Spring 3-2-2018

Physical and Chemical Interactions Affecting U and V Transport from Mine Wastes

Sumant Avasarala

Sumant Avasarala
Candidate

Civil Engineering
Department

This dissertation is approved, and it is acceptable in quality and form for publication:

Approved by the Dissertation Committee:

Dr. Jose M. Cerrato , Chairperson

Dr. Ricardo Gonzalez Pinzon

Dr. Bruce Thomson

Dr. Adrian Brearley

Dr. Mehdi Ali

[redacted]

Sumant Avasarala

B.S., Chemical Engineering, Anna University 2009, India
M.S., Chemical Engineering, Wayne State University, 2012, U.S.

DISSERTATION

Submitted in Partial Fulfillment of the Requirements for the Degree of

Doctor of Philosophy
Engineering

The University of New Mexico

Albuquerque, New Mexico

May 2018

Dedication

I would like to dedicate my PhD to my parents (Seshargiri Rao and Radha), my brother (Ashwin Avsasarala), my friends, and my grandfathers (V.V. Rao and Late Chalapathi Rao) without whose blessings, prayers, and support this journey would have never been possible. Special dedication to my best friend, Dr. Sriraam Ramanathan Chandrasekaran, who guided me and supported me through my rough times. I couldn't think of a better way to indicate your role in my life than dedicating my biggest achievement to you! Thank you for always being there!

Acknowledgement

I never will have enough words to express my gratitude and gratefulness towards my advisor, Dr. José Cerrato, who offered me a PhD position despite many red flags on the way. His exceptional support, advisement, and love for his students (in this case, me) has always kept me driven and motivated—so motivated that it has finally allowed me to see light towards the end of a long, cheerful, fun, and challenging PhD tunnel. Thank you very much, José, for transforming me from a naïve graduate student to an eligible independent researcher. I really appreciate it! I am forever in your debt!

Of course next on my list is Dr. Mehdi Ali for his continuous "It's working, it's not." There is not a day when I have not felt I could talk to you about any challenge that I ran into. You have always comforted, guided, and supported me in both on a professional and personal level. I have relished all moments spent with you from the weekend brunches (green Chile cheese omelets) to all the laughs we shared. Thank you very much, Dr. Ali, for making my journey a lot more memorable and fun.

I am also very thankful to my committee members Dr. Ricardo Gonzalez, Dr. Adrian Brearley, and Dr. Bruce Thomson for all their help, guidance, and support during my PhD research.

I am also very thankful to all my co-authors without whose efforts reaching this point would have been extremely difficult. Special thanks to Dr. Brearley for his patience towards my constant harassment for data.

Finally, my acknowledgement would be incomplete without my friends and lab mates. I consider myself extremely lucky to have had the opportunity to pursue a PhD alongside such smart, supportive, and loving friends. You have always been there to cheer, hold, and encourage me during my difficult times. I have learned so much from all of you, and I wish the best for you all. Thank you.

I have learned so much from each and every one of you that I am forever in your debt. I hope someday I can return the favor.

[redacted]

Sumant Avasarala

B.S., Chemical Engineering, Anna University 2009, India
M.S., Chemical Engineering, Wayne State University, U.S.

Abstract.

This research investigates the physical and chemical interactions that affect the transport of uranium (U) and vanadium (V) from uranium mine waste sites by integrating laboratory experiments and reactive transport modelling with various spectroscopy, microscopy, and diffraction techniques. The document consists of results from three related studies. In the first study (Chapter 3), the reactive transport of U and V was investigated by sequentially reacting mine wastes collected from Blue Gap/Tachee Claim-28 mine site, AZ with 10mM $NaHCO_3$ (7.9) and 10mM CH_3COOH (3.4) during continuous flow through column experiments. Under both of these conditions (pH 3.4 and 7.9), dissolution of U-V bearing minerals predominant at the site were identified as a key mechanism affecting the reactive transport of U and V. The equilibrium (K_{eq}) and reaction rate constants (k_m) for U-V bearing mineral dissolution were estimated to be $K_{eq} = 10^{-44.81}$ and $k_m = 4.8\text{x}10^{-13}$ mol cm^{-2} sec^{-1} at circumneutral conditions, and $K_{eq} = 10^{-38.65}$ and $k_m = 3.2\text{x}10^{-13}$ mol cm^{-2} sec^{-1} under acidic conditions. These results, coupled with electron microscopy data, suggest that the release of U and V is affected by difference in

solution pH and crystalline structure of U-V bearing minerals. Identifying the crystal chemistry of these U-V bearing minerals was the task in the second study (Chapter 4) of the dissertation. Using various diffraction and microscopy tools, the U-V bearing minerals were identified as hydrated carnotite.

Finally, the mobility of U from co-occurring submicron U(IV) and U(VI) mineral phases in mine wastes from the Jackpile mine in Laguna Pueblo, NM was investigated under oxidizing conditions. Co-occurrence of U(VI) and U(IV) at a 19:1 ratio mostly as coffinite ($USiO_4$) and U-phosphate was observed in these mine waste solids. The highest U release from these mine wastes was observed during batch reactions with 10 mM $NaHCO_3$ solution containing ambient dissolved oxygen concentrations. Results from these investigations provide an improved understanding on the role of thermodynamics, crystallinity, stoichiometry, and solution chemistry in the reactive transport of U and V from mine wastes that affect the water quality of surface and ground water resources.

[redacted]

Following the Second World War (WWII), many Federal and Native American lands were intensively mined for uranium (U) to meet the increasing demands for nuclear weapons. Between 1944 and 1986, nearly 30 million tons of uranium ore were extracted from land that was part of the Navajo Nation,[1, 8-9] leaving significant quantities of post-extraction waste materials. Improper disposal and handling of these wastes have resulted in many sites across the United States (US) that have contaminated the surrounding land, the water (groundwater and surface water), and the air resources. Therefore, there is an increased need to understand the mechanisms that affect the transport of U and other co-occurring metals from mine wastes under relevant environmental conditions to propose appropriate remediation strategies.

The research described in this dissertation was intended to improve the current understanding about the reactive transport of U, vanadium (V), and other co-occurring metals in two mines on Native American Land: 1) Blue Gap/Tachee Claim-28 mine waste site, NE Arizona and 2) Jackpile-Paguate mine, Laguna Pueblo, NM. This dissertation is divided into six chapters and two appendices.

Chapter 1 provides an overview of the pivotal research issues and of the dissertation as a whole. Chapter 2 is a summary of the scientific knowledge on 1) mining and its impacts, 2) the physical and chemical processes that affect U mobility, and 3) the existing research gaps. Chapters 3, 4, and 5 form the main body of work for this dissertation are formatted as research papers.

Chapter 3, published in the journal *Environmental Science &Technology* (ES&T), describes the investigation of the reactive transport of U and V from the Blue Gap/Tachee Claim-28 mine waste site using laboratory experiments, reactive transport modelling, and electron microscopy. In this chapter, we estimated the thermodynamic and kinetic constants for dissolution of U-V bearing minerals (which have been detected in the mine waste[1]) at circumneutral and acidic pH by modelling the batch and column experiments using the multicomponent-multiphase model, PFLOTRAN. Appendix A presents supplementary data obtained for this study.

The main objective of Chapter 4 (unpublished) is to determine the crystal chemistry of the U-V bearing minerals that were previously identified in the Blue Gap/Tachee Claim-28 mine wastes using spectroscopy, electron microscopy and X-ray diffraction. In this chapter, we provide insights on the physiochemical characteristics of U and V (i.e., structure, chemistry, morphology, and presence of inclusions) that are fundamental to understanding their material behavior when subjected to weathering processes in mine waste piles. Results from this chapter improve our understanding of the fate and transport of U and V from such sites under environmentally relevant conditions.

The objective of Chapter 5 (unpublished) study was to investigate the effect of oxidizing conditions on the co-occurring submicron U(IV) and U(VI) phases in Jackpile-Paguate mine wastes, AZ, using laboratory experiments, spectroscopy, and electron microscopy techniques. This chapter provides insights on the reactivity of these submicron U(IV) and U(VI) minerals and the relevant mechanism that affects U mobility after reaction with bicarbonate under ambient dissolved oxygen concentrations, and

strong oxidizing conditions. Appendix B for this chapter summarizes supplementary data obtained for this study.

This dissertation improves our understanding of physical and chemical mechanisms that affect the dynamic release and accumulation of U and V from abandoned mine wastes sites by integrating knowledge from geochemistry, thermodynamics, kinetics, mineralogy and hydrology.

[redacted]

Background and Significance

Uranium mining operations occurred during the 1900s to meet the federal government's demand for nuclear weapons after the Manhattan is project [2, 3] and, to a more limited extent, for nuclear energy generation.[4, 5] These mining activities left a legacy of thousands of abandoned mines all over the United States. For example, just in the western US, approximately 15,000 abandoned uranium mine waste sites have been identified, the majority of which are located in Colorado, Utah, New Mexico, Arizona, and Wyoming.[6-7] Seventy five percent of these sites are on federal and tribal lands.[6-7] To exemplify the national problem, about 1100 abandoned uranium mine waste sites located on the Navajo Nation have been overlooked for decades.[1, 8-9]

Mining operations generate two types of waste: mine waste and mill tailings. Mine wastes are unregulated higher concentration U ores that have been abandoned after the mining operations ceased, while the mill tailings are the federally regulated low concentration wastes left after processing the ore for U.[1, 10] Since this dissertation focuses on mine wastes which are generated during mining operations; limited focus has been directed towards discussing mill tailings. Mine wastes contain mixtures of uranium (U), vanadium (V), and other co-occurring metals.[11-13] These wastes pose environmental and health risks to nearby communities. However, before effective remedies can be proposed, we need to know relevant details about the sites and the distribution means for the waste.

In an attempt to remediate such sites after the mine closures, these wastes were regulated based on the Surface Mining Control and Reclamation Act of 1977 (SMCRA). The SMCRA mandated burying the wastes under clean soil covers as an approach to

naturally eliminate potential health hazards.[12] This method was adopted to naturally attenuate the threat metals, especially carcinogenic metals like U. [14-18] However, natural erosion of these soil covers has caused metal migration to the surface and into the groundwater resources where these toxic metals have contaminated the water and negatively impacted those who consume it. [18-19] For example, elevated metals concentrations (with respect to their respective maximum contamination limits (MCL), for e.g. U MCL = 30µg L^{-1}) in the water resources surrounding such contaminated abandoned uranium mine waste sites in southwestern United States have been reported.[1, 20] These dissolved metals have the ability to act as Lewis acids, complexing with the hydroxyl group (OH^-) and causing a drop in pH. Acidic conditions in these sites can also be caused due to acid mine drainage; that is, the outflow of acidic water from a mining site that primarily comes from oxidation of iron sulfide (FeS_2) or pyrite. [21-22] An acidic environment is generally toxic to biota and less favorable for many other organisms than is an environment at circumneutral pH conditions.[23]

Elevated concentrations of U and V in water resources pose a concern for health risks to individuals in the surrounding communities. [14-16] For example, the adverse toxic effects of U and V are well documented in human exposures by inhalation and by ingestion. [24-29] Uranium exposure has long been known to cause cancer (e.g., bone, reproductive, and gastric), kidney toxicity, miscarriages, birth defects, and heart diseases. [14, 27, 30-33] Uranium has also been linked to adverse developmental outcomes in animals.[34-35] Additionally, recent studies in Navajo communities have linked exposures to mine wastes with an increased likelihood for developing one or more chronic diseases including hypertension, kidney disease, and diabetes.[36] Therefore there is an increased

need to understand the mobility and transport of U and V to develop informed and appropriate strategies to remediate abandoned sites.

Adequate management and cleanup of abandoned mine waste sites are challenging due to complex regulatory, social, and political factors. For instance, the Comprehensive Environmental Response, Compensation, and Liability Act, commonly known as the Superfund program, was created to provide assistance to clean these sites.[37] However, despite the known elevated metal concentrations identified in many abandoned mine wastes sites, limited or no action has been taken to remediate thousands of these sites due to financial and political constraints.[6-7] Providing necessary scientific data to guide federal, state, and local governments on developing appropriate remediation strategies for such sites is an ongoing challenge.[38]

Study Areas: Blue Gap Tachee Claim-28, AZ and Jackpile-Paguate Mine, NM

Mine waste sites located on Native American lands have been overlooked due to low population densities and site remoteness. The Blue Gap/Tachee Claim-28 mine site in northeastern Arizona and the Jackpile-Paguate mine waste site in Laguna Pueblo, New Mexico, are two such sites that represent the study areas for this dissertation.

The Blue Gap/Tachee Chapter of the central Navajo Nation, located approximately 40 miles west of Chinle, AZ, started operating during the early 1950s. On the mesa tops and steep slopes of this location, 13 different mines operated from 1954-1968.[1] In the early 1990s, initial reclamation efforts agglomerated the wastes in the Claim 28 site under a layer of uncontaminated soil (SMCRA).[13, 39] At Blue Gap/Tachee, the uranium ores occur in tabular and lenticular sandstone units of the Rough Rock Sandstone member in the Toreva formation. A recent study conducted by our research group in the Claim 28

site identified the major mineralogical constituents of this arkosic sandstone to be 59% quartz (SiO_2), 34% potassium feldspar ($KAlSi_3O_8$), and 7% kaolinite ($Al_2Si_2O_5(OH)_4$).[1, 39-40] Furthermore, the dissolution of U-V bearing minerals in mine wastes that were potentially affect the elevated concentrations (with respect to the maximum contaminant level [MCL] for U) in neighboring water resources (67−169 μg/L of U) at the site.[1] These U-V bearing minerals were found to have a structure similar to that of carnotite ($K_2(UO_2)_2(VO_4)_2 \cdot 3H_2O$) or tyuyamunite ($Ca(UO_2)_2V_2O_8 \cdot (5\text{-}8)H_2O$).[1] However, there is no information on the type of uranyl vanadates these U-V bearing minerals represent or the processes that affect U-mobility from these mine wastes. This information is critical to better understand mobility of U and V from many U mines around the world where uranyl vanadates are predominant. For instance, abandoned uranium mines in the Colorado Plateau, South Dakota, southwest China, southern Jordan, Korea and the calcreted drainages of arid and semiarid western and southern Australia are rich in carnotite, tyuyamunite, and other U-V bearing minerals that have affected the water quality of neighboring surface and ground water resources.[41-48]

The Jackpile-Paguate mine is an abandoned uranium mine located on the 1093 Laguna reservation in north-western New Mexico,[49] 45 miles west of Albuquerque, NM, USA. Approximately 600 m away from the Jackpile-Paguate Mine is Paguate, one among the eight major villages of Laguna Pueblo. Just below Paguate lies one of the most extensive uranium deposits in the US. The mining operation at the Jackpile-Paguate mine disturbed approximately 2,656 acres of property[19] and was once the largest operational, open pit uranium mine in the world. The U deposits in the Jackpile-Paguate Mine are present in the Jackpile sandstone found in the uppermost part of the Brushy Basin Shale

Member of the Jurassic and Cretaceous strata.[50-52] Although the combined ores in the Jackpile-Paguate mine are 2 km long and 600 m wide, the semi-tabular U deposits in the Jackpile sandstone are only about ~5 m thick.[50-52]

The Rio Paguate flows from Miocene basalt and andesite flows of Mount Taylor, southeast towards the village of Paguate through the Jurassic Morrison Formation and the abandoned Jackpile-Paguate Mine.[53] Reactions between these surface waters and U mine wastes could affect the water quality and pose a potential human risk. For instance, a recent study by our research group reported seasonal variations in elevated concentrations of U and other co-occurring metals in Rio Paguate (35.3 to 772 mg L^{-1}) that were later identified as a consequence of dissolution of U-bearing minerals from these U-ore deposits.[54] However, the geochemical processes that affect U mobility from these mine wastes is still not well understood.

State of the Knowledge about Processes Affecting U and V Transport from Mine Wastes

The mobility of U and V are affected by a variety of biogeochemical and physical processes. Uranium is an actinide abundantly found in various parts of the southwestern US with alternating valence states among IV, V, and VI depending on the surface and subsurface conditions in which it is present.[55-58] The +6 oxidation state (U(VI)) is the most mobile and toxic form of U. [24-26] The processes that affect U mobility are driven by physicochemical parameters, including pH, Eh, temperature, reaction kinetics, and elemental composition of the system.[59-63] Uranium mobility is enhanced by the presence of complexants like carbonate and bicarbonate that form aqueous complexes like U-Ca-CO_3^{-2} and U-CO_3^{-2}.[22, 64] Combined use of these natural complexants has been reported to

be effective for U mobility in systems with high calcium (Ca), sulfur (S), manganese (Mn), and aluminum (Al) concentrations.[21] Mining industries use these complexants in alkaline leaching for targeted U extraction.[65]

The aqueous complexes formed from such complexation reactions adsorb onto the oppositely charged surfaces of SiO_2, hydrous ferric oxide, ferrihydrite, aluminum hydroxides, clays, and organic matter.[66-72] Uranyl complexes bind strongly onto organic matter through either ion-exchange, coordination/complexation, donor-receptor interactions, or Van der Waal forces at circum-neutral conditions, substantially enhancing U mobility.[71, 73-77] The degree to which the U mobility is enhanced depends on 1) the electrostatic potential between aqueous complexes and organic matter surfaces, 2) hydrophobicity of organic matter, and 3) the ability of U(VI)-organic matter colloids to stay suspended.[73, 78-79] Like aqueous U(VI), monomeric U(IV), which represents non-crystalline U(IV) species, also adsorb onto organic matter aggregates and organic-carbon coated clays that possess higher mobility and toxicity considering their susceptibility to desorb and reoxidize.[72, 80] Only recently were monomeric biogenic U(IV) species found to be present at undisturbed roll front ore deposits.[81] In addition to adsorption, the tetravalent and hexavalent U also form bidentate aqueous complexes with organic matter.[82]

Formation of sparingly soluble, biogenic, and chemogenic U(IV) through reduction reactions has been used as techniques to immobilize aqueous U.[83-85] The reduction of aqueous U(VI) can result in the formation of crystalline, submicron, biogenic, and chemogenic U(IV) phases whose dissolution rates and energetics are very similar to those of coarser U(IV) phases.[86-88] Submicron U particles and U adsorbed onto colloids of

organic matter and oxides form about 30-40% of the total naturally occurring mobile U.[89-90] In addition to sorption, U mobility can also be affected by dissolution/precipitation of U minerals. For instance, U occurs in the environment as vanadate, silicate, phosphate, carbonate and oxide minerals.[91-98]

Similarly, V is a redox active, transition metal that co-occurs with U at oxidation states from II to V.[5, 99-102] Vanadium is most soluble as V(IV), and V(V) [99-102], among which V(V) is considered most mobile and toxic. [24-26] Like U, V is also mobilized by carbonate reagents.[1] However, unlike U, it does not complex with dissolved carbonate. Instead, its oxyanionic behavior causes the formation of aqueous anionic [$V_{10}O_{26}(OH)_2^{4-}$, $V_{10}O_{27}(OH)^{5-}$, $V_{10}O_{28}^{6-}$,$VO_2(OH)^{2-}$, $VO_3(OH)^{2-}$, VO_4^{3-}, $V_2O_6(OH)^{3-}$, $V_2O_7^{4-}$, $V_3O_9^{3-}$ and $V_4O_{12}^{4-}$], cationic [VO^{2+}] and neutral [$VO(OH)_3$] species.[60, 62, 103-104] These aqueous complexes of U and V adsorb onto ferrihydrite, aluminum hydroxides, and clays through electrostatic interactions[62, 104-106 44, 48, 50-52, 86-91], depending on the pH_{pzc} of the solids. Uranium and V could also be immobilized through precipitation of secondary mineral phases such as carnotite ($K_2(UO_2)_2(VO_4)_2 \cdot 3H_2O$ and vanadinite ($Pb_5(VO_4)_3Cl$)[63, 41, 98] These geochemical processes are key to the aqueous and solid speciation of U and V.

In addition to solid and aqueous chemistry of U and V, other factors such as kinetics, thermodynamics, and crystal chemistry of minerals are also critical to understand their reactive transport under relevant environmental conditions. The reactive transport of metals can be described using reactive transport models, e.g., PFLOTRAN, which is the reactive transport model used in this dissertation.

PFLOTRAN is a multicomponent-multiphase model that couples thermodynamics, kinetics, hydrology, and aqueous chemistry to simulate the interfacial mechanisms that affect the mobilization of U and other metals in surface and subsurface environments. Previous studies have used reactive transport modelling to investigate the adsorption behavior of U(VI) complexes onto alluvial aquifer sediments.[107, 108] The subsurface desorption kinetics of U(VI) species suggest a non-equilibrium sorption behavior with Fe-oxides, Mn-oxides, and phyllosilicates.[109-111] Uranium transport can also be attributed to dissolution of mineral phases. For example, U transport from contaminated, subsurface sediments from the Hanford site, WA, was affected by the dissolution of metatorbernite [$Cu(UO_2)_2(PO_4)_2 \cdot 8H_2O$], cuprosklodowskite ($Cu[(UO_2)(SiO_2OH)]_2 \cdot 6H_2O$), and Na-boltwoodite [$NaUO_2(SiO_3OH) \cdot 1.5H_2O$].[95, 110, 112] The development of reactive transport models that represent environmentally relevant oxidizing conditions in abandoned mine waste sites is necessary to better understand the mobility of U and other metals.

[redacted]

The mobility of U and other metals is also affected by the crystal chemistry of the naturally-occurring U-minerals in the mine waste. Crystal chemistry is the study of chemistry principles behind the assembly of crystals and their use in describing structure-property relations in solids. An example about the importance of crystal chemistry is presented in recent studies, which tried to observe the effect of crystallinity on dissolution of glass and natural silicate minerals. These studies reported that dissolution rates increase with increasing Si:O ratio, which is higher in glass than in natural silicate minerals. For example, ultra-mafic glasses (Si:O $\leq$0.28) dissolve at similar rates as correspondingly compositioned minerals, but Si-rich glasses such as rhyolite (Si:O ~

0.40) dissolves ≥1.6 orders of magnitude faster than corresponding minerals.[113-114, 115] Therefore, in order to better understand the transport of U and V from abandoned mine wastes, the effect of crystal chemistry should be considered as these affect biogeochemical and physical processes. For instance, the general formula used to represent several uranyl vanadates is $M^{n+}_{1/n}UO_2AO_4.xH_2O$ where, M is a cation that can be either mono-, di- or tri-valent elements of groups I and II in the periodic table[93, 116-119] that are comprised of $[(UO_2)_2V_2O_8]_n^{-2n}$ layers and water.[117,120-121] Understanding the crystal chemistry is essential to understand the dissolution and reactivity of these U-V-bearing minerals in mine waste sites.

Research Gap and Objectives

Previous studies have identified the factors that affect individual transport of U or V. However, the specific mechanisms affecting the transport of U and other co-occurring metals in abandoned mine waste sites remains poorly understood. For instance, in a recent study the mobility of both U and arsenic (As) from a U mill tailing site in South Dakota were observed.[122] Yet the specific processes affecting the transport of these metals are unknown.[93] In addition, previous investigations have provided limited information on 1) the release of metal mixtures from uranium mine wastes; and 2) the interactions, co-occurrence, and behavior of these metal mixtures in the environment under relevant field conditions. *Scientific knowledge obtained from this study can be applied to other abandoned uranium mines in U.S. that bear a similar mineralogy or geology as the two study sites of focus in this dissertation*.[123-124]

The goal of this research was to *provide essential insights on the mechanisms that*

affect the reactive transport of U and V from abandoned uranium mine wastes. This information on the reactivity and mobility of U and V can be key to understanding the potential metal exposure pathways in abandoned uranium mine waste sites. The approach and the methods used to in this research involve contributions from different disciplines that include *inorganic chemistry, geochemistry, minerology, analytical chemistry, and environmental science; the interdisciplinary nature of the project is relevant to any remediation proposals arising from the study*.

The three specific research objectives of this research include:

1. Investigate the reactive transport of U and V from the Blue Gap/Tachee Claim-28 mine waste site through laboratory experiments, reactive transport modelling, and electron microscopy techniques.
2. Investigate the crystal chemistry of U-V bearing minerals occurring in the Blue Gap/Tachee Clim-28 mine waste using the properties of synthesized primary ores as a reference.
3. Investigate the effect of oxidizing conditions on the co-occurring nano-particulate U(IV) and U(VI) phases in Jackpile mine wastes using laboratory experiments, spectroscopy, and electron microscopy techniques.

Addressing these research objectives in the following order will help to explain the role of thermodynamics, crystallinity, stoichiometry, and solution chemistry on the reactive transport of U and V from such mine wastes that pose as a threat to neighboring surface and ground water quality.

[redacted]

(Published in *Environmental Science & Technology*)

Sumant Avasarala[1], Peter C. Lichtner[2], Abdul-Mehdi S. Ali[3], Ricardo González-Pinzón[1], Johanna M. Blake[4a] and José M. Cerrato[1]*

*Corresponding email address: jcerrato@unm.edu

Telephone: (001) (505) 277-0870

Fax: (001) (505) 277-1918

[1] Department of Civil Engineering, MSC01 1070, University of New Mexico, Albuquerque, New Mexico 87131, USA.

[2] OFM Research-Southwest, Santa Fe, New Mexico 87507, USA.

[3]Department of Earth and Planetary Sciences, MSC03 2040, University of New Mexico, Albuquerque, New Mexico 87131, USA.

[4]Department of Chemistry, MSC03 2060, University of New Mexico, Albuquerque, New Mexico 87131, USA.

[a] Current address: U.S. Geological Survey, New Mexico Water Science Center, 6700 Edith Blvd NE., Albuquerque, New Mexico, USA.

[redacted] **Abstract**

The reactive transport of uranium (U) and vanadium (V) from abandoned mine wastes collected from the Blue Gap/Tachee Claim-28 mine site, AZ, was investigated by integrating flow-through column experiments with reactive transport modelling, and electron microscopy. The mine wastes were sequentially reacted in flow-through columns at pH 7.9 (10 mM $NaHCO_3$) and pH 3.4 (10 mM CH_3COOH) to evaluate the effect of environmentally relevant conditions encountered at Blue Gap/Tachee on the release of U

and V. The reaction rate constants (k_m) for the dissolution of uranyl-vanadate (U-V) minerals predominant at Blue Gap/Tachee were obtained from simulations with the reactive transport software, PFLOTRAN. The estimated reaction rate constants were within one order of magnitude for pH 7.9 (k_m = 4.8x10^{-13} mol cm^{-2} sec^{-1}) and pH 3.4 (k_m = 3.2x10^{-13} mol cm^{-2} sec^{-1}). However, the estimated equilibrium constants (K_{eq}) for U-V bearing minerals were more than 6 orders of magnitude different for reaction at circumneutral pH (K_{eq} = 10$^{-38.65}$) compared to acidic pH (K_{eq} = 10$^{-44.81}$). These results coupled with electron microscopy data suggest that the release of U and V is affected by water pH and the crystalline structure of U-V bearing minerals. The findings from this investigation have important implications for risk exposure assessment, remediation and resource recovery of U and V in locations where U-V-bearing minerals are abundant.

Introduction

The legacy of mill tailings and wastes from mining operations has resulted in the release of elevated concentrations of metals and radionuclides, which pose imminent environmental and human health concerns.[125, 126] For instance, the negative health impacts of human exposure to uranium (U) and vanadium (V) through inhalation and ingestion have been well documented.[24, 36] Uranium and V co-occur at numerous abandoned mine waste sites on Navajo Nation territory near the Four Corners region of the southwestern U.S.[127, 1] Uranium and other co-occurring metals from these mine wastes can be released into neighboring water resources affecting their water quality.

The aqueous and solid chemical speciation of U and V at mine waste sites could be affected by a variety of interfacial geochemical processes. These mine waste

sites are usually exposed to ambient surface oxidizing conditions in which U(VI) is predominant.[1, 109] Aqueous U(VI) can complex with OH^- and CO_3^{2-} or can react with alkaline earth metals and CO_3^{2-} to form neutral or negatively charged ternary complexes (e.g. U-Ca- CO_3^{2-}) that affect U mobility in water.[128, 129] Vanadium preferentially forms anionic [$V_{10}O_{26}(OH)_2^{4-}$, $V_{10}O_{27}(OH)^{5-}$, $V_{10}O_{28}^{6-}$, $VO_2(OH)^{2-}$, $VO_3(OH)^{2-}$, VO_4^{3-}, $V_2O_6(OH)^{3-}$, $V_2O_7^{4-}$, $V_3O_9^{3-}$ and $V_4O_{12}^{4-}$], cationic [VO^{2+}], and neutral [$VO(OH)_3$] species of oxyanions and aqueous complexes.[62, 104] These oxyanions and aqueous complexes of V and U(VI) can adsorb onto charged surfaces of aluminum (Al) oxides, iron (Fe) oxides, and clay minerals.[67, 104-105, 129-134] Uranium and V can also be present in solid form as oxide, phosphate, carbonate, vanadate, and silicate mineral phases.[93, 135-136] For instance, their co-occurrence as carnotite [$K_2(UO_2)_2V_2O_8$], tyuyamunite [$Ca(UO_2)_2V_2O_8 \cdot (5\text{-}8)H_2O$], metahewettite [$CaV_6O_{16} \cdot 3(H_2O)$], melanovanadite [$CaV_4O_{10} \cdot 5(H_2O)$], and V-bearing clays has been observed at the Rough Rock Sandstone of the Cretaceous Mesa Verde Group study region located in southwestern US.[137] Uranium oxides such as schoepite [$(UO_2)8O_2(OH)_{12} \cdot 12(H_2O)$] are commonly occurring minerals that also influence uranyl solubility under oxic and suboxic environments between pH 6-9.[41, 138] These geochemical processes, which are key to the aqueous and solid speciation of U and other co-occurring metals, should be considered when investigating the reactive transport of metals in abandoned mine wastes.

Reactive transport modelling can be a useful tool to investigate the interfacial mechanisms that affect the surface and subsurface mobilization of U and other metals. Previous studies have used reactive transport modelling to investigate the adsorption behavior of U(VI) complexes onto alluvial aquifer sediments.[107, 108] The subsurface

desorption kinetics of U(VI) species suggest a non-equilibrium sorption behavior with Fe-oxides, manganese (Mn) oxides, and phyllosilicates.[109-111] Uranium transport can also be attributed to dissolution of mineral phases. For example, U transport from contaminated subsurface Hanford Sediments was affected by the dissolution of metatorbernite [$Cu(UO_2)_2(PO_4)_2 \cdot 8H_2O$], cuprosklodowskite ($Cu[(UO_2)(SiO_2OH)]_2 \cdot 6H_2O$), and Na-boltwoodite [$NaUO_2(SiO_3OH) \cdot 1.5H_2O$].[95, 110, 112] The development of similar reactive transport models that represent environmentally relevant oxidizing conditions in abandoned mine waste sites is necessary to better understand the mobility of U, V, and other metals.

Previous laboratory-based studies have shown that U and V can interact through precipitation reactions forming uranyl vanadate minerals with potassium and calcium (e.g., carnotite [$K_2(UO_2)_2(VO_4)_2 \cdot 3H_2O$] and tyuyamunite [$Ca(UO_2)_2V_2O_8 \cdot 5\text{-}8(H_2O)$]).[93, 139] These studies used batch experiments and thermodynamic predictions to identify precipitation of uranyl vanadates as an effective method to immobilize U and V below the U-maximum contaminant level (MCL, 30 μg L^{-1}) between pH 5.5-7. [93, 139] The thermodynamic estimations calculated in these studies were in agreement with those previously calculated by Langmuir.[140] However, these theoretically estimated thermodynamic constants are limited to synthetic minerals that have been subjected to specific reactivity conditions that could differ from those of U-V bearing minerals occurring in the environment.

A recent study conducted by our research group at the Blue Gap/Tachee Claim-28 mine site located in Northeastern Arizona reported that the dissolution of U-V bearing minerals affects the mobility of U and V at pH conditions observed in the field,

which range from 3.8 to 7.4.[1] Results showed that U and V co-occur in mine wastes predominantly as U(VI) and V(V). The Extended X-Ray Absorption Fine Structure (EXAFS) fittings suggest that U and V coordination in these mine waste samples is similar to that of minerals such as carnotite [$K_2(UO_2)_2(VO_4)_2 \cdot 3H_2O$] or tyuyamunite [$Ca(UO_2)_2V_2O_8 \cdot 5\text{-}8(H_2O)$]. Additionally, results from this study suggest dissolution of these U-V bearing minerals are a potential source to the elevated metal concentrations in neighboring surface water resources.[1] Although this study represents a valuable first attempt to identify the co-occurrence of U and other metals at this abandoned mine waste site, the mechanisms affecting the reactive transport of U, V, and other metals remain unknown.

The objective of this study is to investigate the reactive transport of U and V from the Blue Gap/Tachee Claim-28 mine waste site through laboratory experiments, reactive transport modelling, and electron microscopy. In the current investigation we seek to determine the equilibrium and reaction rate constants for dissolution of these U-V bearing minerals at circumneutral and acidic pH by modelling the batch and column experiments performed in this study with PFLOTRAN.[27-28, 33] This study was developed based on our prior evidence that suggested U-V bearing mineral phases as the potential source to U and V release from Blue Gap/Tachee mine wastes.[1] Our integrated approach of using microscopy and reactive transport modelling serves as a foundation to better understand the mechanisms affecting the reactivity of mine wastes and the transport of U and V under environmentally relevant conditions.

Materials and Methods

[redacted]

Mine waste and background sediments were collected from the Blue Gap/Tachee Claim-28 mine site in January, 2014, to identify the processes and phases that affect the U and V transport into neighboring surface and ground water resources. Sediment samples from the site included mine waste and Baseline Reference Soil (background soil) previously characterized by Blake et al., 2015.[1] The Blake et al. study used powder X-ray diffraction to identify quartz (SiO_2; 59%), potassium feldspar ($KAlSi_3O_8$; 34%), and kaolinite ($Al_2Si_2O_5(OH)_4$; 7%) as the major mineralogical constituents. Additionally the co-occurrence of U and V and predominance of U(VI) and V(V) were identified using microscopy, X-Ray Photoelectron Spectroscopy (XPS), and X-Ray Absorption Near Edge Spectroscopy (XANES) techniques. Furthermore, the coordination numbers obtained from EXAFS fits suggested the structure of the U-V bearing mineral to be similar to that of carnotite or tyuyamunite.[1]

[redacted]

We conducted batch experiments to model the U and V release at circumneutral (8.3) and acidic (3.4) pH and determined the equilibrium and reaction rate constants for dissolution of U-V bearing mineral phases. The determined equilibrium constant was then used to obtain the reaction rate constants for U-V bearing mineral dissolution during column experiments. Briefly in the batch experiments, we reacted 0.1 g of mine wastes and background soil samples that were sieved to <63 μm size (using U.S. standard sieve series number 230), with 50 mL 10 mM $NaHCO_3$ (pH 8.3) and 10 mM $C_6H_8O_6$ (pH 3.8) through gentle shaking in 50 mL centrifuge tubes for 264 hours, as described in Blake et al.[1] During the experiments we collected 2 mL aliquots 0.5, 1, 2, 6, 24, 48, 96, and 264 h

after the experiment began. We diluted these aliquots and analyzed for elemental concentrations using Inductively Coupled Plasma Optical Emission Spectroscopy and Mass Spectroscopy (ICP-OES/MS). All batch experiments were conducted in triplicates.

[redacted]

A column experiment was conducted to investigate the transport of U and V from Blue Gap/Tachee Claim-28 sediments. An initial set of experiments consisted of reacting mine waste and background soil with 18MΩ water at pH 5.4 to evaluate the release of water-soluble U and V. Another set of experiments were performed in parallel where the mine waste and background soil were sequentially reacted at pH 7.9 (using 10 mM $NaHCO_3$) and pH 3.4 (using 10 mM CH_3COOH). These pH values and concentrations represent environmentally relevant conditions observed at the study site.[1] We prepared samples by crushing and homogenizing sediments with a Spex shatter box and sieving through U.S. standard sieve with series 120-45 to obtain particle sizes between 125-355 µm. The homogenized sieved fractions were then packed into cylindrical Pyrex glass columns with an inner diameter of 1 cm and a height of 10 cm using vacuum filter pumps. Solutions of 10 mM $NaHCO_3$ and 10 mM CH_3COOH were prepared using 18MΩ deionized water, $NaHCO_3$, and 17.4N CH_3COOH. The prepared solutions were pumped against gravity through the packed columns at 0.9 mL min-1 using a Masterflex L/S series 8-channel peristaltic pump. The column experiments were conducted on eight columns in parallel (Appendix A: Figure 7.1). We chose 0.9 mL min-1 based on existing literature[109-110, 141] as a typical groundwater rate to evaluate how solutions at circumneutral and acidic conditions would react with mine wastes. Columns 1, 2, 5, and 6 were packed with mine waste and columns 3, 4, 7, and 8 were packed with background

soil. Columns 1-4 were reacted with 18MΩ water for 90 minutes with a total of 23 (columns 1-2) and 31 (columns 3-4) pore volumes (PV) at the rate of 3.53, and 2.65 cm3 PV-1, respectively. Columns 5-8 were sequentially reacted for one week each (10,080 min) with 10 mM $NaHCO_3$ and 10 mM CH_3COOH (Appendix A: Figure 7.1). The one week reaction time resulted in 2570 PV for columns 5 and 6 and 3450 PV for columns 7 and 8. Samples were collected at 10, 20, 30, 40, 50, 60, 70, 80, and 90 min of reaction time from the outlets of columns 1, 2, 3, and 4. Samples were collected columns 5–8, at 30, 180, 540, 1440, 2880, 4320, 5760, 7,200, and 10,080 min after sequential reaction with 10 mM $NaHCO_3$ and 10 mM CH_3COOH solutions. The sample aliquots were filtered using a 0.45 μm syringe filter and diluted accordingly for analyses. All experiments were performed at room temperature (25° C) and, consequently, that temperature was set for the reactive transport of modelling.

[redacted]

We used a PerkinElmer Optima 5300DV inductively coupled plasma-optical emission spectrometer (ICP-OES) and a PerkinElmer NexION 300D (Dynamic Reaction Cell) inductively coupled plasma-mass spectrometer (ICP-MS) to obtain the trace metal concentrations in experimental aliquots and total acid extracts of mine waste and background soil. The solution pH was measured using a Thermo Scientific Orion Versastar Advanced Electrochemistry pH meter. Additional technical details of these methods are described in the Supporting Information (SI).

[redacted]

We used PFLOTRAN a surface-subsurface multiphase, multicomponent reactive flow and transport model [110-111, 142] to determine the equilibrium constants for U-V bearing

mineral dissolution at circumneutral and acidic pH (batch experiments) and to identify the processes controlling the reactive transport of U and V from mine waste (column experiments).

In order to model the batch and column experiments, we used various U and V bearing aqueous species and mineral, their associated thermodynamic equilibrium constants (K_{eq}), and stoichiometric reaction coefficients (Tables 7.1 and 7.2) as inputs for PFLOTRAN. Most of the listed parameters were fixed except for the equilibrium constant of carnotite and reaction rate constants of the U-V bearing minerals, metaschoepite [$(UO_2)8O_2(OH)_{12}\cdot 12(H_2O)$], and rutherfordine [$(UO_2)CO_3$] that were varied to fit the experimental data and to obtain the equilibrium and reaction rate constants for dissolution of U-V bearing minerals. At circumneutral pH, minerals such as metaschoepite and rutherfordine were considered in the model as they are commonly occurring oxides and carbonates of U that affect U transport. [41, 143-145] In addition to metaschoepite and rutherfordine, surface complexation reactions for $>SOUO_2OH$ and $>SOHUO_2CO_3$ were also considered in order to understand the effect of sorption on the reactive transport of U.[146] The equilibrium constants estimated for U-V bearing minerals by modelling the batch experiments at circumneutral and acidic pH were used to estimate their reaction rate constants during column experiments.

Some key assumptions made in the model include: 1) U-V bearing minerals are the dominant U phase in the mine waste sample, 2) the U-V bearing minerals have similar properties to those of carnotite [$K_2(UO_2)_2(VO_4)_2\cdot 3H_2O$], and 3) the U-V bearing mineral particles are spherical in shape. These assumptions were made based on our previously published information on the Blue Gap/Tachee mine site, where the EXAFS

fits of U-V bearing minerals, which were dominant in the mine waste, suggested similar coordination as carnotite or tyuyamunite.[1] The spherical shape of the U-V bearing minerals was assumed for calculation simplifications.

Using PFLOTRAN, we modelled the water movement through the column considering fully saturated sediments under oxidizing conditions. The governing mass conservation equation that accounts for the unidirectional change in the total dissolved concentration of the jth primary species is given by (Eq. 1):

$$\frac{\partial}{\partial t}(\varphi\Psi_j) + \frac{\partial}{\partial z}(q\Psi_j - \varphi D \frac{\partial}{\partial z}\Psi_j) = Q_j - \sum_m v_{jm} I_m - \frac{\partial S_j}{\partial t} \quad (1)$$

where z [L] is the height of the column (10cm), t [T] is the time for which column experiments were conducted, Ψ_j [ML^{-3}] denotes the total concentration, D [L^{-2}T^{-1}] denotes hydrodynamic dispersion coefficient, Q_j [M L^{-3}T^{-1}] is a source/sink term, I_m [ML^{-3}T^{-1}] the reaction rate of the m^{th} mineral, v_{jm} [-] is the stoichiometric coefficient for mineral reactions, S_j [ML^{-3}] is the sorbed concentration, q [LT^{-1}] is Darcy's flux calculated to be approximately 1.15 cm min^{-1} based on the flow rate used for the column experiments, 0.9 mL min^{-1} and φ [-] is porosity. Dirichlet boundary conditions were used to model the 1D reactive transport of metals during reaction at pH 7.9 (using 10 mM $NaHCO_3$) and pH 3.4 (using 10 mM CH_3COOH). Additional information and other supporting equations used in the model are explained in the Supplementary Information. (SI equation 2-13)

[redacted]

Solid characterization using JEOL 2010 High resolution Transmission Electron Microscopy (HR-TEM) was performed crystallinity of U-V bearing minerals in the mine waste sample. Synchrotron Micro- X-ray Fluorescence mapping (µ-SXRF) was

conducted in beamline (BL) 10-2 in Stanford Synchrotron Radiation Lightsource (SSRL). Additional technical details of these methods are described in the Supporting Information (SI).

Results and Discussion

[redacted]

We investigated the potential release of water-soluble U and V from mine waste solids by reacting columns with 18MΩ water as a function of pore volumes and time (Appendix A: Figure 7.2). Aqueous concentrations as high as 2.3×10^{-7} M U and 74×10^{-6} M V were measured. For reference, the concentrations of U released from this reaction (~2.3×10^{-7} M) were similar to the concentrations observed in one of the water sources proximate to the site (spring concentrations equal to 2.8×10^{-7} M), as was shown in a previous study conducted by our group.[1] These mobilized concentrations were almost two times higher than the regulated U.S. Environmental Protection Agency Maximum Contaminant Level (MCL) of U, i.e., 1.3×10^{-7} M (30 µg L^{-1}).[8] The U and V concentrations released after reaction of background soil (control) with 18MΩ water were either below the MCL for U or below the detection limit of the ICP-OES/MS instruments. The presence of U and V in the effluent solution can be attributed to possible contributions from electrostatically bound chemical species in the diffused layer or dissolution of soluble oxide phases, such as schoepite [$(UO_2)_8O_2(OH)_{12} \cdot 12(H_2O)$] and V oxides as observed in other investigations.[147-149] The mobility of such labile aqueous species from mine waste is environmentally relevant. Further investigation of the reactive transport of U and V based on co-occurring U-V bearing mineral phases was conducted by sequentially reacting mine waste and background soil with circumneutral and acidic reagents.

The reactive transport model developed for batch experiments reacting mine waste with 10 mM $NaHCO_3$ identified dissolution of U-V bearing minerals as the key process affecting the dissolved concentrations of U and V (Figure 3.2A, B). The equilibrium constant (K_{eq}) for U-V bearing mineral dissolution was estimated to be $10^{-44.81}$ (Table 3.1), which was almost 12 orders of magnitude lower than that reported in literature for carnotite (Keq = $10^{-56.38}$).[150] The difference between the K_{eq} for dissolution of U-V bearing minerals and carnotite can be attributed to a difference in reactivity conditions and crystallinity between U-V bearing minerals in the mine wastes and carnotite. In addition, the estimated reaction rate constant (k_m) for U-V mineral dissolution was $2.13x10^{-14}$ mol cm^{-2} sec^{-1} (Table 3.1). Similarly, the estimated km values for precipitation of metaschoepite and rutherfordine were approximately $1x10^{-15}$ and $2x10^{-16}$ mol cm^{-2} sec^{-1}, respectively (Table 7.3). The nature of a reaction (i.e., dissolution or precipitation) can be identified from the sign convention of the reaction rate (I_m) appearing in PFLOTRAN; that is, negative for dissolution and positive for precipitation. These results are in agreement with observations previously made at the nearby Colorado Plateau deposits where precipitation of metaschoepite from aqueous U concentrations between pH 6-10 was reported.[41] The equilibrium constants estimated by modelling these batch experiments at circumneutral conditions were then used as a foundation for identifying the reaction rate constants for U-V bearing mineral dissolution in the column experiments.

A linear correlation with a slope of 1.45 and a R^2 of 0.993, observed between molar concentrations of U and V (Appendix A: Figure 7.3A) that were mobilized during mine waste reaction with 10 mM $NaHCO_3$, suggested dissolution of U-V bearing mineral phases as a potential source. These results agree with a previous study from our research group where a linear correlation between U and V was observed (slope= 0.636 and R^2 = 0.95) in batch experiments reacting mine wastes with 10 mM $NaHCO_3$ at pH 8.3.[1] The U and V release patterns obtained from these experiments were then simulated using PFLOTRAN to further understand the processes affecting the reactive transport of U and V.

Similar to modelling results from the batch experiments, the reactive transport model for flow-through column experiments on reaction with 10 mM $NaHCO_3$ suggested dissolution of U-V bearing minerals as the primary mechanism affecting U and V transport. The effluent concentrations of U and V, reported as a function of pore volumes (Figure 3.2C, D) and time (Appendix A: Figure 7.4), were compared to those obtained from the reactive transport model (PFLOTRAN). PFLOTRAN used the estimated K_{eq} = $10^{-44.811}$ for U-V bearing mineral dissolution from batch experiments to adequately fit the flow-through column experiments data and to estimate the k_m and fitting parameter (n_m) for U-V bearing mineral phase dissolution. The fitting parameter n_m, to which the non-linear water-rock reactions are sensitive (SI equations 5, 8), and k_m were estimated to be 5.2 and 4.8×10^{-13} mol cm^{-2} sec^{-1}, respectively. In addition, the negative reaction rate (I_m) suggested the dissolution of U-V bearing minerals. The k_m estimated for the dissolution of U-V bearing minerals (4.8×10^{-13} mol cm^{-2} sec^{-1}) during column experiments was different from that estimated for the batch experiments i.e., k_m = 2.13×10^{-14} mol cm^{-2} sec^{-}

[1] (Table 3.1). The increase in k_m cannot specifically be attributed to a single process. However, the difference in the effective reaction rate constant ($k_{effective} = k_m * a_m^0$), estimated using the average surface area, can be attributed to differences in grain size and reactivity conditions, which include flow and heterogeneity in sample composition (Table 3.1). Observing the effect of grain size on the reactive transport of U and V is also important[151, 48] as the sieved samples may contain nanocrystals of U-V and other co-occurring U and V minerals that were bound electrostatically to the surface of coarser particles.[78] After the effect of grain size was introduced into PFLOTRAN, by adding U-V bearing minerals of variable sizes and surface areas, their effective reaction rate constants ($k_{effective}$) were estimated (Table 7.4). The change in the estimated $k_{effective}$ for various U-V bearing mineral phases was negligible (Table 7.4), leading to the inference that the effect of grain size on the reactive transport of U and V is minimal (Appendix A: Figure 7.5).

Other secondary mineral phases of U like oxides, phosphates, silicates, and vanadates soluble at circumneutral pH that have not been considered in this model could also contribute to the release of U and V from mine waste.[139, 147, 152-153] For instance, a Back Scatter Electron- Scanning Electron (BSE-SEM) micrograph that shows the association of V with Fe and K was collected (Appendix A: Figure 7.6). The co-occurrence of U with other elements (e.g., Se and Sr) was also observed using synchrotron µ-XRF mapping (Appendix A: Figure 7.7). The contribution of these secondary mineral phases can be expected especially considering 1) the heterogeneity of mine waste, 2) the discrepancies between experimental and model U concentrations, and 3) the initial experimental V concentrations are much higher than the model.[149] However, after 3-4 hours of reaction, the experimental V concentrations agree well with the model

suggesting a major contribution from U-V bearing mineral dissolution. Following the column experiments with 10 mM $NaHCO_3$, the mine waste and background soil were sequentially reacted under acidic conditions to further understand the reactive transport U and V.

The reactive transport model for batch reactions with mine waste under acidic conditions (pH 3.8) suggests dissolution of U-V bearing mineral phase as a primary contributor to the reactive transport of U and V. We used PFLOTRAN to estimate the equilibrium (K_{eq} = $10^{-38.65}$) and reaction rate constant (k_m = 6.4x10^{-14} mol cm^{-2} sec^{-1}) for U-V bearing mineral dissolution (Figure 3.3 A, B). This estimated K_{eq} under acidic conditions was different from that of synthetic carnotite (K_{eq} - $10^{-56.38}$) and from that obtained at circumneutral conditions (K_{eq} = $10^{-44.81}$).[150] Similar to observations made in the reactive transport model at circumneutral pH, the difference between the K_{eq} of U-V bearing minerals and carnotite at acidic pH can be attributed to difference in reactivity conditions and crystallinity. We also observed a negative reaction rate (I_m) for U-V bearing minerals that represents their dissolution at acidic pH. The K_{eq} for U-V bearing mineral phase dissolution, identified by modelling the batch reaction under acidic conditions, was then used to estimate the reaction rate constants for U-V bearing mineral dissolution during column experiments.

Consistent with the results obtained for experiments at circumneutral pH, the dissolution of U-V bearing minerals was identified as the key process affecting the reactive transport

of U and V during column experiments under acidic conditions. A linear correlation (slope of 0.862 and a R^2 of 0.983) between effluent molar concentrations of U and V was also observed in column experiments under acidic conditions (Appendix A: Figure 7.3B). However, the rates of dissolution obtained for column experiments at acidic conditions are higher compared to those at circumneutral conditions (Table 3.1). Given that the pK_a of CH_3COOH is 4.74, >90% of CH_3COOH remains protonated. Therefore, more contribution from dissolution by acetic acid (protonated form) over complexation or reduction reactions caused by acetate (non-protonated form) at pH 3.4 is expected.[154] These results agree with observations made in our previous study at Blue Gap/Tachee where linear correlations with a slope of 1.08 and a R^2 of 0.996 between molar concentrations of U and V were observed.[1] Additionally, 99.1% U and 92.8% V of the total elemental content present in the mine waste were extracted through the sequential reaction of solids in column experiments with 10 mM $NaHCO_3$ and CH_3COOH. Note that the acid extractable content of unreacted mine wastes was 1912.12 mg Kg^{-1} U and 858.01 mg Kg^{-1} V (Table 7.5). The U and V concentrations released during these continuous sequential reactions showed strong agreement with the modelled U and V concentrations, suggesting dissolution of U-V bearing minerals as a primary contributor to the reactive transport of U and V.

Different K_{eq} and k_m values for dissolution of U-V bearing minerals were obtained for mine waste reaction under circumneutral and acidic conditions during flow-through column experiments (Figure 3.3 C, D and Appendix A: Figure 7.8). The reactive transport model constructed, with a known K_{eq} for metaschoepite ($-10^{5.26}$)[148] and K_{eq} for U-V bearing mineral phase ($-10^{-38.651}$) estimated from batch reaction under acidic

conditions, was used to identify the k_m constants for dissolution of U-V bearing minerals. The estimated k_m for U-V bearing mineral phase, 3.2×10^{-13} mol cm^{-2} sec^{-1}, was slightly different from those estimated for batch reactions ($k_m = 6.4 \times 10^{-14}$ mol cm^{-2} sec^{-1}) (Table 3.1). As discussed previously for column experiments at circumneutral pH (7.9), this decrease in k_m for U-V bearing mineral dissolution cannot specifically be attributed to a single process. However, the change in the effective reaction rate constant ($k_{effective}$) can be attributed to differences in grain size and reactivity conditions that include flow and heterogeneity in sample composition (Table 3.1). The effect of grain size was not particularly tested for the sequential reaction of mine waste with CH_3COOH, as the electrostatically bound micron sized U-V bearing minerals would already be lost during reaction with 10 mM $NaHCO_3$. In addition, the fitting parameter 'n_m', necessary to model the non-linear dissolution of U-V bearing mineral phase, was estimated to be 4.5 (SI equations 5, 8). Our PFLOTRAN simulations also estimated the reaction rate (I_m) of U-V bearing mineral phase to be negative suggesting dissolution of U-V bearing mineral phase. However, the reaction rate for metaschoepite and rutherfordine remained unchanged, suggesting minimal contribution from metaschoepite and rutherfordine in the reactive transport of U and V. Although, our experimental and model concentrations agree well with each other, the early release of lower experimental U and V concentrations can be attributed to 1) sample heterogeneity, 2) restricted access to incorporated U-V bearing mineral phases, and 3) precipitation of an unidentified U and V phase.

The difference in the reactive transport of U and V after reaction under circumneutral and acidic conditions could be attributed to the dissolution of different co-

existing U-V bearing mineral phases, possibly amorphous and crystalline, as identified in the unreacted mine waste. The co-existence of amorphous and crystalline U-V bearing minerals was identified through Selected Area Electron Diffraction (SAED) and Energy Dispersive Spectroscopy (EDS) analyses performed using a High Resolution-Transmission Electron Microscopy (HR-TEM) (Figure 3.4). For instance, Figure 3.4A, D represents the Back Scatter Electron image (BSE) of two nanoparticulate grains that were identified as uranyl vanadates co-occurring with other minerals based on the EDS elemental composition spectrum in Figure 3.4B, E. Diffused rings in the SAED pattern (Figure 3.4C) suggested the identified U-V bearing mineral phase in figure 3.4A to be amorphous. However, unlike Figure 3.4C, definite patterns in Figure 3.4F suggested the presence of crystalline U-V bearing mineral that co-occurs with other crystalline mineral phases within a particular grain of the mine waste sample. This co-existence of crystalline and amorphous U-V bearing minerals in unreacted mine waste samples can be a result of nucleation[155, 156] or 2) polymorphism[157], which are common in natural samples due to their heterogeneity in site and reactivity conditions. These results agree with observations made in other studies that have shown that crystallinity can affect the solubility of mineral phases.[114, 115] Future work will focus on identifying the crystalline chemistry of these U-V bearing minerals to better understand the factors affecting the reactive transport of U and V from Blue Gap/Tachee.

It is possible that other secondary mineral phases like uranium-bearing oxides, hydrous ferric oxides, and uranium phosphates that have not been considered in the reactive transport model but are soluble at acidic pH can also affect the reactive transport of U and V.[148, 158-159] For instance, analyses conducted using and synchrotron-based micro

XRF mapping on the mine waste sample indicate that U co-occurs with other elements (Appendix A: Figure 7.7). Despite the chemical complexity of these samples, our reactive transport model can reasonably represent the release of U and V by considering the dissolution of U-V bearing minerals as the key contributing process. However, we acknowledge that contributions from other mineral phases, heterogeneity, and other aqueous processes were not accounted in the reactive transport for U and V, which represent a limitation of this study. Therefore, future research should focus on trying to understand the role of other reaction processes such as the contribution of other secondary mineral/nanoparticulate phases of U and V and the influence of mineral structure of the U-V bearing minerals on the reactive transport U and V from such mine waste sites.

Environmental Implications.

This work integrates reactive transport modeling, electron microscopy, and aqueous chemistry methods to evaluate the mechanisms affecting the transport of U and V from mine wastes from a site in northeastern Arizona. One outcome from this investigation includes the determination of solubility and reaction rate constants for the dissolution of U-V bearing mineral phases at circumneutral and acidic pH that can serve as a foundation to better understand their reactivity at relevant field conditions. This information can be useful to better understand the mobility of U and V in neighboring community water sources to assess risks for human exposure. Additionally, the identification of factors affecting the dissolution of U-V bearing minerals under environmentally relevant conditions evaluated in this study is relevant to inform remediation and resource recovery

initiatives in sites where these U-V bearing minerals are abundant. For instance, the results from this study have implications for other abandoned uranium mines in the Colorado Plateau, South Dakota (Black Hills), southwest China, southern Jordan, Korea, and the calcreted drainages of arid and semiarid western and southern Australia where carnotite ($K_2(UO_2)_2(VO_4)_2 \cdot 3H_2O$), tyuyamunite ($Ca(UO_2)_2V_2O_8 \cdot (5\text{-}8)H_2O$), and other U-V bearing minerals are commonly found.[41-48]

Spectroscopy and microscopy analyses suggest that U is associated to different elements, which is indicative of the complex mineralogy of these solids. These results are consistent with those reported in the previous study from our research group.[1] Despite the chemical and mineralogical complexity of these mine wastes, dissolution of U-V bearing minerals was identified as the key mechanism controlling the reactive transport of U and V under the environmentally relevant conditions selected for this study. In addition, the integrated methodology used for this study is transferable to other mining and milling sites and to abandoned U mine waste sites where a better understanding of the reactive transport of U and its co-occurring elements is necessary.

Table 3.1 Parameters of U-V bearing minerals estimated by modelling the reactive transport of U and V during mine waste reaction at circumneutral and acidic pH. The surface area of U-V bearing minerals was estimated using the average U-V bearing mineral diameter (Appendix A: Table 7.2) and equation [13]. The effective reaction rate constant (keffective = k*a_m^0) accounts for the effect of grain surface area on the reactive transport of U and V, where k is the reaction rate constant and a_m^0 is the surface are of U-V bearing minerals.

Experiments	**Equilibrium constant (K_{eq})**	**Average U-V bearing mineral surface area(a_m^0) (cm^2 cm^{-3})**	**Reaction rate constants (k_m) (mol cm^{-2}-sec^{-1})**	**Effective reaction rate constant ($k_{effective}$ = (k_m*a_m^0) (mol cm^{-3}-sec^{-1})**
Batch circumneutral (pH 8.3)(<63 µm)	$10^{-44.811}$	468.8	$2.13x10^{-14}$	$9.99x10^{-12}$
Batch acidic (pH 3.8)(<63 µm)	$10^{-38.651}$	468.8	$6.4x10^{-14}$	$3x10^{-11}$
Column circumneutral (pH 7.9) (120-355 µm)	$10^{-44.811}$	62.5	$4.8x10^{-13}$	$3x10^{-11}$
Column acidic (pH 3.4) (120-355 µm)	$10^{-38.651}$	62.5	$3.2x10^{-13}$	$2x10^{-11}$

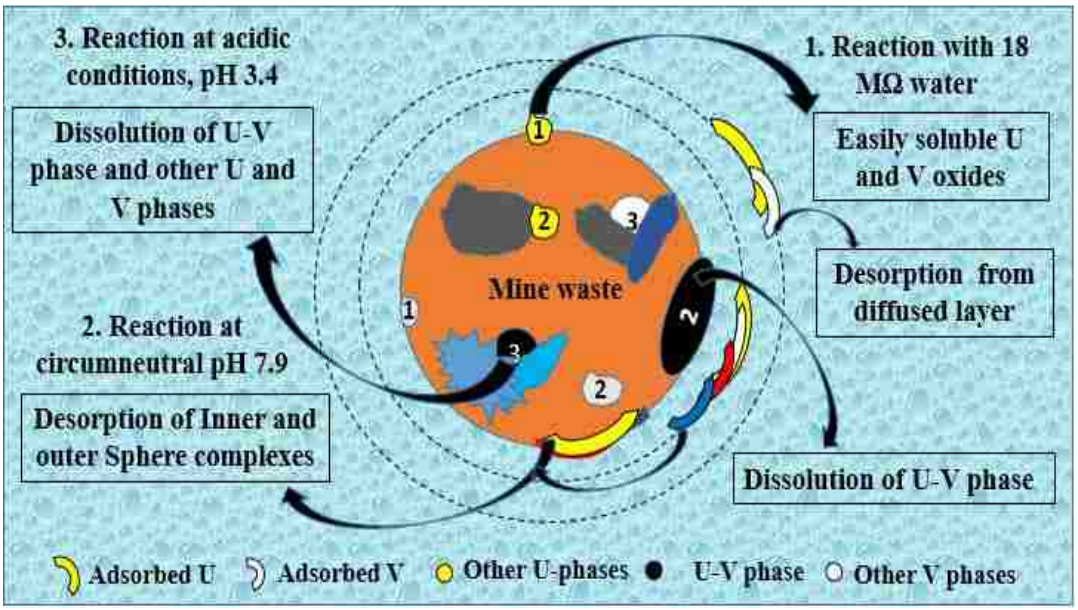

Figure 3.1 TOC art: Conceptual model indicating the geochemical processes acting in various experiments conducted in this chapter.

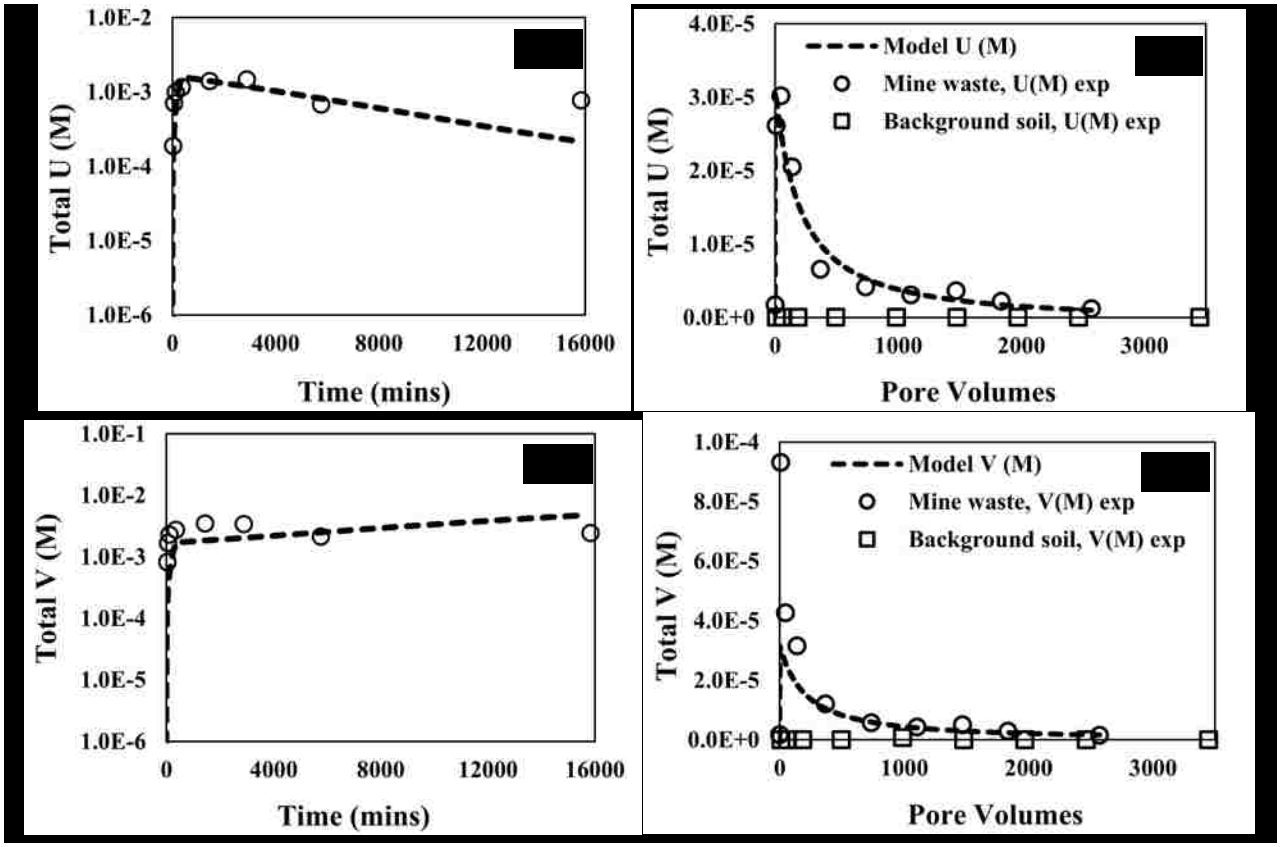

Figure 3.2 Measured effluent concentrations and reactive transport model (PFLOTRAN) of U and V, from mine waste (circle) and background soil (squares) during batch and continuous flow-through column experiments at circumneutral pH (using 10 mM $NaHCO_3$). **A)** U concentrations from batch experiments versus time; **B)** V concentration from batch experiments versus time; **C)** U concentrations from column experiments versus pore volumes; **D)** V concentration from column experiments versus pore volumes. The curve fitting resulting from the reactive transport model are presented with dashed lines.

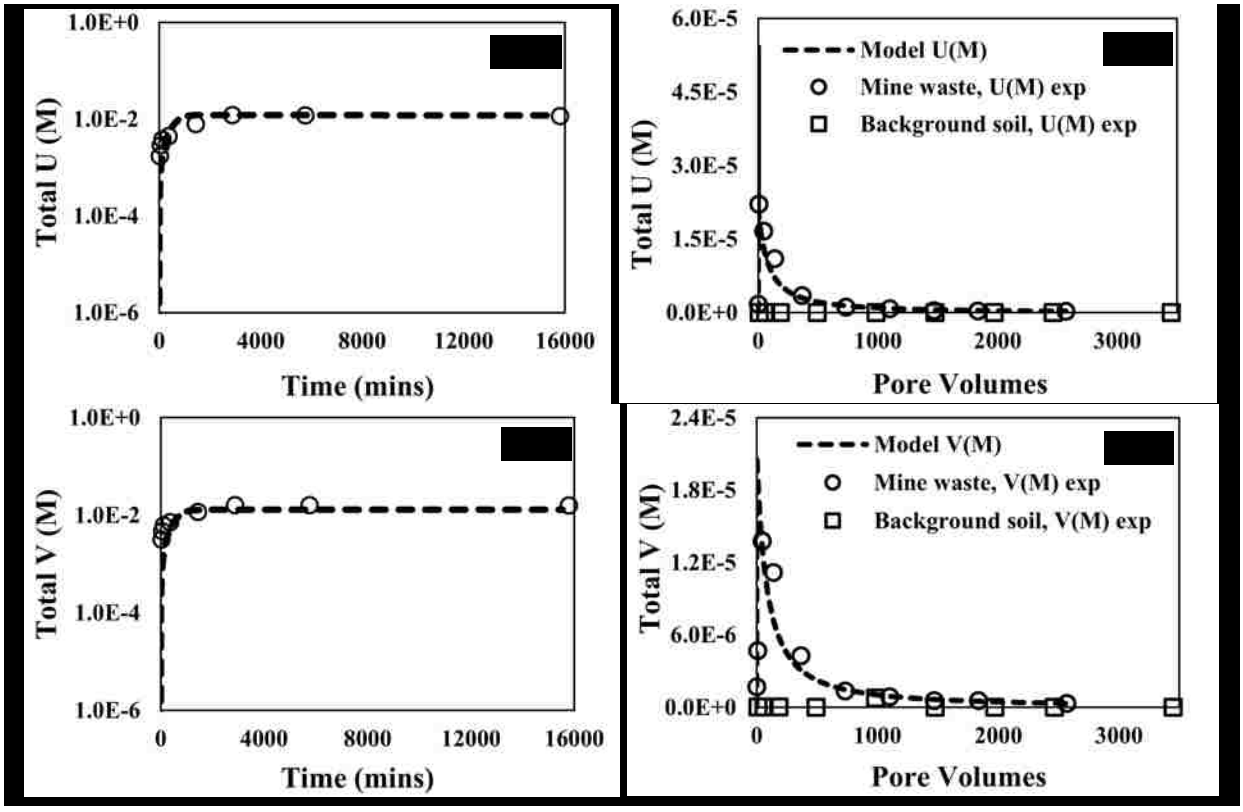

Figure 3.3 Measured effluent concentrations and reactive transport model (PFLOTRAN) of U and V, from mine waste (circle) and background soil (squares) during batch and continuous flow-through column experiments at acidic pH (using 10 mM $C_6H_8O_6$ and CH_3COOH). **A)** U concentrations from batch experiments versus time; **B)** V concentration from batch experiments versus time; **C)** U concentrations from column experiments versus pore volumes; **D)** V concentration from column experiments versus pore volumes. The curve fittings resulting from the reactive transport model are presented with dashed lines.

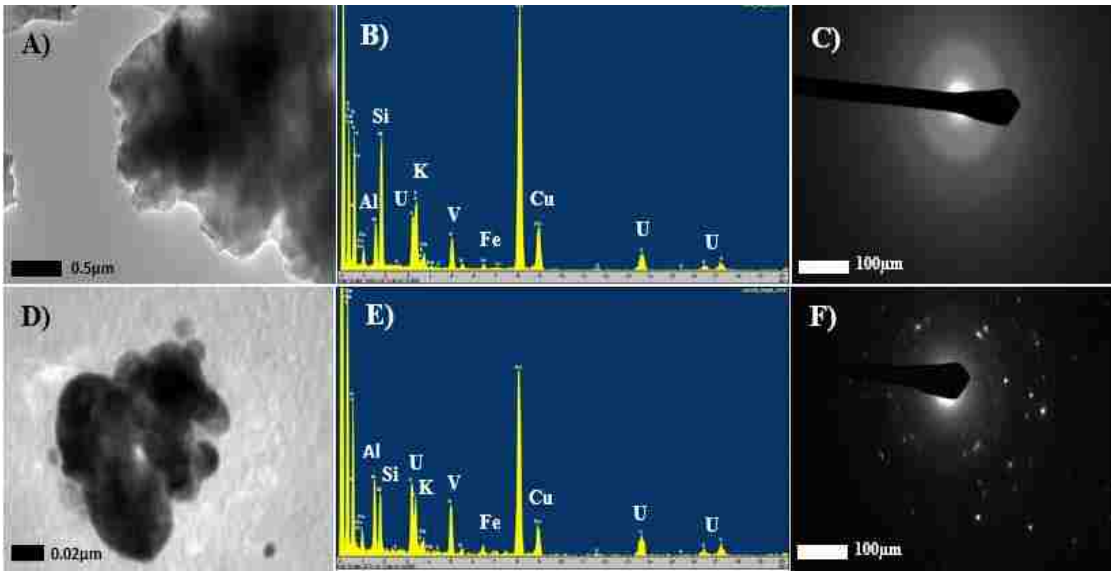

Figure 3.4 Transmission electron microscopy (TEM) images, Energy Dispersive Spectroscopy (EDS) spectra and Selected Area Electron Diffraction (SAED) patterns for unreacted mine waste samples indicating the co-occurrence of amorphous and crystalline U-V bearing minerals. **A, D)** TEM images of U-V bearing mineral phases. **B, E)** EDS spectra identifying the presence of U-V bearing minerals. **C, F)** SAED patterns confirming the co-occurrence of amorphous and crystalline U-V bearing mineral phase.

[redacted]

(To be submitted to *American Mineralogist Journal*)

Sumant Avasarala[1], Michael Spilde[2], Adrian Brearley[2], Eric Peterson[3], Ying Bing Jiang[2,4], and José M. Cerrato[1]

*Corresponding email address: savasarala87@unm.edu,

Telephone: (001) (248) 978-8264

Fax: (001) (505) 277-1918

[1] Department of Civil Engineering, MSC01 1070, Center for Water and the Environment, University of New Mexico, Albuquerque, New Mexico 87131, USA.

[2] Department of Earth and Planetary Sciences, MSC03 2040, University of New Mexico, Albuquerque, New Mexico 87131, USA.

[3]Department of Chemical and Biological Engineering and Center for Micro-Engineered Materials, University of New Mexico, MSC 01 1120, Albuquerque, New Mexico 87131, USA.

[4] Center for Micro-Engineered Materials University of New Mexico, Albuquerque, New Mexico, 87131, USA

[redacted] **Abstract**

The objective of this chapter is to determine the crystal chemistry of uranyl vanadate minerals that naturally occur on ore samples from the Blue Gap/Tachee Claim-28 mine in Northeastern, AZ. Previous investigations on these uranyl vanadate rich ores identified dissolution of uranyl vanadate as the key mechanism affecting reactive transport of U and V. However, the specific crystal chemistry of these naturally occurring uranyl vanadate mineral is unknown. Therefore, to address this research gap we conducted various

spectroscopy, electron microscopy and diffraction analyses on solid chunks of the Blue Gap/Tachee ore samples. Most diffraction lines in the X-ray diffractogram of the uranyl vanadate are in agreement with those of synthetic carnotite data from the literature. Carbon detected by electron microprobe analyses in the uranyl vanadate was found to occur as organic carbon inclusions as suggested by the bright-field transmission electron microscopy (BF-TEM) imaging, energy-filter transmission electron microscopy (EFTEM), and electron energy loss spectroscopy (EELS). Therefore, after excluding carbon (C) from the quantitative electron microprobe analysis, we found that the elemental composition of the uranyl vanadate was 4.45% K_2O, 0.53% CaO, 62.72% UO_2, 0.04% Na_2O, 20.65% V_2O_5, 0.56 Fe_2O_3, 0.09% TiO_2, and 8.65 H_2O at a K:U:V ratio of 1:2:2.1 with an empirical formula of $(K_{0.87}, Na_{0.012}, Ca_{0.088})((Ti_{0.005}, U_{0.99})O_2)_2((Fe_{0.033}, V_{1.05})O_4)$. This empirical stoichiometry is similar to that of the anhydrous carnotite. The d-spacing information of the uranyl vanadate was estimated using the electron diffraction capability in a transmission electron microscope (TEM) that indicated: 1) complete amorphization of uranyl vanadates on short-term exposure to the electron beam (<120s); and 2) minor differences between measured d-spacings of uranyl vanadates and calculated d-spacing of anhydrous carnotite. Minor discrepancies in d-spacing may be attributable to differences in their degree of hydration. Results from this investigation provide an improved understanding on the crystal chemistry of a naturally-occurring uranyl vanadate in abandoned mine wastes. Naturally-occurring carnotites form an important ore mineral in many uranium mines. Characterizing such naturally-occurring uranyl vanadates is also crucial to better understand and predict the long term transport of U in abandoned mine waste sites.

Keywords: Spectroscopy, electron microscopy, Diffraction, uranyl vanadate, Electron energy loss, d-spacing, and stoichiometry

Introduction

Uranium (U) mining operations during the 1900s resulted in the formation of thousands of abandoned uranium mines in the United States. Approximately, 10,000 abandoned U mine waste sites have been identified in the western United States, of which more than 1,000 are located on the Navajo Nation [1, 8-9]. For decades, abandoned mine waste sites located in Native American communities have been overlooked due to the remoteness of the sites, the low population densities, and the social isolation of the population. The Blue Gap/Tachee Claim 28 mine waste site in northeastern Arizona is a good example; it was abandoned after the mining operations were ceased during the 1960s. Discontinuation of the mining operations resulted in mine wastes that were abandoned and, hence, unregulated despite their high U concentrations. In addition to mine wastes, mill tailings were also generated after processing for U[1, 10]. These mill tailings were federally regulated, low concentration wastes.

Uranyl vanadate minerals are abundant and important constituents of many uranium deposits. Uranium and vanadium (V) co-occur as primary U-bearing ore minerals including carnotite ($K_2(UO_2)_2(VO_4)_2 \cdot 3H_2O$), tyuyamunite ($Ca(UO_2)_2V_2O_8 \cdot (5\text{-}8)H_2O$), and other uranyl vanadate. These elements have been reported in abandoned uranium mines of southwestern U.S., South Dakota, southwest China, southern Jordan, Korea, and Australia.[41-48, 127] Recently, we reported the occurrence of uranyl vanadate in abandoned mine wastes from Blue Gap/Tachee Claim-28 site [1]. We also observed that the dissolution of uranyl vanadates was the key mechanism affecting the reactive transport of

U and V from mine wastes at this site[98]. The solubility properties of the main uranyl vanadate in this mine waste sample is similar to that of carnotite [98, 150]. Although some information on the reactivity of uranyl vanadate occurring in the mine waste is available in literature, there is limited information on their occurrence, composition, structure, and crystallinity, which are crucial to better understand the reactive transport of U and V in mine waste materials.

The general formula, $M^{n+}_{1/n}UO_2AO_4.xH_2O$, can be used to represent the stoichiometry of several uranyl vanadates, where M is a cation that can be either mono-, di-, or tri-valent elements of groups I and II in the periodic table and 'A' can be P, As, S or V [93, 116-119]. For example, Krivovichev and Plasil (2013) identified 13 uranyl vanadates that, according to Francevillite anion topology, were comprised of $[(UO_2)_2(V_2O_8)]^{2-}$ sheets and mono, di-, or tri-valent cations[120-121]. Quantification of these interlayer cations (between $[(UO_2)_2V_2O_8]_n^{-2n}$ layers) and water [117] can be challenging due to water loss and interlayer cation migration[160-161]. In addition to uranyl vanadates, a similar arrangement with interlayer occupancy is observed in uranyl phosphates, specifically in the meta-autunite group of minerals.[116, 161-168] Furthermore, most uranyl vanadates consist of V_2O_8 groups that are connected to UO_7 pentagonal bipyramids by a shared edge; but these groups differ in hydration capacity, stoichiometry, bond distance, and bond angles.[116, 162-163, 169] For instance, K-carnotites are anhydrous at ambient atmospheric conditions; on the other hand, Na-carnotite can remain hydrated with up to six water molecules [116, 162] under the same conditions. Differences in hydration capacity and interlayer occupancy of cations between such uranyl vanadates cause changes in structural arrangements and bond distances that, in turn, affect the thermodynamic

stability and crystal chemistry of these minerals [161, 170]. However, similarity in their crystal symmetry (monoclinic) and space group ($P2_1/c$) explains the overlap in their X-ray diffraction (XRD) patterns [162-163]. Raman spectroscopy analysis on various uranyl vanadate minerals (carnotite, curienite [$Pb(UO_2)_2V_2O_8 \cdot 5(H_2O)$], Francevillite [$(Ba,Pb)(UO_2)_2V_2O_8 \cdot 5(H_2O)$], tyuyamunite [$Ca(UO_2)_2V_2O_8 \cdot (5\text{-}8)H_2O$]) showed intense peaks at 800 - 824 cm^{-1} and 965 - 985 cm^{-1}, which can be attributed to UO_2^{2+} and V_2O_8 units, respectively [171]. Uranyl vanadates can also occur in different packing arrangements, such as nano clusters of U-V oxide where the $\{U_2V_{16}\}$ nano-clusters are comprised of two uranyl pentagonal bipyramids and 16 distorted vanadate square pyramids, 14 of which share edges to form a two polyhedral-wide rigid ring [172]. Therefore, these studies indicate that the crystal chemistry of synthetic uranyl vanadates has been widely explored. However, this information may not be directly applicable to natural uranyl vanadate found in environmental samples.

Studying uranyl vanadate in environmental samples can be complex and challenging given that these minerals: 1) may not occur as pure phases but as complex solid solutions; 2) can occur in more than one form of uranyl vanadate or other U minerals; 3) may show varying degrees of crystallinity from amorphous to fully-ordered crystalline materials, and 4) can also be extremely fine-grained minerals that have intergrown with other phases with variable degree of hydration. In addition, studying uranyl vanadates in mine waste samples can be formidable considering their occurrence in concentrations that are below the detection limit of many bulk characterization techniques [173]. Structural incorporation of ions or elements of similar charges can make identification of such U-phases difficult using powder XRD techniques [174]. Therefore,

these incorporations must be studied using other bond and unit cell scale-characterization techniques like Extended X-ray Fine Structure (EXAFS) [173], transmission electron microscopy (TEM), or single crystal XRD to identify the U-phase and its crystal chemistry. Despite the availability of such advanced analytical techniques, limited attempts have been made to identify and understand of the crystal chemistry of naturally-occurring uranyl vanadates that occur in most U mines of southwestern US (Colorado, Utah, Arizona and New Mexico).[39, 127]

Therefore, this study seeks to determine the crystal chemistry and microstructures of uranyl vanadate that occur naturally in mine wastes from Blue Gap/Tachee Claim-28 site in Northeastern, AZ, using spectroscopy, electron microscopy, and X-ray diffraction. A secondary objective of this work is to clarify the association of carbon with uranyl vanadate. This investigation uses essential insights from chemistry, morphology, and presence of inclusions, which are fundamental to understanding material behavior when subjected to weathering processes. Knowledge from this study can shed light on the fate and transport of U and V under environmentally relevant conditions in mine wastes and other mine sites where uranyl vanadate are abundant.

Materials and Methods

Mine waste samples were collected in November, 2015, from Claim-28 mine, an abandoned U mine waste site in Blue Gap/Tachee Chapter in northeastern Arizona. The solid waste samples were collected from the surface within a 0.2 km radius from the erosion channel, a location similar to that reported in Blake et al. (2015)[1]. Spectroscopic assessment of these mine waste samples in Blake et al. (2015) suggested that U is present

at concentrations less than 1% weight of the total sample. [1] Mine wastes samples used in this investigation were present as rocks emitting very high gamma radiations (>10mRad) almost as high as ore samples. These radiation measurements were made using a Ludlum Model 19 MicroR Geiger counter. Fragments from these mine waste rock samples were used for various spectroscopic, microscopic, and diffractions analyses throughout this study.

Uranium ores in the Blue Gap/Tachee region occur in tabular and lenticular sandstone units of the Rough Rock Sandstone member in the Toreva formation. This arkosic sandstone is a much younger deposit formed by a less extensive transgression of the cretaceous sea in the northern Black Mesa that forms the uppermost unit of the Torreva formation [40]. The major mineralogical components of these deposits include quartz, potassium feldspar, clays, and uranyl vanadates[1, 39-40].

[redacted]

Small fragments of the mine waste rock samples were embedded in epoxy; the surface was ground flat and polished using successive grits of silicon carbide and alumina to a surface smoothness of 0.05µm, suitable for electron microprobe analyses. Samples and standards were coated with approximately 150 nm of gold rather than carbon in order to measure carbon quantitatively. Scanning electron microscopy (SEM) imaging was also conducted on the surface of the epoxy embedded mine waste fragments to register the physical characteristics of the uranyl vanadates in the mine wastes.

X-ray quantitative mapping analyses were acquired on a JEOL 8200 electron microprobe equipped with five wavelength spectrometers; automation of the microprobe

and data reduction was carried out using Probe for EPMA(TM) (Probe Software, Inc.). Operating conditions were 15 kV accelerating voltage, 10 nA beam current, and a beam diameter of 5-10 µm. Natural mineral standards were used for calibration. Kaersutite and hematite from the Harvard Mineralogical Museum[175] were used for O, Na, Al, K, Ca, Ti, and Fe; dolomite and olivine mineral standards from the Smithsonian Institution[176] were used for C, Mg and Si; SRM 663 Cr-V steel for V; and a natural sample of uraninite for U. Counting times were 60 seconds on peak for C and O, 40 seconds for V, and 20 for all other elements; total background counting times were the same as on-peak times. Interference corrections were applied to V by Ti, to C for interference by U, and O for interference by V[177]. A blank correction was utilized for Au N5-N6 overlap with C[178]. Area Peak Factors[179] were utilized to correct x-ray intensities of C for wavelength peak shift and shape changes. The resulting detection limit for C was 0.016 wt%.

[redacted]

Mine waste collected from Blue Gap/Tachee Claim-28 site was analyzed using a Rigaku SmartLab powder X-ray diffractometer. The Rigaku SmartLab XRD is fitted with a Cu K_α X-ray source with 1D silicon strip detector (D/teX™) and a Ni filter Bragg Brentano geometry with a 2/3° incident slit. Mineral phases were identified using Rietveld refinements that were performed using the Jade™ (MDI) software package. Because of the beam divergence resulting from the 2/3° S6 incident slit, beam spillover during data collection occurred at angles below 20˚ 2θ and caused clay fractions to be somewhat underestimated. The analysis was conducted on a mine waste rock sample that was prepared by grounding together some of its smaller fragments using an alumina

mortar/pestle. The ground sample was processed through three different sample preparation techniques to concentrate the nano-crystalline uranyl vanadate for improved diffractograms. The first pattern was collected on randomly oriented mine waste powder sample prepared using standard procedures. The second pattern was measured on the suspended fraction of the ground powder, which was obtained by mixing the powder with deionized water and allowing the solution to settle overnight[180]. However, due to a preferred orientation of this sample, the analysis was repeated using a more randomly oriented suspended fraction that was obtained by reducing the settling time to <30s.

[redacted]

We prepared an ultrathin section of the uranyl vanadate for transmission electron microscope (TEM) analysis using the focused ion beam (FIB) in situ lift out technique described in Abreu et al., 2010.[181] The FIB samples was prepared using a FEI Quanta 3D Dualbeam® FEGSEM/FIB instrument equipped with an EDAX Apollo 40 SDD EDS system. A Ga ion beam voltage of 30 kV and beam currents ranging from 3 nA to 10 pA were used to perform sample extraction and final ion milling. During the sample preparation, a protective layer of Pt, 2 µm in thickness was deposited on the surface of the sample prior to minimize ion beam damage. After the initial cutting stage, the FIB section was lifted out using an Omniprobe 200 micromanipulator and transferred onto a Cu TEM half grid for ion milling to a final thickness of about 100 nm.

[redacted]

The TEM analysis was conducted on the FIB section and handpicked grains of the uranyl vanadate from the mine waste to reveal the microstructure and composition at the submicron scale. The handpicked uranyl vanadate (yellow) grains were taken from

minute fragments of the mine waste rock sample and gently disaggregated under acetone using an agate pestle and mortar. A droplet of the disaggregated sample suspension in acetone was deposited on a holey carbon TEM grid and allowed to dry prior to TEM analysis. Both types of sample uranyl vanadate were studied using Bright-Field TEM imaging (BFTEM), Selected Area Electron Diffraction (SAED) and Energy Dispersive Spectroscopy (EDS) using a high JEOL 2010F Field Emission Gun scanning transmission electron microscope **(**STEM) (FEG/STEM) instrument. This instrument is equipped with a GATAN GIF 2000 and an Oxford AZTec EDS system with an ultrathin window $XMax^N$ 80 mm^2 SDD EDS detector. In addition, the FIB section was also studied using High-Angle Annular Dark-Field Scanning Transmission Electron Microscopy (HAADF STEM), full spectral STEM X-ray mapping, Energy Filtered TEM imaging (EFTEM), and Electron Energy Loss Spectroscopy (EELS). The JEOL 2010F was operated at 200 kV for all analyses except for EFTEM imaging, which was performed at197 kV. The EELS analysis was operated at an accelerating voltage of 200 kV and energy resolution of 0.7ev.

Results and Discussion

Diffraction analysis on the Blue Gap/Tachee Claim-28 mine waste samples identified most diffraction peaks of the uranyl vanadate to agree with that of the carnotite reported in literature. However, due to <1% weight of U in the mine waste samples as reported in a previous study by our research group [1], the occurrence of uranyl vanadate could not be detected in the diffractogram of the powdered mine waste (Figure 4.1, green). The absence of identifiable diffraction peaks for uranyl vanadate could also be attributable to

the fact that some of these phases could be amorphous, based on observations made in another recent investigation by our research group.[98] In addition, the diffractogram is dominated by peaks from minerals such as quartz, kaolinite, and microcline that are abundant in the host rocks as previously reported at this site [1]. Therefore, we tried to concentrate the uranyl vanadates in the mine wastes following the procedure described in the methods section and analyze them for their diffraction patterns. The diffractogram obtained by Method 2 (overnight settling time) showed preferential orientation, where only the peaks of a certain orientation for uranyl vanadates in the sample matched with those of anhydrous carnotite [$K_2(UO_2)_2V_2O_8$] reported in the literature.[116] This result suggests that the uranyl vanadate in the mine waste has a structure similar to that of carnotite. In addition, the diffractogram also suggested the presence of fernandinite [$CaV_8O_{20}\bullet 4H_2O$] and lanthanite [$(REE)_2(CO_3)_3(H_2O)_8$] (Figure 4.1, blue). To overcome the preferential orientation issue and acquire a randomly oriented sample, we prepared another sample using Method 3. Diffraction results on this randomly oriented sample (Figure 4.1, red) showed many uranyl vanadate peaks in agreement with those of carnotite, unlike observations made in samples prepared using Method 2. Additional confirmation on the presence of lanthanite [$REE_2(CO_3)_3(H_2O)_8$] and fernandinite [$CaV_8O_{20}\bullet 4H_2O$] was also acquired on samples prepared using method 3. Although these results suggest that the uranyl vanadate in the mine waste sample is carnotite, there are some differences between the natural-occurring and synthetic materials. Therefore, more research using electron microscopy was conducted to better understand the crystal chemistry of the uranyl vanadate.

[redacted]

The electron microprobe X-ray mapping analysis of a U-bearing ore grain in the mine waste samples shows that U is commonly associated with V, potassium (K), calcium (Ca), and, to a lesser extent, O (Figure 4.2). The distribution of these elements is variable within this grain, but there are clear regions such as that in the upper half of the ore grain that shows a strong spatial correlation among U, V, K, and oxygen (O). This correlation qualitatively suggests that the naturally occurring uranyl vanadate has a composition that is consistent with that of carnotite, as indicated by the XRD analyses. However, the lower half shows lower K and V contents, but higher Ca, suggesting that an additional U–bearing phase such as tyuyamunite may be intergrown with carnotite. The apparent low concentrations of O in the U-bearing phases based on the O X-ray map (Figure 4.2E) are due to the elevated concentrations of O in the surrounding quartz grains. In addition, a V-rich phase with low U contents is present, is associated with the U-rich phase, and is a fibrous V-Fe phase that appears darker gray in the backscattered electron images. This phase has been discussed by Avasarala et al. 2017 [98]. The two types of uranyl vanadate (carnotite and tyuyamunite) identified in the ore grain appear to be intergrown and precipitated as secondary mineral on the surface of a V-Fe phase.

Back-scattered electron imaging showed that the uranyl vanadate mineral in the mine waste contains numerous submicron, low Z inclusions distributed homogeneously throughout individual grains. These grains are aligned parallel to the elongation direction of the grains, and the grains ranged in size from 100 to 200 nm. Qualitative EDS analysis showed that these inclusions were rich in carbon. Back Scatter Electron (BSE) image and

Energy Dispersive Spectroscopy (EDS) identified uranyl vanadate to co-occur with C that could be included in the uranyl vanadate structure (Figure 4.3). The white areas in the secondary electron image (Figure 4.3A) were identified as uranyl vanadate based on an EDS analysis conducted on them (Figure 4.3B). However, a C map was not added in figure 4.2, as it was difficult to discriminate the C in the uranyl vanadate from the C in the epoxy.

Quantitative microprobe analysis of the identified uranyl vanadate was conducted on several different regions of the polished section of the epoxy embedded mine waste sample. Carbon was included in the analytical setup based on the fact that the EDS spectra indicated that C was present. However, as discussed in later subsection, TEM analyses show that this C is actually present in submicron inclusions that were disseminated throughout the uranyl vanadate grains. Ignoring the included carbon from the quantitative microprobe analysis (4.8% C as elemental carbon), the elemental composition of uranyl vanadate was 4.45 wt% K_2O, 0.53 wt% CaO, 62.72 wt% UO_2, 0.04 wt% Na_2O, 20.65 wt% V_2O_5, 0.56 Fe_2O_3, and 0.09 wt% TiO_2 at a K:U:V atomic ratio of 1:2:2.1 (Table 4.1). These concentrations were similar to that of carnotite $[K_2(UO_2)_2(V_2O_8)\cdot 1{-}3H_2O]$ reported by Anthony (2000), which had a reported composition of 10wt%% K_2O, 0.66% CaO, 62.26% UO_3, 0.16% Na_2O, 20.57% V_2O_5, 0.55 Fe_3O_3, and 4.90 H_2O (total 99.1%).[182] However, analytical tools consistently estimated less than 100 wt% (91.35%), which was due to the presence of H_2O. Therefore, the percentage of water in uranyl vanadates was theoretically estimated to be 8.65%, after subtracting total estimated weight 91.35% from 100%. Our EPMA analysis had lower K and H_2O concentrations because we excluded the C in the analysis, which was clearly not

present within the carnotite itself. The major discrepancy between our data and the literature and theoretical compositions is the much lower K_2O content. We attribute the low K_2O content to migration of K from within the electron beam excitation volume despite using a broad beam of 10-15 µm for the analyses[161, 183]. Stubbs et al. (2010) documented the analytical challenges of determining the compositions of copper (Cu)-bearing uranyl phosphates using electron microprobe. Copper, as an interstitial cation, was highly mobile in these analyses. We can reasonably expect that K is even more mobile, based on its well documented mobility during EPMA analyses of feldspars and alkali-bearing glasses.[184-185] The calculated empirical formula of the uranyl vanadate phase is $(K_{0.87}, Na_{0.012}, Ca_{0.088})((Ti_{0.005}, U_{0.99})O_2)_2((Fe_{0.033}, V_{1.05})O_4)_2{\cdot}2H_2O$, which can be simplified to $K(UO_2)_2(VO_4)_2{\cdot}\ 9H_2O$.

[redacted]

We used TEM and STEM analyses to investigate the crystal structure and microstructures of the U-V-bearing phase in the mine waste. We also extracted a FIB section from a region of the U-V phase that contained the low-Z inclusions. Bright-field TEM and electron diffraction analyses were performed on the samples prior to STEM imaging and STEM X-ray mapping. The BF-TEM imaging showed that the uranyl vanadate consisted of crystalline, elongated, platy grains between 1-5 µm in size with a significant intergranular porosity. The grains often had their elongation direction parallel to subparallel. The STEM X-ray mapping showed that U, V, K, and O were homogeneously distributed throughout the individual uranyl vanadate grains in the Blue Gap/Tachee mine waste (Figure 4.4). There was no evidence of intergrowths of any phase with a different

composition with the exception of carbon-rich inclusions, which are discussed below. The uranyl vanadate grains showed no evidence of compositional zoning or for the presence of tyuyamunite in this thin section.

Dark-field STEM and EFTEM imaging were used to characterize the occurrence of C within the uranyl vanadate phase. In DF-STEM images (Fig 5a), distinct, submicron grains were distributed throughout individual grains. They ranged in morphology from sub-rounded to elongate grains that ran parallel to the elongation direction of the uranyl vanadate grains. Their sizes ranged from 20 nm to 50 nm for the largest elongate grains. The EFTEM imaging using the C edge at 284 eV showed that the grains were C-rich: no other elements were detected within these inclusions. A complicating issue with this analysis was that abundant epoxy was present in the interstitial space between the uranyl vanadate grains. We, therefore, restricted our analyses to those morphological regions that was clearly included within individual uranyl vanadate grains and not due to the epoxy impregnation at interstitial spaces. The EFTEM image shown in Figure 4.5 is an example grain of a grain which was on the edge of a uranyl vanadate grain in a region that was thin enough for conducting EFTEM analysis.

We performed Electron Energy Loss Spectroscopy (EELS) analyses on several of these C-rich inclusions to determine their characteristics in the uranyl vanadates that naturally occur in Blue Gap/Tachee mine wastes. Figure 4.6A shows a DF-STEM image of C-bearing inclusions in the region of the uranyl vanadate where the EELS analysis was conducted. An example of a specific inclusion that was analyzed is indicated in Figure 4.6B. The EELS spectrum from this inclusion showed the presence of a broad peak characteristic of σ* bonding with no evidence of a pre-edge π* bond signal at the C-edge.

These features of the C edge are consistent with amorphous carbon. The analysis was complicated by the fact that the C K-edge at 284eV is overlapped by the potassium L edge, which occurs at an energy of 294 eV (Figure 4.6C). Although the electron beam was focused on the inclusion, to avoid beam damage we defocused the electron beam and overlapped it with the uranyl vanadate, resulting in a contribution from K in the host uranyl vanadate in the EELS spectrum. In EELS spectra of amorphous and graphitic carbons, an increase in the π^*/σ^* ratio (i.e. more π^* bonding), occurred with increasing degree of graphitic character [186] as the transition from amorphous C to graphitized C (turbostratic or poorly-graphitized carbon) and then to crystalline graphite. The strong sp^2 bonding in graphite is indicated in EELS spectra by a distinct, sharp σ^* peak [187], whereas amorphous C, which did not contain sp2 bonding, did not show the σ^*. We concluded that 1) the broad and featureless shape of the σ^* peak and 2) the small π^*/σ^* ratio showed that the inclusion in the uranyl vanadate was amorphous C (Figure 4.6C). The presence of amorphous C could be due to organic matter from carbonaceous plant material that was found to co-occur with U in these deposits [39]. For example, we also conducted the EELS analysis on the epoxy (Figure 4.6A), that showed a high resolution EELS spectrum of the C-edge with distinct σ^* bond. This observation indicates that the inclusion was not epoxy but was indigenous to the uranyl vanadate. Several EELS spectra were also conducted on regions of the uranyl vanadate away from any obvious carbon inclusions (Figure 4.6E). These spectra showed no evidence of a C-edge; thus, the C detected in the electron microprobe analyses is present in carbonaceous inclusions and was not incorporated into the structure of the uranyl vanadate in the mine waste.

To supplement the powder XRD data, which suggest that carnotite is the uranyl vanadate mineral in the mine waste, we carried out TEM studies on grain mounts of the fine-grained fraction from the mine waste. Specifically, we focused on obtaining electron diffraction data from single crystal to confirm the identification of carnotite. Bright field TEM imaging (Figure 4.7A-C) detected that the uranyl vanadate occurred in the TEM grain mount as clusters of submicron crystals (Figure 4.7A-C). Several different clusters were examined in order to determine if there was any variability in the characteristics of the clusters. Morphologically, the crystals appeared to be platy, frequently lying on top of one another and to have subhedral shapes with weakly developed facets, and grain sizes that range from <0.2 μm to ~ 1 μm. Electron diffraction studies of individual clusters indicated that the uranyl vanadate was indeed crystalline but that it rapidly amorphized during electron beam exposure. In order to obtain images and electron diffraction patterns of the sample, the grains were located on the TEM sample grid at extremely low electron fluxes with a highly defocused electron beam giving very low illumination. After location of a grain cluster, an electron diffraction pattern was obtained immediately at the same low level of electron irradiation. This diffraction resulted in ring patterns. However, due to the limited number of crystals within the diffraction aperture, the rings were incomplete but well defined. To avoid excessive exposure of the grains to the electron beam, EDS analysis of the study area was only carried out after collection of the electron diffraction data. A sequence of electron diffraction patterns was then obtained for several different clusters of crystals. The electron diffraction patterns were taken under the same conditions with only the time interval to collect and save the individual electron diffraction patterns (~20 secs) between each pattern (Figure 4.7D-G). The resulting

patterns showed the progressive amorphization of the sample, indicated by disappearance of diffraction maxima with high reciprocal lattice spacings and the development of diffuse electron diffraction intensity as rings within the patterns.

From the first diffraction pattern obtained from each sequence of patterns, lattice spacings were calculated for each of the diffraction rings (Table 4.2) and compared with the calculated *d*-spacing data for anhydrous carnotite using Single Crystal software. There is reasonable agreement between the measured data and the calculated data except for the highest *d*-spacings. In addition, a significant number of diffraction maxima were absent from the measured *d*-spacings compared to the calculated spacings. There are a number of possibilities for these discrepancies. The only crystal structure determination available for carnotite was for synthetic anhydrous carnotite reported by Sundberg and Sillen (1950)[188]. Anhydrous, synthetic carnotite is monoclinic with space group $P2_1/c$; however, the naturally occurring uranyl vanadate is hydrated and based on various studies of the Ca analog of carnotite, tyuyamunite, is likely to have variable states of hydration. Previous studies have shown that the progressive hydration of hydrated uranyl vanadates results in the expansion of interlayer spacing, changing the dimensions of the unit cell [161, 189]. Stern et al. (1956) showed that complete dehydration of tyunamunite results in the formation of metatyunamunite, a phase that Stern et al. (1956) suggested was structurally distinct from tyuyamunite based on X-ray diffraction data [189]. Donnay and Donnay (1954) determined the structure of tyuyamunite and found that it is orthorhombic with space group P*nan* when compared with a monoclinic structure for anhydrous carnotite [190]. The expansion of the unit cell due to variable degrees of hydration may account for the discrepancies between the calculated and measured values.

In addition, the absence of a number of diffraction maxima in the ring pattern of carnotite can reasonably be attributed to the fact that there is a preferential orientation of the clusters of particles of the TEM grid with the plates of carnotite lying with their (001) planes parallel to holey carbon film. These patterns only represent a small volume of reciprocal lattice space. Despite the discrepancies between the measured and calculated patterns, which may be attributable to differences in the degree of hydration, the data for the naturally-occurring uranyl vanadate in Blue Gap/Tachee mine waste appear to be consistent with carnotite. Importantly, the data show conclusively that the carnotite is crystalline but rapidly amorphizes under the electron beam.

Implications

Outcomes from this investigation suggest that the uranyl vanadate minerals in the Blue Gap/Tachee mine waste site were crystalline, elongated and platy grains (1-5 μm) of hydrated carnotites with significant intergranular porosity, rich in carbon inclusions (20-50 nm). These hydrated carnotites were susceptible to rapid amorphization on short-term exposure (<120s) to the electron beam, based on *d*-spacing information obtained using the electron diffraction capability in a TEM. This information on the crystal chemistry of naturally occurring uranyl vanadate is critical to improve our understanding on their solubility that contribute to an improved understanding on the transport of U and V from these mine wastes. For instance, results from this investigation are coherent with our previous observations at Blue Gap/Tachee Claim-28 mine waste site, where the solubility of this hydrated carnotite (equilibrium constant: K_{eq} at circumneutral pH = $10^{-38.65}$ and acidic pH K_{eq} = $10^{-44.81}$) was similar to that of synthetic carnotite reported in literature

(K_{eq} = $10^{-56.38}$).[98] However, there were minor discrepancies in their solubility information that could be attributed to differences in crystal chemistry, highlighting the importance of crystal chemistry while understanding the reactive transport of metals. Knowledge obtained from this manuscript and the integrated methodology used to obtain this information can be transcribed to other mine waste sites where uranyl vanadates are abundant.[41-48, 127].

Table 4.1 Electron microprobe data for carnotite from the Blue Gap Tachee mine waste.[182]

Element	Average Element Weight % (C as elemental carbon)	Oxides	Average Oxide Weight %	Reference	Reference Weight% Carnotite
C	4.81	C	4.81	-	-
K	3.54	K_2O	4.45	K_2O	10.00
Ca	0.37	CaO	0.53	CaO	0.66
U	52.20	UO_2	62.72	UO_2	62.26
Si	0.22	SiO_2	-	SiO_2	-
Na	0.03	Na_2O	0.041	Na_2O	0.16
Al	0.45	Al_2O_3	-	Al_2O_3	-
Ti	0.05	TiO_2	0.09	TiO_2	-
V	11.5	V_2O_5	20.65	V_2O_5	20.57
Fe	0.41	Fe_2O_3	0.56	Fe_2O_3	0.55
H	-	H_2O	-	H_2O	4.90
O	17.8	O	0	O	-
Total without C	91.35	Total	90.75	Total	99.1
Total with C	91.35 + 4.81 = 96.16	Total with C	90.75+4.81 = 95.56	Total with C	99.1

Table 4.2 Electron diffraction data of measured *d*-spacings (in Å) for the uranyl vanadate occurring in the Blue Gap/Tachee mine waste compared to the calculated *d*-spacing for synthetic anhydrous carnotite ($K_2UO_2VO_4$) [188]. Lattice spacing data <2.5 Å has been omitted.[188]

Calculated*	h	k	l	Measured[1]
6.4626	0	1	1	7.04
6.3886	1	0	0	6.09
5.75				
5.0857	1	1	0	5.17
4.9478	1	1	1	4.87
4.68				
4.5438	1	0	2	4.58
4.3320	0	1	2	
4.2243	1	1	1	4.27
4.2015	0	2	0	
3.9969	1	1	2	3.95
3.8799	0	2	1	3.79
3.5620	1	0	2	
3.5104	1	2	0	
3.4640	1	2	1	3.41
3.2795	1	1	2	
3.2313	0	2	2	3.21
3.1943	2	0	0	
3.1858	1	2	1	
3.1282	0	1	3	
3.1022	1	1	3	
3.0848	1	2	2	
3.0607	2	0	2	3.05
3.0606	2	1	1	
2.9859	2	1	0	
2.8759	2	1	2	2.90
2.7170	1	2	2	2.71
2.7004	2	1	1	
2.6993	0	3	1	
2.6290	0	2	3	
2.6136	1	2	3	2.603
2.5885	2	2	1	2.596
2.5865	1	1	3	
2.5767	1	0	4	
2.5653	1	3	0	
2.5470	1	3	1	2.53

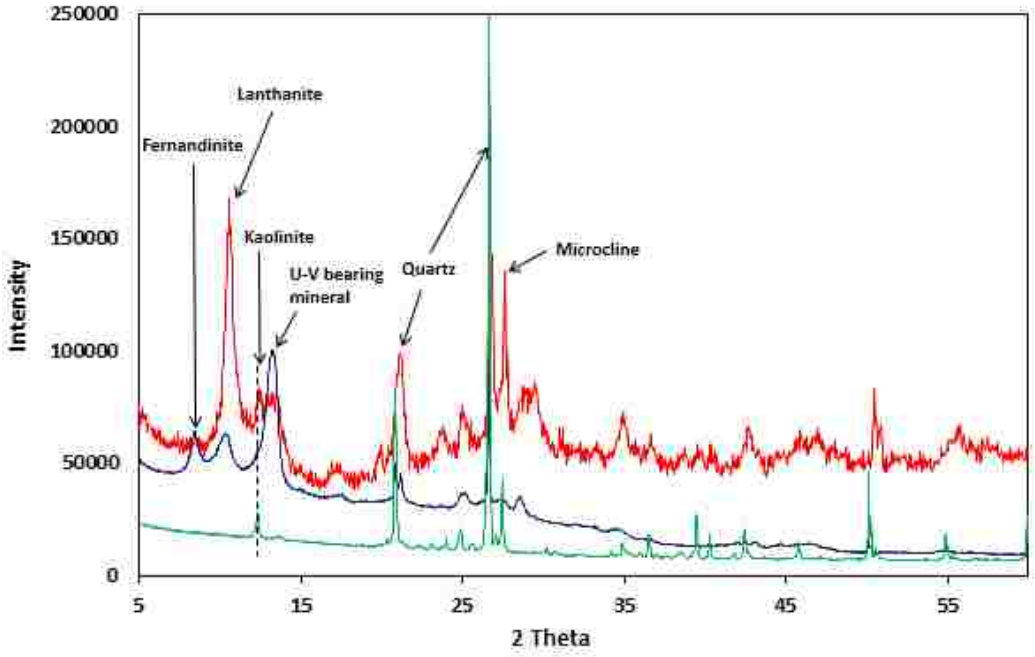

Figure 4.1 Powder X-ray Diffraction of Blue Gap Tachee mine waste. The green curve represents the diffractogram of the powdered mine waste without any separation. The blue curve represents diffractogram of an oriented mine waste sample obtained from suspended fraction of a water separation technique with an overnight settling time. The red curve represents diffractogram of a randomly oriented mine waste sample obtained from the suspended fraction of a water separation technique with a settling time of <30s.

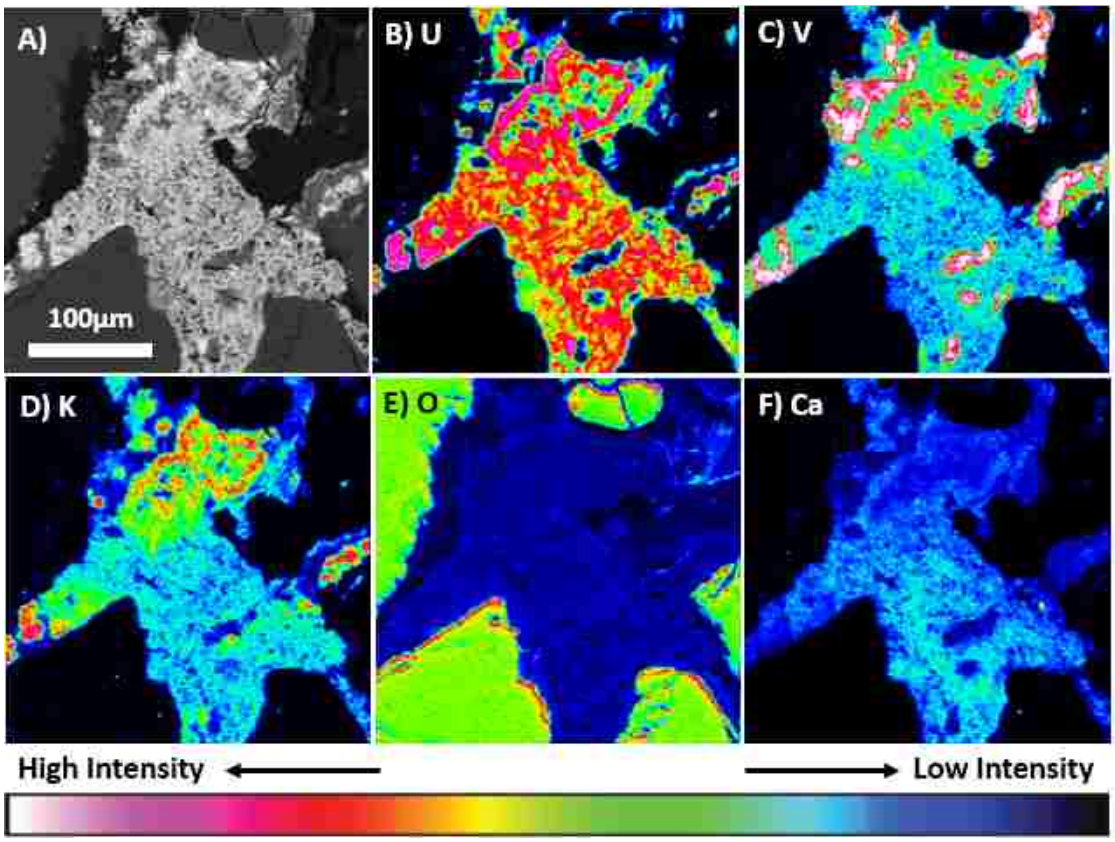

Figure 4.2 Qualitative electron microprobe X-ray maps of elemental distributions in an ore sample from mine waste from the Blue Gap Tachee site, showing complex correlation of U with V, K, Ca and O. **A)** Back-scattered electron image of the mapped area, **B)** U M_{α} map, **C)** V K_{α} map, **D)** K K_{α} map **E)** O K_{α} map and **F)** Ca K_{α} Map.

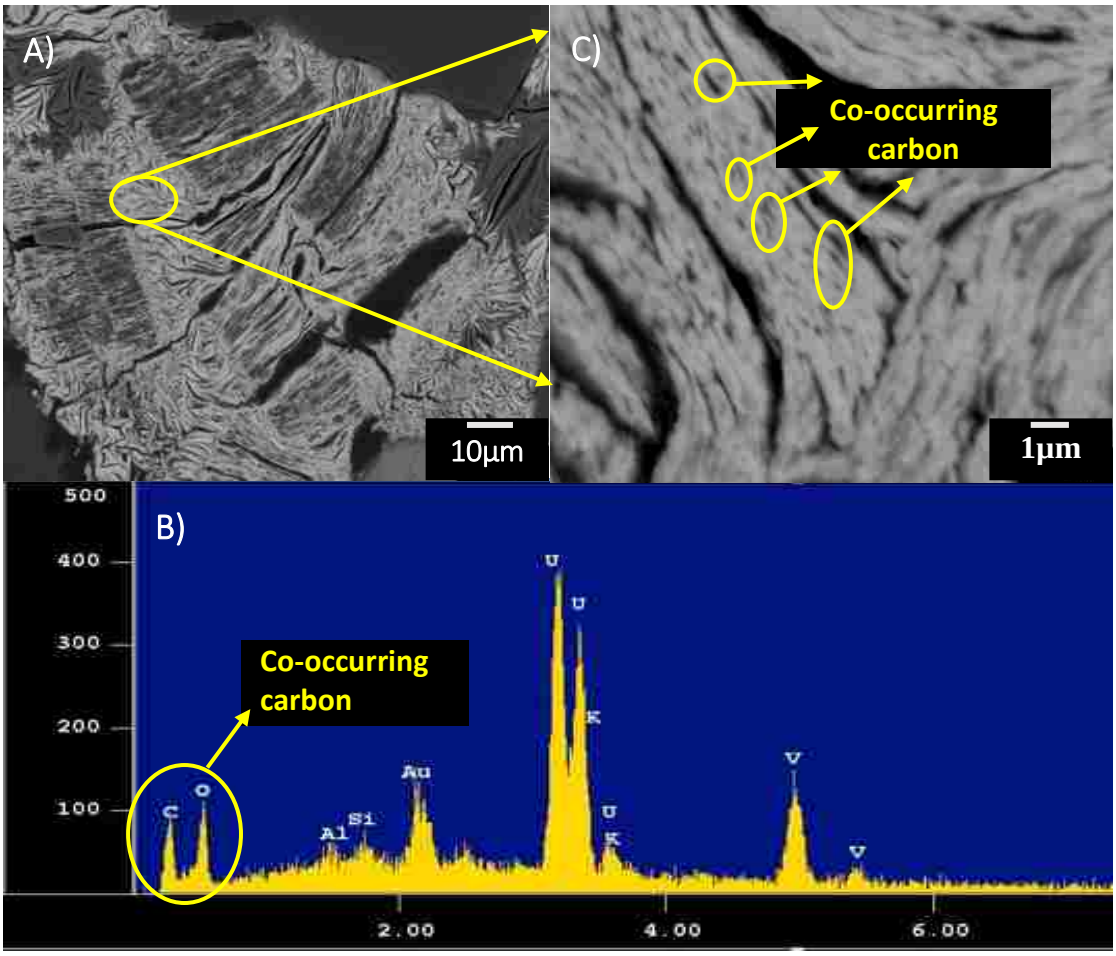

Figure 4.3 A) Back-scattered electron image of complex intergrowth of U-V bearing mineral phase occurring in the Blue Gap/Tachee mine waste. **B)** Energy Dispersive Spectrum (EDS) of the yellow circled area in image A showing presence of low Z inclusions. **C)** Higher magnification BSE image showing occurrence of submicron, low-Z inclusions (yellow circles) in the uranyl vanadate which EDS indicates are carbon rich.

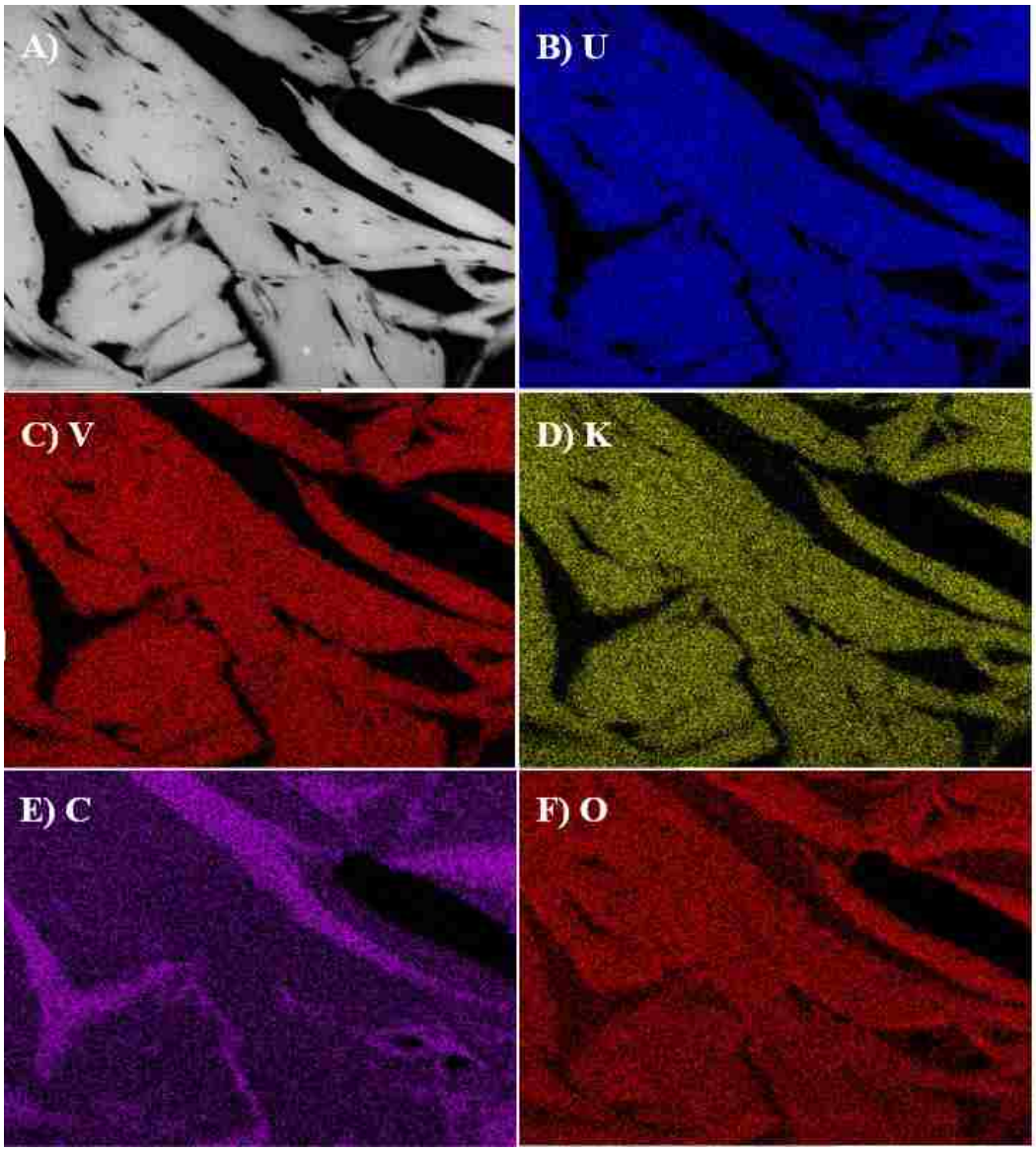

Figure 4.4 Scanning Transmission Electron Microscopy (STEM) image and STEM EDS X-ray maps obtained from a FIB section of the Blue Gap Tachee mine waste. **A)** HAADF image of the FIB section, **B-F**) X-ray lines of **B)** U M_{α}, **C)** V K_{α} **D)** K K_{α}, **E)** C K_{α} and **F)** O K_{α}, were used for the analysis. The X-ray map of carbon shows the presence of low nanometric Z inclusions within the grain and also the presence of epoxy in which the grains were embedded that are not indigenous to the sample.

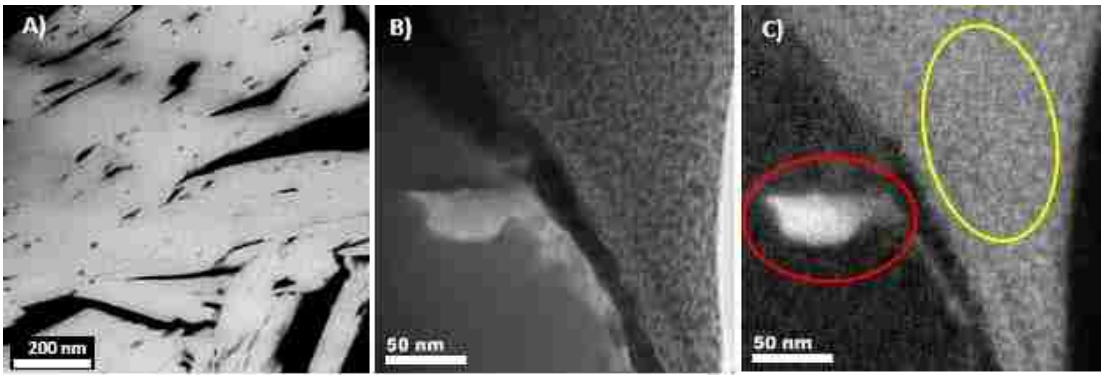

Figure 4.5 A-D) A) Dark Field HAADF images in Scanning Transmission Electron Microscopy (STEM) mode showing the co-occurrence of C with in the U-V mineral of the Blue Gap Tachee Claim-28 mine waste. **B) and C)** Energy Filtered Transmission Electron Microscopy (EFTEM) images confirming the C co-occurrence to be an inclusion in the uranyl vanadate. The area in red is the distinct form of a C inclusion and the area in yellow indicates the carbon incorporated into the organic platinum structure that is used to coat the FIB section.

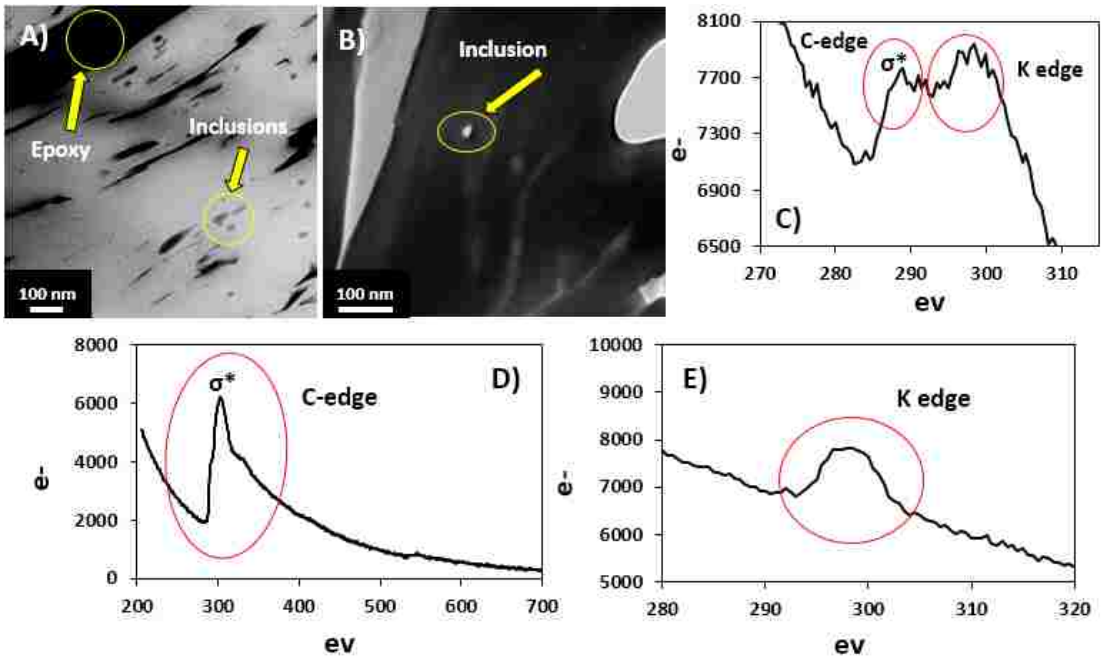

Figure 4.6 Electron Energy Loss Spectroscopy (EELS) analysis of the carbon inclusions and epoxy. **A)** HAADF Scanning Transmission Electron Microscopy (DF-STEM) image of the inclusions and epoxy (yellow arrows) in the Focused Ion Beam (FIB) section of the uranyl vanadate. **B)** BF-TEM image of an inclusion that was analyzed using EELS. **C)** EELS spectrum of the C inclusion showing the presence of C and K-edge. **D)** EELS spectrum of the epoxy showing the presence of C-edge. **E)** EELS spectra of the uranyl vanadate away from the inclusion showing the presence of only K-edge. The C L edge at 284 eV is missing demonstrating that the carbon is present only in the inclusions.

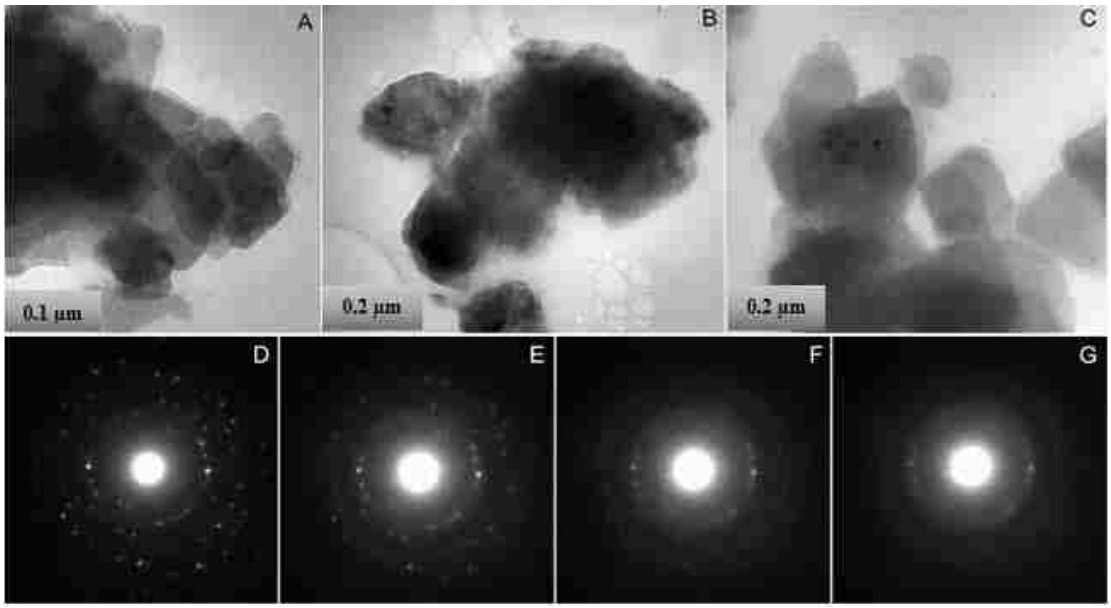

Figure 4.7 Bright-field TEM images and electron diffraction patterns of clusters of uranyl vanadate crystal from the Blue Gap/Tachee ore. **A-C)**: Bright-field TEM images showing the morphology and grain size of different uranyl vanadate clusters. The crystallites consist of plates with anhedral to subhedral outlines that are overlapping one another, parallel to the plane of the supporting holey carbon film. **D-G**): sequence of ring electron diffraction patterns taken at time intervals of ~20 secs, showing the rapid amorphization of the uranyl vanadate due to electron beam irradiation. Discrete diffraction maxima disappear and are replaced by diffuse intensity consistent with an amorphous phase.

[redacted]

(To be submitted to *Chemical Geology*)

Sumant Avasarala[1*], Chris Torres[2], Abdul-Mehdi S. Ali[3], Bruce M. Thomson[1], Michael N. Spilde[3], Eric J. Peterson[3], Kateryna Artyushkova[2], Elena Dobrica[3], Juan S. Lezama-Pacheco[5], and José M. Cerrato[1]

*Corresponding email address: savasarala87@unm.edu,

Telephone: (001) (248) 978-8264

Fax: (001) (505) 277-1918

[1] Department of Civil Engineering, MSC01 1070, University of New Mexico, Albuquerque, New Mexico 87131, USA.

[2] Department of Chemical and Biological Engineering, MSC01 1120, University of New Mexico, Albuquerque, New Mexico 87131, USA

[3] Department of Earth and Planetary Sciences, MSC03 2040, University of New Mexico, Albuquerque, New Mexico 87131, USA

[4] OFM Research-Southwest, Santa Fe, New Mexico 87507, USA.

[5] Department of Environmental Earth System Science, Stanford University, California 94305

[redacted] **Abstract.**

We investigated the effect of oxidizing conditions on the submicron U(IV) and U(VI) mineral phases in mine wastes from Jackpile-Paguate mine, Laguna Pueblo, New Mexico, by integrating laboratory experiments, spectroscopy, microscopy and diffraction techniques. Concentrations exceeding 7000 mg Kg^{-1} U were measured in these sediments

using X-ray fluorescence. Results from X-ray Photoelectron Spectroscopy (XPS) analysis suggested co-occurrence of U(VI) and U(IV) at a ratio of 19:1 at the surface. These results agree with observations made using X-ray Diffraction (XRD) and electron microprobe where coffinites ($USiO_4$) and U-P-K phases were identified. The U-phosphate phase (U-P-K phase) was the predominant submicron crystalline U-phase encapsulated by carbon, based on results from scanning transmission electron microscopy imaging (STEM), energy dispersive spectroscopy (EDS), and STEM mapping. Laboratory experiments also measured the effect of bicarbonate and oxidizing agents (e.g., dissolved oxygen (DO) and OCl^-) on the submicron U(IV) and U(VI) minerals. Despite exposing the mine wastes to strong oxidizing conditions, the highest aqueous U concentrations were obtained from mine waste reaction with 10mM $NaHCO_3$ at pH 7.5. The reaction of these organic rich mine wastes with bicarbonate under ambient dissolved oxygen concentrations can result in considerable mobilization of U in water, which has relevance for environmental conditions observed at the Rio Paguate across Jackpile mine. Results from this investigation provide a better understanding on the reactivity of carbon encapsulated submicron U-phases under oxidizing conditions and has important implications in uranium recovery, remediation, and risk exposure assessment.

Introduction.

The occurrence of uranium (U) in water and soils after mining operations has occurred at thousands of uranium mines throughout the United States. This study is focused on the Jackpile-Paguate on Laguna Pueblo, NM, which, at one time, was the largest open pit U mine in the world. The Jackpile deposit was discovered in 1951 during an airborne

radioactivity survey.[53] Since then extensive studies of its geologic deposit have been conducted by the U.S. Geological Survey[50, 191], the Atomic Energy Commission[192], and the Anaconda Company.[193] These extensively studied geologic deposits were then mined from 1953 to 1980, affecting approximately 3,141 acres of land, among which 2,656 acres were yet to be reclaimed as of 1985[194].

The Jackpile sandstone at the Jackpile-Paguate mine is a medium-grained, cross-stratified, 33 mile long sandstone in which the U deposits are composed of one or more semi-tabular ore layers. Unoxidized parts of these tabular U deposits are rich in U(IV) phases such as uraninite and coffinite that co-occur with the vegetative carbonaceous matter as primary minerals imparting a gray to black shade with increasing organic content.[50, 195] Oxidation of these U(IV) phases resulted in the formation of secondary U(VI) minerals such as carnotite [$K_2(UO_2)_2(VO_4)_2$. $3H_2O$], tyuyamunite [$Ca(UO_2)_2(VO_4)_2$. $7\text{-}10H_2O$], meta-tyuyamunite [$Ca(UO_2)_2(VO_4)2$. $5H_2O$], and uranophane [$Ca(UO_2)_2(SiO_3)_2(OH)_2$].[196] Additionally, other U(VI) mineral phases such as autunite [$Ca(UO_2)_2(PO_4)_2$.$10\text{-}12H_2O$] and phosphuranylite [$Ca(UO_2)_2(PO_4)_2(OH)_4$.$7H_2O$] that are not a consequence of oxidation are also dominant in these deposits. Given that surface waters of Rio Paguate and Rio Moquino flow through these abandoned U deposits, the co-occurring U(IV) and U(VI) pose potential sources of elevated concentrations of U and other co-occurring metals[54, 1].

The mobility of U from U(IV) and U(VI) phases at the Jackpile-Paguate mine can be affected or mediated by a number of geochemical mechanisms at the mineral-water interface. For instance, physical and chemical characteristics of the mine waste (e.g., mineralogy, reaction kinetics, and crystallinity) and water chemistry (i. e., pH, Eh, and

solution composition) are some key factors that affect U mobility[59, 61, 98, 197]. Uranium mobility is substantially enhanced when aqueous U(VI) species bind strongly onto organic matter through either ion-exchange, coordination/complexation, donor-receptor interactions, or Van der Waal forces at circumneutral conditions[71, 73-77]. The degree of mobility depends on 1) the sorption ability of aqueous U(VI) onto solid organic matter surfaces, 2) hydrophobicity and alkyl carbon content in organic matter, and 3) the presence of the U(VI)-organic colloids[73, 78-79]. Aqueous U(VI) also adsorbs onto SiO_2, hydrous ferric oxide, goethite, and montmorillonite surfaces[71, 91-92]. The adsorption of U(IV) may also occur in organic matter aggregates [e.g. mononuclear or monomeric U(IV)] and organic-carbon coated clays[72, 80]. Recently, biogenic amorphous U(IV) species were found to be a major component of undisturbed roll front ore deposits[81]. Formation of such sparingly soluble biogenic and chemogenic U(IV) through reduction have been proposed as methods to immobilize aqueous U in contaminated ground waters[83-85]. Reduced U(VI) results in the formation of crystalline submicron biogenic and chemogenic U(IV) phases whose dissolution rates are similar to those of coarser U(IV) phases[86-88]. Submicron U and U adsorbed onto colloids of organic matter and oxides can form about 30-40% of the U mobilized from similar U mining sites[89-90]. In addition to sorption, U mobility can also be affected by dissolution/precipitation of U mineral phases. For instance, U occurs in the environment as vanadate, silicate, phosphate, and oxide solid mineral phases[91-98]. Uranium mobility from such aqueous and solid mineral U(IV) and U(VI) species has been widely explored; however, there is limited literature on the reactivity of submicron U phases from natural U-deposits and mine wastes under environmentally relevant conditions.

Previous studies have tried to understand the mobility of U from organic-rich, U-deposits at the Grants Mineral District and sediments along Rio Paguate. Deditius et al. (2008) investigated the process of formation and alteration of three different coffinites under reducing and oxidizing conditions[198]. This investigation suggested that the coffinites occur as secondary submicron-crystals within layers of organic matter that were formed as a result of alteration under oxidizing conditions[198]. Dissolution of coffinite and other U-bearing minerals from these U-ore deposits were later suggested as potential sources of elevated U concentrations (35.3 to 772 mg L^{-1}) in the Rio Paguate[54]. However, no reactivity experiments on these carbon-rich mine wastes were conducted to support this hypothesis.

This objective of this study is to investigate the reaction of different oxidizing agents (O_2 and hypochlorite OCl^-) and bicarbonate with submicron U(IV) and U(VI) phases in Jackpile-Paguate mine wastes by using laboratory experiments, spectroscopy, and electron microscopy techniques. Results from this investigation will improve our understanding about: 1) U mobility from naturally-occurring formations; 2) transport and remediation of contaminants at mine waste sites; and 3) U resource recovery.

Experimental.

Mine waste samples collected in 2015 from the exposed beds in the mineralized zone of north Jackpile-Paguate mine site (35° 8'28.09"N, 107°20'19.67"W), Laguna Pueblo, New Mexico, USA, and were used for the solid analyses and batch experiments presented in this study. These mine waste samples were organic-rich, black in color with a solid rock

texture (loss on ignition of upto 21.8% were found in these samples), and were used in a previous investigation on ground water quality restoration after in situ leach mining.[199] The samples were pulverized and homogenized using a Spex shatterbox and then sieved to a fraction of <63µm. Only the sieved fraction (<63) was used for all spectroscopic and microscopic characterizations and batch experiments. These homogenized Laguna mine waste samples were addressed as 'waste' throughout this investigation.

The Jackpile-Paguate mine site is roughly 13 miles wide, 33 miles long, and up to 65 m deep; the mine is located in the Grants-Laguna District near the village of Paguate. This location raises concerns about the mine's impact on ground water quality, the sole source of water supply for the village. Major U deposits of the Jackpile-Paguate mine are embedded in the Jackpile Sandstone of the Jurassic and Cretaceous strata[50-54] . Recently the Jackpile-Paguate mine was investigated for U mobility and accumulation from sediments of the Rio Paguate, where U in mine waste samples occurred with silicon (Si), phosphorus (P), iron (Fe), and vanadium (V) as coffinite and other unidentified mineral phases.[54]

[redacted]

Batch experiments were conducted under oxidizing conditions to investigate the effect of oxidizing conditions on the reactivity of U in waste samples. About 2 g of the <63µm fraction of waste was reacted with: 1) 18MΩ water, pH 5.4; 2) 10 mM $NaHCO_3$, pH 7.5; 3) 6% NaOCl, pH 7.5; and 4) 10 mM $NaHCO_3$ + 6% NaOCl, pH 7.5 at room temperature. The pH of all reagents except 18MΩ water were adjusted to 7.5 using concentrated nitric acid, 0.5N NaOH, and 0.1M HCl. A pH 7.5 was chosen as it was

proximate to the pKa of NaOCl [200], represents the pH of surface water at the site[54], and was the recommended pH to effectively oxidize the organic matter[201-202]. Furthermore, 10mM $NaHCO_3$ was selected to mimic the alkalinity and pH conditions measured in the Rio Paguate that flows through the Jackpile-Paguate mine site[54]. The 18MΩ water reaction with waste approximately represents the first flush of waste in the field where the weakly bound U is easily mobilized. The 6% NaOCl solution, purchased commercially from Fisher Scientific, was used as a strong oxidizing agent to increase the release of U through oxidation of organic carbon (C) and reduced mineral phases. All experiments were conducted in triplicate. The batch oxidation studies were conducted for two weeks, and aliquots were collected periodically after 0.5, 2, 4, 8, 24, 72, 144, 218, 288, and 336 hours of reaction. The aliquots were then filtered through 0.45µm filters and diluted to 10x or 100x depending on whether the elemental concentrations were measured using Inductively Coupled Plasma – Optical Emission Spectroscopy (ICP-OES) or Mass Spectroscopy (ICP-MS).

[redacted]

The concentrations of metals in the waste leachates were measured using a PerkinElmer Optima 5300DV ICP-OES and a PerkinElmer Nexion 300D (Dynamic Reaction Cell) ICP-MS. Trace metal concentrations below detection limit of ICP-OES were measured using ICP-MS that has a 100-1000 times lower detection limit than ICP-OES. Both ICPs were calibrated with a 5-point calibration curve, and QA/QC measures were taken to ensure quality results. The solution pH was measured using a Thermo Scientific Orion Versastar Advanced Electrochemistry pH meter. Additionally, at the end of the leaching experiment the dissolved organic carbon (DOC) was measured using the UV persulfate

method in a Tekmar-Dohrmann Phoenix 8000 TOC analyzer. Additional information on the DOC analysis and acid extractable procedure is provided in the supplementary information (SI).

[redacted]

Characterization of waste samples was conducted using various spectroscopy, microscopy, and diffraction techniques. Specifically, we used X-ray Fluorescence (XRF), X-ray diffraction (XRD), and Electron microprobe analysis (EPMA), High resolution Scanning Transmission Electron Microscopy (HR-STEM), X-ray photoelectron spectroscopy (XPS), synchrotron micro X-ray Fluorescence spectroscopy (μ-SXRF), and Zeta were used to obtain information on the occurrence of U-minerals in the mine waste and their overall surface charge. Additional information on these methods is provided in the supporting information (SI).

[redacted]

The aqueous complexes and solid phases of U formed during reactions with 18MΩ water, 6% NaOCl and 10 mM $NaHCO_3$ were estimated using MINEQL+ v4.6[203] to better explain the U trends observed from our experiments. Inputs to these chemical equilibrium simulations were provided based on alkalinity, pH and Ca and U concentrations measured during the experiments. MINEQL database that was previously updated with critical thermodynamic reactions such as aqueous cation-uranyl-carbonate complexes was used instead of the default MINEQL database that is supplied with the software.[128, 204-206]

[redacted] **Results and Discussion.**

[redacted]

The results of X-ray photoelectron spectroscopy (XPS) suggested the co-occurrence of U(VI) and U(IV) near the surface (top 5-10 nm) of the unreacted wastes (<63 µm). Results from XPS survey scan found that the elemental composition of the waste surface was 47.8% C, 37.5% O, 9.0 % Si, 0.2% N, and 0.1% U (Table 8.1). Approximately, 95% of the U detected at the waste surface was U(VI), and the remaining 5% was U(IV). Both measurements were based on XPS narrow scans conducted using U(IV) (uraninite [UO_2]) and U(VI) standards (becquerelite [$Ca(UO_2)_6O_4(OH)_6 \cdot 8H_2O$]) as a reference (Figure 5.2A-C, Appendix B: Table 8.2). Recent investigations have reported the possibility of using satellite peaks in the U4f spectra to differentiate oxidation states of U.[207] However, the waste samples contained nitrogen (N), magnesium (Mg), and other elements that coincide with the position of satellite peaks of U. Therefore, the XPS fits used in this study are reported based on fits of just U4f 5/2 and 7/2 peaks. These results agreed with observations made in the past where co-occurrence between autunite, phosphuranylite, and coffinites was reported in U-deposits at the Jackpile-Paguate mine[196, 198] Additional microscopy and diffraction analyses were conducted to obtain more specific information about these U(IV) and U(VI) mineral phases.

[redacted]

Results from microscopy, diffraction, and spectroscopy analyses on unreacted wastes suggest that the submicron U(IV) and U(VI) phases such as coffinite ($USiO_4$) and U-P-K phases are encapsulated by carbon (Figure 5.3, 8.2). Electron microprobe analyses using back scatter electron imaging (BSE) identified submicron U-minerals (bright white spots, Figure 5.3A) that occurred with P and C (red circles, Figure 5.3D-G). Similarly, the occurrence of U, P, and Si was observed using micro synchrotron x-ray fluorescence (µS-

XRF) mapping analysis (Appendix B: Figure 8.1). The minerals were encapsulated by carbon-rich material (possibly organic matter)[198] similar to observations made using back scatter electron image (Figure 5.3A). It is worth noting that a past investigation reported loss on ignition of up to 21.8% in the same organic-rich waste used for this study,[199] which could possibly be attributed to organic matter in these samples. The co-occurrence of U, P, and Ca could correspond to uranyl phosphates (autunite [$Ca(UO_2)_2(PO_4)_2.10$-$12H_2O$] and phosphuranylite [$Ca(UO_2)_2(PO_4)_2(OH)_4.7H_2O$]) that were previously identified at the Jackpile-Paguate mine[50, 195]. Associations between U, Fe, sulfur (S), and V in addition to occurrence of U, P, Si, and C phases were also reported in a recent study by our research group at the Jackpile-Paguate mine[54].

Electron microprobe and XRD analyses on unreacted waste samples suggested the co-occurrence of coffinite ($USiO_4$) and U-P-K phases with other primary minerals such as kaolinite ($Al_2Si_2O_5(OH)_4$), quartz (SiO_2), and microcline ($KAlSi_3O_8$). Additionally, based on theoretical estimations using Jade® software (Smartlab XRD), 47% of waste was amorphous (Appendix B: Figure 8.2), consistent with other data reported from the same site[54, 198]. The presence of amorphous phases in these samples could be from the clays and organic conglomerates that are characteristic of sandstone formations such as the Jackpile-Paguate, which is a member of the Morrison formation. Furthermore, the identification of coffinite, kaolinite, quartz, and microcline in the unreacted mine wastes using XRD analyses was consistent with observations reported previously in other investigations (Appendix B: Figure 8.2)[50, 54, 195, 198]. These results also confirmed the observations made using S-µXRF mapping where U and Si were found (Appendix B: Figure 8.1). The presence of a U-P-K phase in the mine waste was identified using

electron microprobe BSE imaging and energy dispersive spectroscopy (EDS) analyses. The U-P-K phases were similar to observations made using microprobe mapping and previously reported (Figure 5.3B, C)[50, 195]. However, the specific U-minerals formed by U, P, and K remain unknown.

The scanning transmission electron microscopy (STEM) analysis suggested the presence of carbon encapsulated crystalline U-P-K phase in the waste samples (Figure 5.4). Specifically, bright field TEM imaging and EDS analyses were used to observe that the U-P-K phase was both submicron and predominant (black features, Figure 5.4A, B). In addition, the patterned fringes (in yellow) obtained using high resolution TEM imaging suggested that these U-P-K phases were crystalline (Figure 5.4C). These submicron U-P-K phases co-occurred with C and Ca (Figure 5.4A) and were consistent with observations made by electron microprobe analysis (Figure 5.3). We prepared a STEM map of these U-P-K grains (Appendix B: Figure 8.3) because the C map suggested that the C occurs as an encapsulation, similar to the electron microprobe mapping results (Appendix B: Figure 8.3B). This carbon layer, composed of 33.3% C and 66.6% O (spectrum 3, Appendix B: Figure 8.4), could be from vegetative organic matter that was reported to intricately co-occur with U-minerals in the mine waste[50, 195, 198]. The composition of the U-P-K phase was also estimated to be 10.7% U, 3.79% K, 9.15% P, 6.49 Si, and 69.86% O (Spectrum 1, 2 and 4, Appendix B: Figure 8.4). In another study, the sustained presence of U(IV) minerals, such as coffinites in the Jackpile-Paguate mine wastes, was reported as a consequence of reducing conditions preserved by this vegetative organic matter[198]. However, the interaction of organic matter with U is still not well understood. Future investigations could conduct a more detailed

spectroscopy (EELS, NMR etc.) and microscopy (STXM) analyses to confirm the nature of C in the mine wastes, which is beyond the scope of the present study. Additional experiments were conducted to evaluate the reactivity of these co-occurring submicron U-minerals under oxidizing conditions at circumneutral pH.

[redacted]

Leaching the mine waste samples with 18MΩ water resulted in U concentrations as high as 200 µg L^{-1} (Figure 5.5A). The concentrations mobilized in the first 30 minutes of the reaction; 70 µg L^{-1} could be attributed to the first flush removal of the weakly bound U. However, after eight hours of reaction, the steady increase in U concentrations upto 200 µg L^{-1} could be due to desorption or dissolution of readily souble U phases, such as schoepite [$(UO_2)_8O_2(OH)_{12}\cdot 12(H_2O)$] or metaschoepite [$UO_3\cdot 2H_2O$] etc. could occur at circumneutral pH (Appendix B: Figure 8.5A)[41, 138, 147-148]. After about 300 hours of reaction, the U concentrations decreased to ~20 µg L^{-1}. To better understand this behavior and evaluate reactions that could possibly occur under these experimental conditions, chemical equilibrium modelling using MINEQL was conducted. Chemical equilibrium simulations suggest that this decrease in U concentrations could be due to precipitation of schopepite (Saturation Index = 0, MINEQL, Appendix B: Table 8.3). The decrease in U could also be attributed to readsorption of positively charged aqueous complexes (UO_2OH^+, $(UO_2)_3(OH)_5^+$) onto the negatively charged mine waste surfaces (measure surface charge is -25mV as shown in Appendix B: Figure 8.6A)[82, 128, 208]. After the deionized water (DI) water leach was complete, an acid digestion was performed to

determine the remaining total acid extractable content of the samples. This analysis found a 3.7% loss on the total acid extractable U content (Appendix B: Table 8.5). Results from this experiment provide an improved understanding of the contributions from weakly bound U relevant to the first flush reactions that happen during rainfall events. These mine wastes were later subjected to more aggressive leach solutions containing 10 mM $NaHCO_3$ under ambient DO concentrations and 6% NaOCl solution to observe the reactivity and mobilization of U under oxidizing conditions.

[redacted]

The highest release of U by leaching experiments was obtained using a 10 mM $NaHCO_3$ leachate at, pH 7.5 under ambient DO conditions. For instance, 25000 µg L^{-1} of U was released into solution during this experiment (Figure 5.5B). Rapid leaching during the first eight hours of reaction, (~15000 µg L^{-1}) suggested the occurrence of U desorption was due to complexation with carbonate or dissolution of U-bearing minerals.[41, 138, 147-148] Contributions from organic matter and oxidative dissolution of U(IV) submicron minerals reacting with DO was also possible. However, oxidation of U(IV) minerals such as coffinite is sufficiently slow that this possibility seems unlikely[86, 209]. The release could also have been a consequence of oxidative dissolution of U-bearing organic matter, as suggested by the increase in DOC (2.6 mg L^{-1}) concentrations compared to those observed during reaction with 18 MΩ water (1.6 mg L^{-1}) (Appendix B: Table 8.4). After eight hours of reaction, however, a steady increase in U concentrations suggested the possible dissolution of U-bearing mineral phases. Other investigations reported the dissolution of uranyl phosphates such as ankoleite and meta-ankoleite $[K_2(UO_2)_2(PO_4)_2 \cdot 6(H_2O)]$ at circumneutral pH to be slow but steady.[210]

In order to futher identify the complexes that potentially affect U speciation during this experiment and explain the U behavior under circumneutral conditions, chemical equilibrium simulations using experimentally measured alkalinity, pH, and concentrations of Ca and U were conducted. Results from these simulations suggested that neutral or negativily-charged U-Ca-CO_3^{2-} aqueous complexes such as $UO_2(CO_3)_3^{4-}$, $CaUO_2(CO_3)_3^{2-}$ and $Ca_2UO_2(CO_3)_3^0$ were predominant at pH 8 (Appendix B: Table 8.3, Figure 8.7B). These neutral or negatively charged aqueous complexes potentially repelled negative solid surfaces, which inhibited readsorption, unlike observations made with 18 MΩ water (Appendix B: Figure 8.5B, Figure 8.6B).[128] After the experiment, the XPS analysis on the reacted mine waste surfaces indicated an increase in U(VI)% from 95% (unreacted) to 100% (reacted). This increased suggested oxidation of U(IV) phases due to DO. However, the increase in U(VI)% could also be attributed to sample hetrogeneity. Additionally, post leach acid digestions of the reacted mine waste samples found that 17% of the total acid extractable U was extracted by the 10 mM $NaHCO_3$ leachate (Appendix B: Table 8.5). This percentage loss in U was highest among all experiments and was of greater environmental relevence as these conditions represent relevant conditions observed at the site. Subsequent experiments were perfomed to understand the reactivity of these co-occurring U(IV)-U(VI) phases under strong oxidizing conditions.

[redacted]

The concentrations of U released by leaching with 6% NaOCl was significantly less than those obtained from leaching by $NaHCO_3$ solution. Despite our using strong oxidizing conditions, the concentrations of U (8000 µg L^{-1}) released after leaching with 6% NaOCl were less than one-third of those released during leach study with 10 mM $NaHCO_3$, pH

7.5 (Figure 5.5C). These 8000 µg L^{-1} U concentrations were released within the first two hours of reaction with 6% NaOCl. However, between the second and eighth hours of reaction, the U concentrations dropped to ~2000 µg L^{-1}. In order to better understand this change in U behavior, chemical equilibrium simulations using experimentally measured pH and Ca and U concentrations were conducted.

Attributing the decrease of U in solution over time to a single process in these experiments is not possible given that the specific mineraology and organic matter chemisry of the mine wastes remain unknown. There are a variety of scenarios that could be considreed. For instance, chemical equilibrium simulations suggested that positively charged aqueous complexes UO_2OH^+ were prevalant at pH 6-7 (Appendix B: Table 8.3, Figure 8.5C). Given that the mine waste surfaces were negatively charged (Appendix B: Figure 8.6C), the positively charged aqueous complexes UO_2OH^+ may readsorb to the solids. The decrease in U concentrations may also be due to precipitation of schoepite as indicated in results from chemical equilirbium calculations (Appendix B: Table 8.3). Since U (~8000 µg L^{-1}) and DOC (5.5 mg L^{-1}) concentrations (Figure 5.5C, Appendix B: Table 8.4) were measured in solution in these experiments, it is possible that the readsorption process was affected by U-organic matter aqueous complexes. Uranium can form stable U-organic matter complexes[82]. Since little is known about the chemistry and characteristics of the organic matter type, the specific U(IV)/U(VI)-aqueous complexes are also not known. Future investigations are necessary, to understand the chemistry of organic matter in the mine wastes and idnetify relevant interfacial inoganic and organic reactions between U and organic matter.

After eight hours of reaction, the steady increase in U concentrations to ~9000 µg L^{-1} could be due to dissolution of U-bearing minerals that are soluble under acidic conditions, pH <4 (Figure 5.5C, 8.6C). It is not possible to attribute this release to any specific U phase such as coffinite, U-P-K, and other U-bearing minerals that were identifed in the waste based on XRD and microprobe results discussed in the previous sections. Other U-bearing minerals included uranyl sulfates, silicates - (Na, K)-boltwoodite [(Na, K) ($UO_2SiO_3OH \cdot H_2O$)], and vanadates that were previously identified as products of coffinite and uraninite oxidation[196, 198]. These secondary uranyl minerals—such as Na-boltwoodite, meta-ankoleite, uranyl vanadates—were capable of dissolving under acidic conditions at pH >4 based on results reported in other investigations[98, 210-211]. However, more research is necessary to understand the specific U-phases and mechanisms that affect the mobility of U from these mine wastes.

Finally after the experiment, the reacted wastes were subjected to XPS analysis that found an increase in the U(VI)% from 95% to 100% possibly due to the oxidation of U(IV) phases at the waste surface (Appendix B: Figure 8.8 and Table 8.2). The waste solids were subjected to acid digestions after the NaOCl leaching that found a 12% loss of the total acid extractable U from waste despite exposure to strong oxidizing conditions. This result was less than that found by leaching with 10 mM $NaHCO_3$ (Appendix B: Table 8.5).

[redacted]

The solid samples were subjected to a combined reaction with 6% NaOCl and 10 mM $NaHCO_3$ to determine the combined effect of oxidation and complexation on U leachability at pH 7.5. There was no noticeable increase in the U leachability obtained

from the combined reaction (oxidation + complexation) of 10 mM $NaHCO_3$ + 6% NaOCl with mine wastes compared to results from individual reactions with 10 mM $NaHCO_3$ or 6% NaOCl. A leachate concentration of 8000 µg L^{-1} was mobilized in the first two hours, which was similar to that observed during reactions with 6% NaOCl (Figure 5.5D). However, the U release was unaffected by the presence of $NaHCO_3$, possibly because the buffering capacity of carbonate and bicarbonate was masked by HOCl and OCl^- in these experiments.

After two hours of reaction, the U concentrations decreased in a manner similar to observations made during reaction with 6% NaOCl. This decrease in U concentrations could not be attributed to a specific process. However, based on chemical equilibrium modelling were conducted using measured alkalinity, pH, and Ca and U concentrations, readsorption was unlikely due to similarity in charges of aqueous complexes (UO_2CO_3 (aq), $UO_2(CO_3)_2^{-2}$, $Ca_2UO_2(CO_3)_3^0$ and $CaUO_2(CO_3)_3^{2-}$), and waste surfaces (Appendix B: Table 8.3, Figure 8.5, 8.7 D,E) at pH 5.9. Readsorption of U as U-organic matter aqueous complexes is also possible considering the presence of ~3.3 mg L^{-1} of DOC and ~8000 µg L^{-1} of U in the leachates (Appendix B: Table 8.4, Figure 5.5D). Aqueous U and organic matter can associate to form stable U-organic matter aqueous complexes as reported in a previous study[82].

Unlike observations made during reaction with 6% NaOCl, we found that the U concentrations during mine waste reaction with 10 mM $NaHCO_3$ + 6% NaOCl did not increase again after eight hours of reaction. This behavior could be attributed to the improved buffering capacity of the system that prevented acidic conditions and maintained the pH at ~6. Existing literature suggests that most uranyl minerals are

soluble under either circumneutral (7-9)[212] or acidic conditions (<4). Yet only a limited number of U-bearing minerals, such as easily soluble U(VI)-oxides, are soluble between pH 5-7, which could explain the lack of increase in U concentrations after eight hours of reaction during this experiment.

After the experiment, XPS analysis on the leached samples found an increase in the U(VI)% from 95% to 100% in the surface (top 5 nm). This difference in U(VI)% could be due to sample hetrogeneity (Appendix B: Figure 8.8, 8.9 and Table 8.2). The leached samples were also subjected to acid digestions that found 23% total extractable U was removed by the leach process with 10 mM $NaHCO_3$ + 6% NaOCl. This result could be due to sample hetrogeneity as the losses estimated from this leach process were greater than those observed during reaction with 10 mM $NaHCO_3$. Therefore, more research is necessary to overcome this uncertainity and better understand the role of organic matter in U mobility and the identification of specific minerals phases that affect the reactive transport U and other co-occurring metals from these mine wastes.

Conclusions.

Based on results from XPS analysis, submicron U(VI) and U(IV) phases were found in solid samples from the Jackpile Mine at a 19:1 ratio. Additionally, microscopy and XRD analyses on these mine wastes identified cofinites and U-P-K phases as the principal U solid phases that were encapsulated by organic carbon[54, 196, 198]. The association of U with different elements was indicative of the complex mineralogy of these solids. Results from mine waste leaching with $NaHCO_3$ and strong oxidants suggest that dissolution of U-phases and subsequent sorption and/or precipitation are key processes affecting U

mobility. The highest U concentrations were mobilized on leaching with 10 mM $NaHCO_3$ solution containing ambient DO concentrations. These results partially explain the presence of elevated U concentrations in the Rio Paguate (35.3 to 772 mg L^{-1}) under relevant alkalinity and pH conditions (average pH 7.5, 70 – 372 mg L^{-1} $CaCO_3$) as reported by others[54]. This information can be useful to provide an imporoved understanding on the reactivity and mobility of U from submicron U minerals in abandoned mine wastes into neighboring water resources and to assess risks for human exposure. Knowledge from this study also provides ideas to improve mine waste management strategies through targetted U remediation and resource recovery initiatives. However, several gaps remain in our understanding. We need to find 1) the role of organic matter in the reactivity and mobility of U from these submicron U minerals and 2) the reactvity and solubility of different U minerals under relevant field conditions. More research is necessary to overcome these research gaps to better understand the mechanisms that affect the mobility of U from organic rich mine wastes.

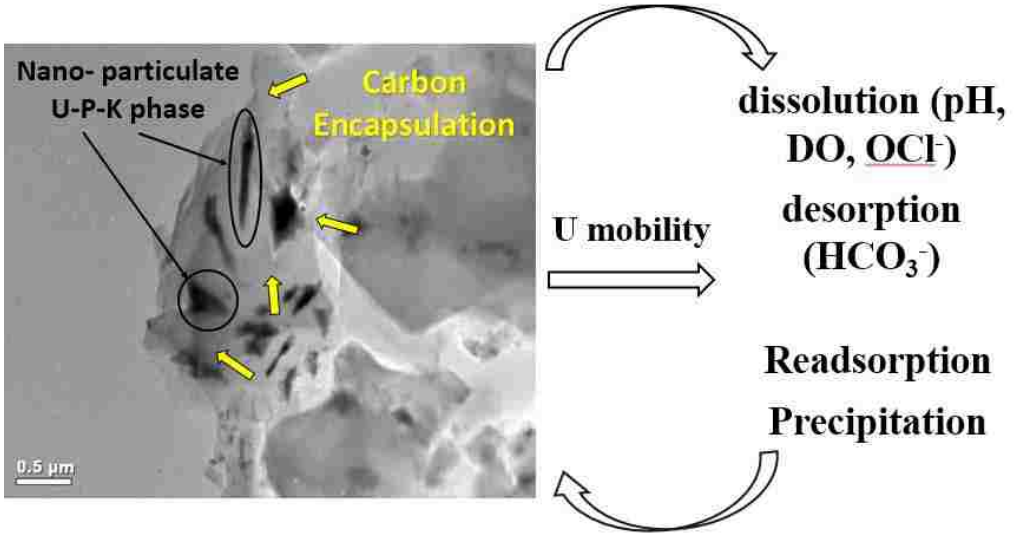

Figure 5.1 TOC art used in the paper showing the presence of submicron U(IV) and U(VI) phases whose mobility is goverened by few processes explained in the conceptual model.

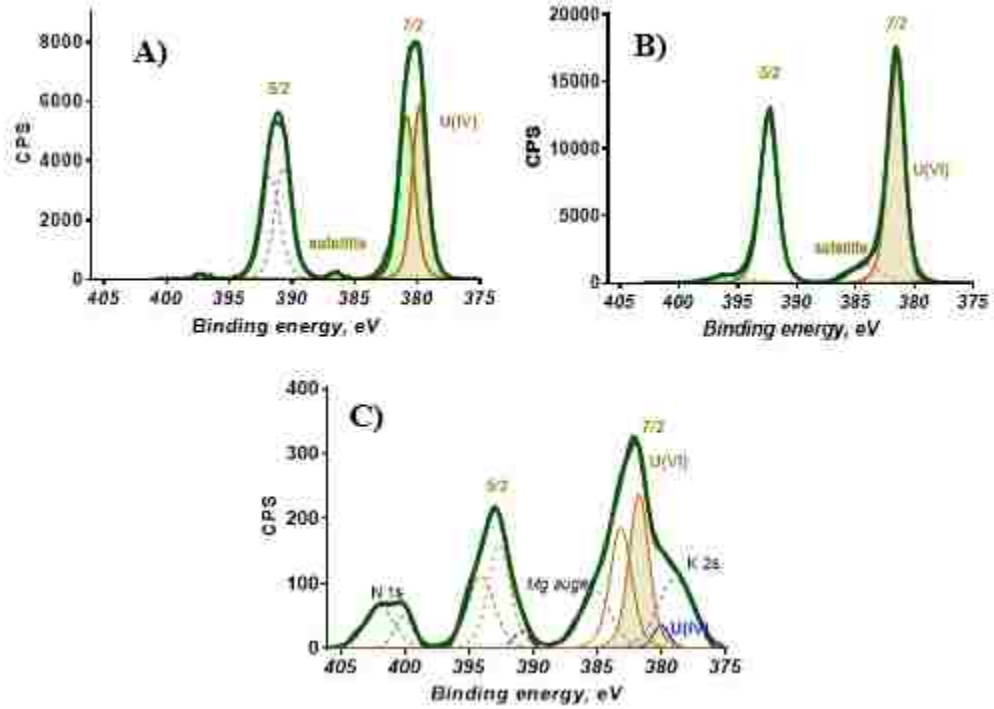

Figure 5.2 Oxidation states (bulk and surface) and co-ordination of U in unreacted Jackpile-Paguate mine waste samples. **A)** Reference XPS spectra for U(IV) using uraninite [UO_2] **B)** Reference XPS spectra for U(VI) using becquerelite [$Ca(UO_2)_6O_4(OH)_6 \cdot 8(H_2O)$] **C)** High resolution X-ray Photoelectron Spectroscopy (XPS) spectra of U in unreacted waste.

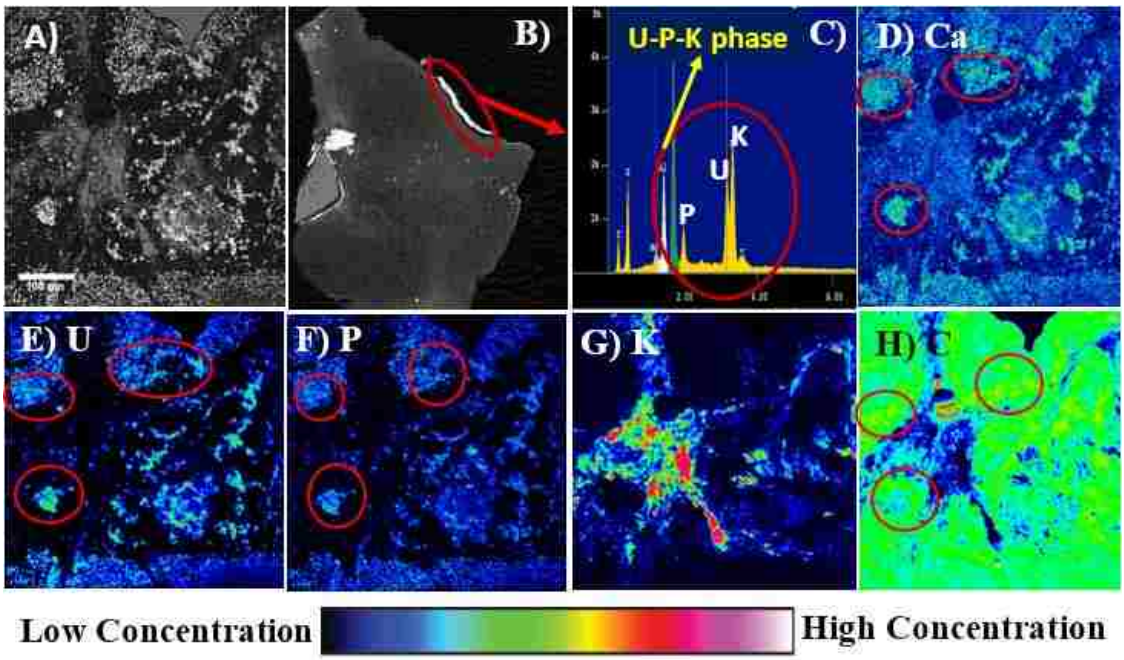

Figure 5.3 Electron Microprobe (EM) analysis of the Jackpile-Paguate mine waste sediments. **A)** BSE image (leftmost) showing the presence of submicron U-phases encapsulated by carbon where, the mapping was performed. **B)** Electron Microprobe (EM) BSE image of a polished sample showing rock fragments with surface aggregates of U-P-K (red arrow). **C)** Energy Dispersive Spectrum (EDS) confirming the presence of a U-P-K phase showing distinct U, P and K peaks (red circle). **D)** Calcium map **E)** Uranium map **F)** Phosphorous map **G)** pottasium map **H)** Carbon map. Green, yellow, pink and white represent high concentrations of elements and dark blue represents lower concentrations of elements.

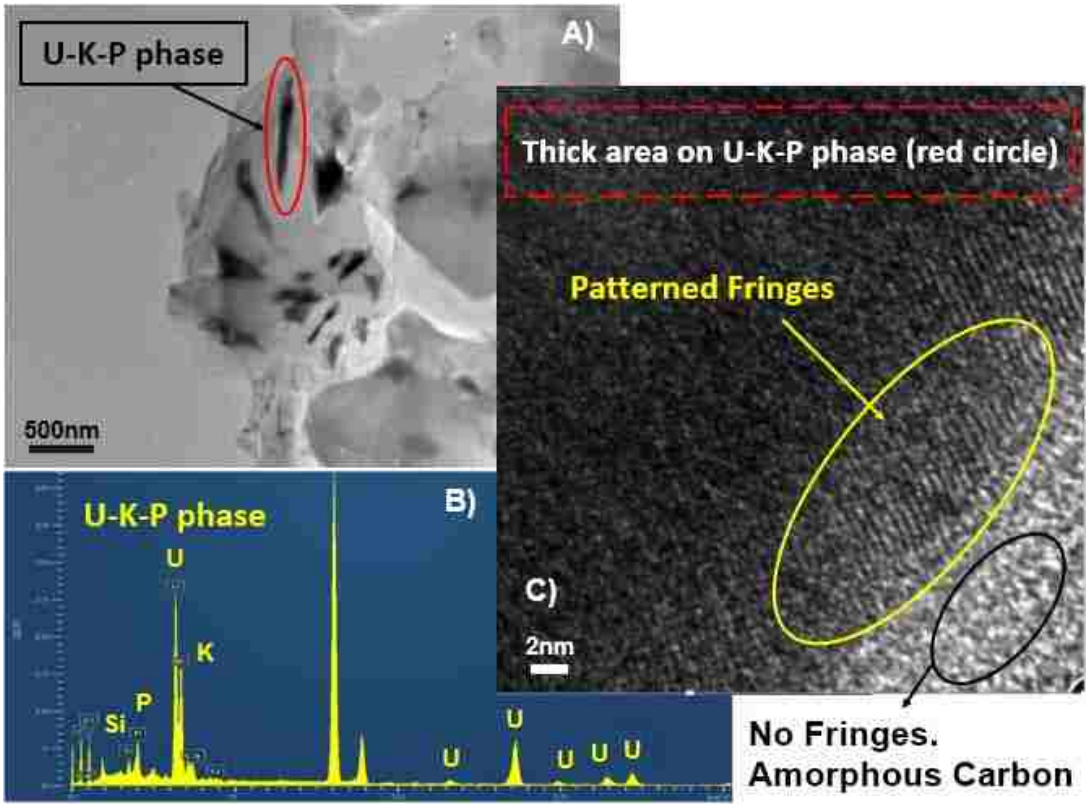

Figure 5.4 Scanning Transmission Electron Microscopy (STEM) imaging of U phases within the mine waste sample. A) STEM image of U-K-Si-P phases in black. B) Energy Dispersive Spectrum (EDS) on grain 1, confirming the presence of a U-K-Si-P phase. C) High Resolution Selected Area Electron Diffraction (HR-SAED) analysis on grain 1 (U-K-Si-P phase) showing patterned fringes (in yellow) suggesting the phase to be crystalline. The lack of patterned fringes around the U-K-Si-P phase suggests the presence of an amorphous phase possible organic matter in the mine waste sample.

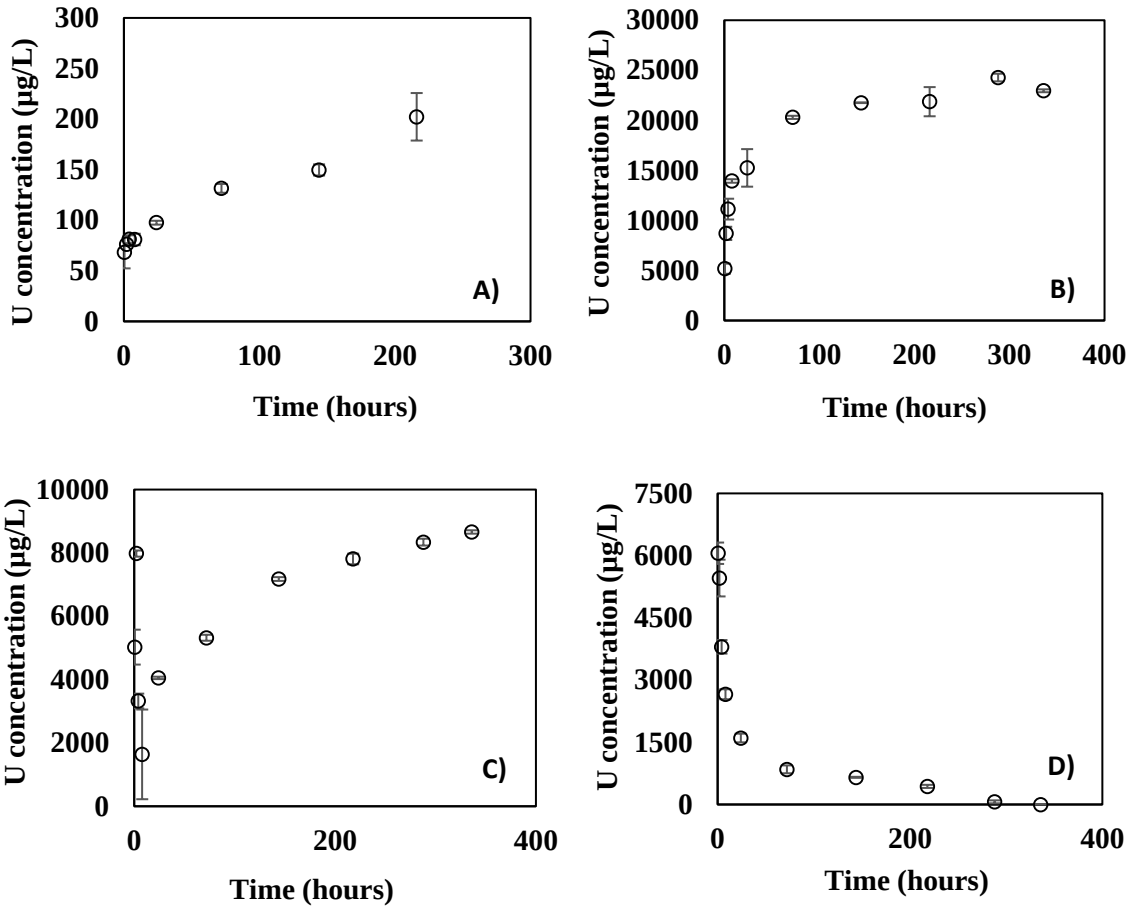

Figure 5.5 Uranium trends for batch experiments on Laguna ore samples reacted with A) 18MΩ water pH 5.4 B) 10mm bicarbonate ($NaHCO_3$) solution pH 7.5 C) 5.6-6% NaOCl solution, pH 7.5 D) 5mM $NaHCO_3$ + 2.8-3% NaOCl solution, pH 7.5 and E) 10mM $NaHCO_3$ + 5.6-6% NaOCl solution, pH 7.5. The pH of the reagents used in B-E were adjusted using 0.5N NaOH, 0.1N HCl and 35.6N HNO_3.

[redacted]

[redacted] Conclusion.

This dissertation contributes a better understanding of processes affecting the transport of U and V from abandoned mine wastes collected from the Blue Gap/Tachee Claim-28 mine, AZ and Jackpile-Paguate mine, Laguna, NM. Chapter 3 reports on how the Blue Gap/Tachee Claim-28 mine wastes were sequentially reacted in flow-through columns at pH 7.9 (10 mM $NaHCO_3$) and pH 3.4 (10 mM CH_3COOH) to evaluate the effect of environmentally relevant conditions encountered at Blue Gap/Tachee on the release of U and V. The reaction rate constants (k_m) for the dissolution of uranyl-vanadate (U-V) minerals predominant at Blue Gap/Tachee were obtained from simulations with the reactive transport software, PFLOTRAN. The estimated reaction rate constants were within one order of magnitude for pH 7.9 (k_m = 4.8x10^{-13} mol cm^{-2} sec^{-1}) and pH 3.4 (k_m = 3.2x10^{-13} mol cm^{-2} sec^{-1}). However, the estimated equilibrium constants (K_{eq}) for U-V bearing minerals were more than six orders of magnitude different for reaction at circumneutral pH (K_{eq} = 10$^{-38.65}$) compared to acidic pH (K_{eq} = 10$^{-44.81}$). These results coupled with electron microscopy data suggest that the release of U and V is affected by water pH and the crystalline structure of U-V bearing minerals.

Chapter 4 describes the crystal chemistry of U-V bearing minerals occurring in the Blue Gap/Tachee mine wastes that was investigated using various spectroscopy, electron microscopy and diffraction techniques. The diffraction lines in the X-ray diffractogram of these U-V bearing minerals showed agreement with most peaks of the synthetic carnotite from literature. The C in the U-V bearing mineral phase was found to co-occur as an organic carbon inclusion based on results from the bright field

transmission electron microscopy (BFTEM) imaging, energy filter transmission electron microscopy (EFTEM), and electron energy loss spectroscopy (EELS). Quantitative electron microprobe analysis suggested the elemental composition of U-V bearing minerals was at a K:U:V ratio of 1:2:2.1 with an empirical stoichiometry similar to that of the anhydrous carnotite that differ in d-spacing. Discrepancies between measured (U-V bearing minerals) and calculated (anhydrous carnotite) diffraction ring patterns can be attributed to differences in the degree of hydration, suggesting the U-V bearing minerals were hydrated crystalline carnotite. Results from this investigation provide an improved understanding on the crystal chemistry of naturally occurring U-V bearing minerals in abandoned mine wastes.

Chapter 5 documents the mobility of U from submicron U(IV) and U(VI) mineral phases in the Jackpile-Paguate mine wastes under oxidizing conditions that was investigated by integrating laboratory experiments, spectroscopy, microscopy, and diffraction techniques. Submicron U(VI) and U(IV) phases were found to co-occur at the mine waste surfaces at a 19:1 ratio, based on results from XPS. Additionally, microscopy and XRD analyses on these mine wastes identified these U-minerals to occur predominantly as coffinites and U-P-K phases that were encapsulated by organic carbon. Results from mine waste reactions with 10 mM $NaHCO_3$ mobilized the highest U concentrations under ambient DO concentrations. The results from this study provide relevant information about how the reactivity of submicron U-bearing mine wastes in the Jackpile-Paguate Mine can affect U mobility. For instance, elevated U concentrations (35.3 to 772 mg L-1) have been measured at alkalinity and pH conditions (average pH 7.5, 70 – 372 mg L^{-1} $CaCO_3$) in the Rio Paguate just across the Jackpile-Paguate Mine.[20]

The pH and alkalinity conditions selected for the experiments conducted in Chapter 5 are relevant to the Rio Paguate. This information provides insights about the reactivity of U-micro particles in abandoned mine wastes into neighboring water resources to assess risks for human exposure.

Contribution of this Dissertation to the Body of Knowledge.

The work presented in this dissertation provides the following contributions to the body of knowledge:

- Dissolution of the U-V bearing mineral is a relevant mechanism that affects the reactive transport of U and V from the Blue Gap/Tachee Claim-28 abandoned U mine. (Chapter 3).
- The U-V bearing minerals in the Blue Gap/Tachee mine wastes were identified as hydrated carnotites that contain carbon inclusions. (Chapter 4).
- The presence of submicron U(VI) and U(VI) phases was identfied in the organic rich sediments of the Jackpile-Paguate mine. The presence U-P-K bearing and coffinite were also identified in these mine wastes. (Chapter 5).
- The highest U release was observed during batch reactions with 10 mM $NaHCO_3$ solution containing ambient dissolved oxygen concentrations. (Chapter 5).

This dissertation offers an improved understanding on the role of thermodynamics, crystallinity, stoichiometry, and solution chemistry on the reactive transport of U and V from mine waste sites that pose as a threat to neighboring surface and ground water quality. This knowledge is important for the development of risk assessment and remediation strategies that benefit the communities proximate to such sites. Additionally, outcomes this work have relevant implications for resource recovery.

Additional Materials and Methods.

Acid digestions were conducted to assess the total acid extractable metal concentrations between unreacted and reacted mine wastes. For unreacted mine waste 3 mL of hydrochloric acid (HCl), 3 mL of nitric acid (HNO_3^-) and 3 mL of hydrofluoric acid (HF) were added into 50 mL Teflon digestion tubes containing 1 ± 0.002 g of mine waste sample. Similarly for reacted mine waste (collected after reaction with CH_3COOH) 1 mL of each reagent (HCl, HF and HNO_3^-) was added to 50 mL Teflon digestion tubes containing 0.1 ± 0.002 g of mine waste sample. All reagents are of Ultra High Purity (UHP) grade. The digestion tubes were then heated using a Digi prep MS SCP Science block digester at 95°C for 2 h, followed by dilution of acid extracts from reacted and unreacted mine waste to 50 (unreacted) and 25 (reacted) mL using 2% HNO_3. The diluted samples are then filtered using 0.45 μm filters to remove any suspended or undissolved solids before analysis.

Acid extracts and aliquots from column experiments were analyzed for elemental concentrations using a PerkinElmer Optima 5300DV ICP-OES. Trace metals below the detection limit of ICP-OES were measured using PerkinElmer NexION 300D (Dynamic Reaction Cell) Inductively Coupled Plasma-Mass Spectrometer (ICP-MS). Both ICPs are calibrated with calibration standards and QA/QC measures are taken to ensure quality data.

A TEM analysis was conducted on mine waste samples to identify the crystallinity of various U-V bearing minerals using a Selected Area Electron Diffraction technique (SAED). A JEOL 2010 High Resolution Transmission Electron Microscope (HR-TEM) fitted with a GATAN Orius high speed CCD camera and an Oxford INCA system with an ultra-thin window Energy Dispersive Spectroscopy (EDS) detector was used in sample analysis. Drops of unaltered sediments suspended in acetone were dropped onto standard holey carbon film-covered Cu TEM grids using a pipette. Acetone was allowed to evaporate in air and then the dry samples were loaded onto a Gatan cryotransfer holder to observe frozen hydrated specimens for cryo-electron microscopy. Before loading the grid, zeolite crystals inside the cryotransfer holders were allowed to dry overnight using a vacuum pump to avoid cooling obstruction due to frozen water inside the holder. The dry and loaded cryotransfer holders were then loaded into the HR-TEM and allowed to reach a temperature of -180oC using liquid nitrogen before the analysis. The INCA EDS detector was used to determine the elemental composition of the specific targeted crystal. After identification, SAED analysis was performed on the identified crystals to observe their crystallinity.

[redacted]

A polished section of the mine waste sample was mapped for elemental distribution using the µ-SXRF beam line (BL) 10-2 at the Stanford Synchrotron Radiation Light Source (SSRL). The maps were collected using a Si (111) phi, 90 double crystal monochromator at a 50 µm resolution upto 17200 eV X-ray energies, just above the U L_{III} edge. All data processing was conducted using the Microanalysis Toolkit software program.

[redacted]

Below are the supporting equations that were used in PFLOTRAN to calculate the change in concentration while taking the dominant processes into account. The total aqueous concentrations (Ψj) [ML-3] for a particular species j is given by equation [2], where Cj and Ci [ML-3] represent concentrations of jth primary species from 1 to Nc and ith secondary species that varies from 1 to Nsec in the liquid phase.

$$\Psi_j = C_j + \sum_{i=1}^{N_{sec}} v_{ji} C_i \quad (2)$$

The secondary species concentrations (C_i) are estimated in terms of primary species concentration using equation [3] with known values of equilibrium constant K_{eq_i} [-], and activity coefficients γ_i and γ_j that are computed using the Debye-Hückel equation that,

$$C_i = (\gamma_i)^{-1} K_{eq_i} \prod_{j=1}^{N_c} (\gamma_j C_j)^{v_{ji}} \quad (3)$$

Correspond to the homogeneous aqueous reactions described in equation [4a] and [4b].

$$\sum_{j=1}^{N_c} v_{ji} A_j \leftrightarrow A_i \quad (4a)$$

$$\sum_{j=1}^{N_c} v_{jm} A_j \leftrightarrow M_m \quad (4b)$$

These reactions are written in their canonical form where A_j denotes the primary species, A_i aqueous secondary species, v_{ji} and v_{jm} [-] stoichiometric coefficient for aqueous and mineral reactions respectively, and M_m denotes minerals.[213] The reaction rate (I_m) [$ML^{-3}T^{-1}$] is given by equation [5] based on the transition state theory where Q_{IAP_m} [$M\ L^{-3}T^{-1}$] is the ion activity product [6], a_m [L^{-1}] is the new specific surface area that is a function of porosity (φ), k_m is reaction rate constant, $\mathcal{P}_m$ [-] is a prefactor that accounts for the pH

dependence and ζ_m [-] is a factor whose value is 0 or 1 depending if $K_{eq_m} Q_{IAP_m} \leq 1$and $\varphi_m = 0$ or $K_{eq_m} Q_{IAP_m} > 1$ and n_m [-] is fitting parameter.[214] Water-rock reactions typically follow a non-linear rate law that is sensitive to this fitting parameter 'n_m' in PFLOTRAN.[214, 215, 216]

$$I_m = -k_m a_m \mathcal{P}_m \left(1 - (K_{eq_m} Q_{IAP_m})^{n_m}\right)\zeta_m \quad (5)$$

$$Q_m = \prod_{k=1}^{N_c} (\gamma_k^l C_k^l)^{v_{km}} \quad (6)$$

The sign convention used in PFLOTRAN is that if the rate is positive the mineral is precipitating and if it is negative the mineral is dissolving. The change in the material properties like porosity φ and surface area a_m due to mineral precipitation and dissolution reactions are accounted through equations [7] and [8], where, φ_m [-], ϕ_m [-], ϕ_m^0 [-] and $a_m{}^o$ [L^{-1}] denote porosity of the m^{th} mineral, volume fraction of the m^{th} mineral, initial volume fraction of the m^{th} mineral and initial mineral specific surface area.

$$\varphi = 1 - \sum_m \varphi_m \quad (7)$$

$$a_m = a_m^0 \left(\frac{\phi_m}{\phi_m^0}\right)^{n_m} \quad (8)$$

The porosity, φ = 0.25, of the Blue Gap/Tachee mine waste sediments were estimated using equation [9] where the bulk density (ρ_b = 1.65 gm cm^{-3} [ML^{-3}]) and particle density (ρ_p = 2.25 gm cm^{-3} [ML^{-3}]) were acquired experimentally.

$$\varphi = 1 - \frac{\rho_b}{\rho_p} \quad (9)$$

However, other material properties like tortuosity (tau) and aqueous diffusion coefficient [M^2T^{-1}] were assumed to be, *tau* = 1 and 10^{-9} m^2 s^{-1} respectively. The assumption for tortuosity was made for simplification purposes, while the assumption for aqueous diffusion coefficient was made based on the diffusion coefficients of H^+, CO_3^{2-}, HCO_3^{2-}, $Ca_2UO_2(CO_3)_3^0$, $CaUO_2(CO_3)_3^{2-}$, $UO_2(CO_3)_2^{2-}$ and Ca^{2+} that were all found to be around 10^{-9} m^2 s^{-1} at 25°C.[217, 218] The dirichlet initial and boundary conditions were imposed on the 1D reactive transport of metals over time during reaction with 10 mM $NaHCO_3$ and 10 mM CH_3COOH. The initial surface area $a_m{}^o$ (L^{-1}) of U-V bearing minerals in the mine waste sediments is calculated using equation [10] in cm^2 cm^{-3}. The specific mineral surface area $a_m{}^o$, [L^{-1}] is defined as

$$a_m^0 = \frac{A_m}{V} = \frac{A_m}{V_m}\frac{V_m}{V} = \frac{a_m}{v_m}\,\phi_m \tag{10}$$

where ϕ_m = V_m/V and V_m are the volume fraction and volume of the m^{th} mineral contained in the REV of volume V, respectively, and a_m [L^{-1}] and v_m [L^3] refer to the area and volume of a single sphere of radius r_m [L],

$$a_m = 4\pi {r_m}^2 \tag{11}$$

$$v_m = \frac{4}{3}\pi {r_m}^3 \tag{12}$$

Thus the surface area a_m^0 [L^{-1}] further simplifies to,

$$a_m^0 = \frac{3}{r_m}\,\phi_m \tag{13}$$

The surface area of the U-V bearing mineral was estimated using equation [13] by considering the average particle size of the mine waste used in batch (<63 µm) and column (120-355 µm) based on the assumption that 1) all of the U-phases in the mine

waste are U-V bearing minerals and 2) the U-V bearing minerals area spherical in shape. The assumptions were made based on prior knowledge on the Blue Gap/Tachee mine site,[1] where U-V bearing mineral was identified as the dominant U-phase in the mine waste. The shape of the U-V bearing minerals was assumed to be spherical for simplifying the calculations.

Table 7.1 Thermodynamic equilibrium constants (at T = 25°C) for aqueous and solid phase U(VI) used in the reactive transport model (PFLOTRAN).

U(VI) Aqueous and Mineral species	Log K_{eq}	Reference	Implement ation in the model
Primary species			
$H_2O = OH^- + H^+$	-14.00	Shock et al., 1988[219, 220]	Fixed
$U^{4+} + 1.5\ H_2O + 0.25O_2 = UO_2^{2+} + 3\ H^+$	-13.2076	Cox et al., 1989[221]	Fixed
$VO^{2+} + 0.5\ H_2O + 0.5O_2 = VO^{2+} + H^+$	-3.8528	Shock et al., 1988[219]	Fixed
$H_3AsO_4 + H^+ = H_2AsO_4^-$	2.2492	Shock et al., 1988[219]	Fixed
$H_2CO_3 = HCO_3^- + H^+$	6.37	Shock et al., 1988[219]	Fixed
$HCO_3^- = CO_3^{2-} + H^+$	10.33	Shock et al., 1988[219]	Fixed
$HCO_3^- + H^+ = H_2O + CO_2$ (aq)	-6.3447	Shock et al., 1988[219]	Fixed
Aqueous complexes			
$Al^{3+} + H_2O = AlOH^{2+} + H^+$	4.971	Pokrovskii et al., 1995[222]	Fixed
$Al^{3+} + 2H_2O = Al(OH)_2^+ + H^+$	10.594	Pokrovskii et al., 1995[222]	Fixed
$Al^{3+} + 3H_2O = Al(OH)_3$ (aq) + $3H^+$	16.1577	Pokrovskii et al., 1995[222]	Fixed
$Al^{3+} + 4H_2O = Al(OH)_4^- + H^+$	22.8833	Pokrovskii et al., 1995[222]	Fixed
$Ca^{2+} + H_2O = CaOH^+ + H^+$	12.85	Baes et al., 1976[223]	Fixed
$Ca^{2+} + HCO_3^- = CaCO_3$ (aq) + H^+	7.0017	Johnson. J. W et al. 1992[224]	Fixed
$Ca^{2+} + HCO_3^- = CaHCO_3^+$	-1.0467	Johnson. J. W et al. 1992[224]	Fixed
$Mg^{2+} + OH^- = MgOH^+$	-2.210	Johnson. J. W et al. 1992[224]	Fixed
$Mg^{2+} + HCO_3^- = MgCO_3$ (aq) + H^+	7.3499	Johnson. J. W et al. 1992[224]	Fixed
$Mg^{2+} + HCO_3^- = MgHCO_3^+$	-1.0357	Johnson. J. W et al. 1992[224]	Fixed

$Mn^{2+} + H_2O = MnOH^+ + H^+$	10.59	Baes et al., 1976[223]	Fixed
$Mn^{2+} + 3H_2O = Mn(OH)_3^- + 3H^+$	34.22	Wagman et al., 1982[225]	Fixed
$Mn^{2+} + 4H_2O = Mn(OH)_4^{2-} + 4H^+$	48.3	Baes et al., 1976[223]	Fixed
$Na^+ + H_2O = NaOH\ (aq) + H^+$	14.79	Johnson. J. W et al. 1992[224]	Fixed
$Na^+ + HCO_3^- = NaHCO_3\ (aq)$	-0.1541	Wagman et al., 1982[225]	Fixed
$K^+ + H_2O = KOH\ (aq) + H^+$	14.46	Baes et al., 1976[223]	Fixed
$H^+ + SO_4^{2-} = HS^- + 2O_2$	132.52	Shock et al., 1988[219]	Fixed
$Fe^{2+} + H^+ + 0.25\,O_2 = Fe^{3+} + 0.5\,H_2O$	-7.765	Shock et al., 1988[219]	Fixed
$Fe^{2+} + H_2O = FeOH^+ + H^+$	9.5	Baes et al., 1976[223]	Fixed
$Fe^{2+} + 2H_2O = Fe(OH)_2\ (aq) + H^+$	20.60	Baes et al., 1976[223]	Fixed
$Fe^{3+} + 2H_2O = Fe(OH)^{2+} + 2H^+$	5.67	Baes et al., 1976[223]	Fixed
$Fe^{3+} + 3H_2O = Fe(OH)_3\ (aq) + 3H^+$	12	Baes et al., 1976[223]	Fixed
$Fe^{2+} + 3H_2O = Fe(OH)_3^- + 3H^+$	31	Baes et al., 1976[223]	Fixed
$Fe^{3+} + 4H_2O = Fe(OH)_4^- + 4H^+$	21.6	Baes et al., 1976[223]	Fixed
$Fe^{2+} + 4H_2O = Fe(OH)_4^{2-} + 4H^+$	46	Baes et al., 1976[223]	Fixed
$Fe^{2+} + CO_3^{2-} = FeCO_3\ (aq)$	5.5988	Turner et al., 1981[226]	Fixed
$Fe^{2+} + HCO_3^- = FeCO_3^+ + H^+$	0.6088	Turner et al., 1981[226]	Fixed
$Fe^{2+} + HCO_3^- = FeHCO_3^+$	-2.72	Mattigod et al., 1979[227]	Fixed
$Li^+ + H_2O = LiOH\ (aq) + H^+$	13.64	Baes et al., 1976[223]	Fixed
$UO_2^{2+} + H^+ = U^{3+} + 0.75O_2 + 0.5H_2O$	62.6291	Grenthe et al., 1992[228]	Fixed
$UO_2^{2+} + 2H^+ = U^{4+} + H_2O + 0.5O_2$	32.4999	Grenthe et al., 1992[228]	Fixed
$U^{4+} + 1.5H_2O + 0.25O_2 = UO_2^{2+} + 3H^+$	-13.2076	Grenthe et al., 1992[228]	Fixed

$UO_2^{2+} + H_2O = UO_2OH^+ + H^+$	5.2073	Grenthe et al., 1992[228]	Fixed
$UO_2^{2+} + 2H_2O = UO_2(OH)_2$ (aq) $+ 2H^+$	10.3146	Grenthe et al., 1992[228]	Fixed
$UO_2^{2+} + 3H_2O = UO_2(OH)_3^- + 3H^+$	19.2218	Grenthe et al., 1992[228]	Fixed
$UO_2^{2+} + 4H_2O = UO_2(OH)_4^{2-} + 4H^+$	33.0291	Grenthe et al., 1992[228]	Fixed
$2UO_2^{2+} + 1H_2O = (UO_2)_2OH^{3+} + H^+$	2.7072	Grenthe et al., 1992[228]	Fixed
$2UO_2^{2+} + 2H_2O = (UO_2)_2(OH)_2^{2+} + 2H^+$	5.6346	Grenthe et al., 1992[228]	Fixed
$3UO_2^{2+} + 4H_2O = (UO_2)_3(OH)_4^{2+} + 4H^+$	11.929	Grenthe et al., 1992[228]	Fixed
$3UO_2^{2+} + 5H_2O = (UO_2)_3(OH)_5^+ + 5H^+$	15.5862	Grenthe et al., 1992[228]	Fixed
$3UO_2^{2+} + 7H_2O = ($ $(UO_2)_3(OH)_7^- + 7H^+$	31.0508	Grenthe et al., 1992[228]	Fixed
$4UO_2^{2+} + 7H_2O = (UO_2)_4(OH)_7^+ + 7H^+$	21.9508	Grenthe et al., 1992[228]	Fixed
$UO_2^{2+} + HCO_3^- = UO_2CO_3(aq) + H^+$	0.6634	Grenthe et al., 1992[228]	Fixed
$UO_2^{2+} + 2HCO_3^- = UO_2(CO_3)_2^{2-} + 2H^+$	3.7467	Grenthe et al., 1992[228]	Fixed
$UO_2^{2+} + 3HCO_3^- = UO_2(CO_3)_3^{4-} + 3H^+$	9.4302	Grenthe et al., 1992[228]	Fixed
$2UO_2^{2+} + 3H_2O + HCO_3^- = (UO_2)_2CO_3(OH)_3^- + 4H^+$	11.2229	Grenthe et al., 1992[228]	Fixed
$2Ca^{2+} + UO_2^{2+} + 3CO_3^{2-} = Ca_2UO_2(CO_3)_3$ (aq)	-30.04	Dong et al., 2006[128]	Fixed
$Ca^{2+} + UO_2^{2+} + 3CO_3^{2-} = CaUO_2(CO_3)_3^{2-}$	-27.18	Dong et al., 2006[128], Bernhard et al.., 2001[229]	Fixed
$VO^{2+} + H^+ = V^{3+} + 0.5H_2O + 0.25O_2$	14.9945	Israel et al. ,1976[230]	Fixed
$VO^{2+} + 0.5H_2O + 0.25O_2 = VO_2^+ + H^+$	-3.8528	Shock et al., 1988[219]	Fixed
$V^{3+} + 3H_2O + 0.5O_2 = VO_4^{3-} + 6H^+$	9.6002	Wagman et al., 1982[225]	Fixed
$VO^{2+} + 2H_2O = (VO)_2(OH)_2^{2+} + 2H^+$	6.67	Baes et al., 1976[223]	Fixed
$VO^{2+} + 2.5H_2O + 0.25O_2 = H_2VO_4^- + 3H^+$	3.2394	Johnson. J. W et al. 1992[224]	Fixed

$VO^{2+} + 2.5H_2O + 0.25O_2 = HVO_4^{2-} + 4H^+$	11.3024	Johnson. J. W et al. 1992[224]	Fixed
$V^{3+} + H_2O = VOH^{2+} + H^+$	2.260	Baes et al., 1976[223]	Fixed
$VO^{2+} + H_2O = VOOH^+ + H^+$	5.67	Baes et al., 1976[223]	Fixed
$VO_4^{3-} + 2H^+ = VO_3OH^{2-}$	-14.26	Baes et al., 1976[223]	Fixed
$V^{3+} + 2H_2O = V(OH)_2^+ + 2H^+$	5.9193	Langmuir et al., 1978[150]	Fixed
$2V^{3+} + 2H_2O = V_2(OH)_2^{4+} + 2H^+$	3.80	Baes et al., 1976[223]	Fixed
$VO_2^+ + 2H_2O = VO(OH)_3$ (aq) + H^+	3.30	Baes et al., 1976[223]	Fixed
$H_2AsO_4^- + H^+ = AsH_3$ (aq) + $2O_2$	149.3941	Sergeyeva et al., 1969[231]	Fixed
$H_2AsO_4^- = H_2AsO_3^- + 0.5O_2$	29.0857	Shock et al., 1988[219]	Fixed
$H_2AsO_4^- = AsO_2^- + 3H_2O + 0.5O_2$	29.0746	Grenthe et al., 1992[228]	Fixed
$H_2AsO_3^- + 4H^+ = As(OH)_3$ (aq)	-9.2048	Grenthe et al., 1992[228]	Fixed
Solid Mineral phases			
Calcite $CaCO_3 + H^+ = Ca^{2+} + HCO_3^-$	1.8487	Helgeson et al. 1978[232]	Fixed
Becquerelite $Ca(UO_2)_6O_4(OH)_6 \cdot 8H_2O + 14H^+ = 6UO_2^{2+} + Ca^{2+} + 18H_2O$	29.23	Casas et al., 1997[233]	Fixed
Quartz $SiO_2 = SiO_2$ (aq)	-3.9993	Helgeson et al. 1978[232]	Fixed
Boehmite $AlO_2H + 3H^+ = Al^{3+} + 2H_2O$	7.5642	Pokrovskii et al., 1995[222]	Fixed
Diaspore $AlHO_2 + 3H^+ = Al^{3+} + 2H_2O$	7.1603	Pokrovskii et al., 1995[222]	Fixed
Gibbsite $Al(OH)_3 + 3H^+ = Al^{3+} + 3H_2O$	7.756	Pokrovskii et al., 1995[222]	Fixed
Hercynite $FeAl_2O_4 + 8H^+ = Fe^{2+} + 2Al^{3+} + 4H_2O$	28.8484	Robie et al. 1995[234]	Fixed

Spinel $Al_2MgO_4 + 8H^+ = Mg^{2+} + 2Al^{3+} + 4H_2O$	37.6295	Helgeson et al. 1978[232]	Fixed
Portlandite $Ca(OH)_2 + 2H^+ = Ca^{2+} + 2H_2O$	22.5552	Robie et al. 1995[234]	Fixed
Wustite $Fe_{0.947}O + 2H^+ = 0.1060Fe^{3+} + 0.8410Fe^{2+} + H_2O$	12.4113	Wagman et al., 1982[225]	Fixed
Periclase $MgO + 2H^+ = Mg^{2+} + H_2O$	21.3354	Helgeson et al. 1978[232]	Fixed
Brucite $Mg(OH)_2 + 2H^+ = Mg^{2+} + 2H_2O$	16.2980	Helgeson et al. 1978[232]	Fixed
Ferrihydrite $Fe_2O_3 + 3H^+ = Fe^{3+} + 3H_2O$	4.896	Stumm and Morgan[235]	Fixed
Goethite $FeOOH + 3H^+ = Fe^{3+} + 2H_2O$	0.5345	Robie et al. 1995[234]	Fixed
Hematite $Fe_2O_3 + 6H^+ = 2Fe^{3+} + 3H_2O$	0.1086	Helgeson et al. 1978[232]	Fixed
Uraninite $UO_2 + 4H^+ = U^{4+} + 2H_2O$	-4.8372	Cox et al., 1989[221]	Fixed
Schoepite $UO_3.2H_2O + 2H^+ = UO^{2+} + 3H_2O$	4.8333	Grenthe et al., 1992[228]	Fixed
Rutherfordine $UO_2CO_3 + H^+ = HCO_3^- + UO_2^{2+}$	-13.9	Meinrath 1993[236]	Fixed
Boltwoodite-Na $Na_{.7}K_{.3}(H_3O)(UO_2)SiO_4.H_2O + 3H^+ = 0.3K^+ + 0.7Na^+ + SiO_2$ (aq)	14.5834	Hemingway et al., 1982	Fixed
Metaschoepite $UO_3.2H_2O + 2H^+ = UO2^{2+} + 3H_2O$	-22.29 (circumneutral), -5.26 (acidic)	Meinrath 1993[236], Riba et al., 2005[148]	Fixed
Uranophane $Ca(UO_2)_2(SiO_3)_2(OH)_2 + 6H^+ = Ca^{2+} + 2SiO2$	17.2850	Wagman et al., 1982[225]	Fixed
$UO_2CO_3 + H^+ = HCO_3^- + UO2^{2+}$	-4.1267	Grenthe et al., 1992[228]	Fixed
$CaUO_4 + 4H^+ = Ca^{2+} + UO_2^{2+} + 2H_2O$	15.9420	Grenthe et al., 1992[228]	Fixed
$UO_3.2H_2O + 2H^+ = UO_2^{2+} + 3H_2O$	4.833	Grenthe et al., 1992[228]	Fixed

Schoepite-dehydrated $0.9UO_3.0.9H_2O + 2H^+ = UO^{2+} + 1.9H_2O$	5.0167	Grenthe et al., 1992[228]	Fixed
$V_2O_4 + 4H^+ = 2H_2O + 2VO^{2+}$	8.5719	Wagman et al., 1982[225]	Fixed
$V_3O_5 + 8H^+ = VO^{2+} + 2V^{3+} + 4H_2O$	13.4312	Wagman et al., 1982[225]	Fixed
$V_4O_7 + 10H^+ = 2V^{3+} + 2VO^{2+} + 5H_2O$	18.7946	Wagman et al., 1982[225]	Fixed
Carnotite $(K_2(UO_2)_2(VO_4)_2)^* = 2K^+ + 2UO2^{2+} VO4^{3-}$	*-56.3811*	*Langmuir et al., 1978[150]*	*Varied*
$Mg_2V_2O_7 + H2O = 2H^+ + 2Mg^{2+} + 2VO_4^{3-}$	-30.9025	Wagman et al., 1982[225]	Fixed
$MgV_2O_6 + 2H_2O = Mg^{2+} + 2VO_4^{3-} + 4H^+$	-45.8458	Wagman et al., 1982[225]	Fixed
Tyuyamunite $Ca(UO_2)_2(VO_4)_2 = Ca^{2+} + 2UO_2^{2+} + 2VO_4^{3-}$	-53.3757	Langmuir et al., 1978[150]	Fixed
Arsenopyrite $FeAsS + 1.5H_2O = 0.5H^+ + 0.5AsH_3$ (aq)	-14.4453	Wagman et al., 1982[225]	Fixed
Arsenolite $As_2O_3 + 3H_2O = 2H^+ + 2H_2AsO_3^-$	-19.8365	Robie et al. 1995[234]	Fixed
$(UO_2)_2As_2O_7 + 2H^+ + H_2O = 2H_2AsO_4^- + 2UO_2^{2+}$	7.7066	Grenthe et al., 1992[228]	Fixed
$(UO_2)_3(AsO_4)_2 + 4H^+ = 2H_2AsO_4^- + 3UO_2^{2+}$	9.3177	Grenthe et al., 1992[228]	Fixed
$KUO_2AsO_4 + 2H^+ = H_2AsO^{4-} + K^+ + UO_2^{2+}$	-4.1741	Wagman et al., 1982[225]	Fixed
$LiUO_2AsO_4 + 2H^+ = H_2AsO_4^- + Li^+ + UO_2^{2+}$	-0.7862	Wagman et al., 1982[225]	Fixed
$UO_2(AsO_3)_2 + 2H_2O = UO_2^{2+} + 2H_2AsO_4^-$	6.9377	Grenthe et al., 1992[228]	Fixed
Surface Complexes			
$>SOUO_2OH$	6.448	Bond et al., 2007[146]	Fixed
$>SOHUO_2CO_3$	2.033	Bond et al., 2007[146]	Fixed

Table 7.2. Other parameters used in the reactive transport model to simulate the experimental release of U and V from mine waste.

Parameter	Value	Implementation in the model
Reaction rate constant (k_m) of carnotite	-	Varied
Reaction rate constant (k_m) of Rutherfordine (UO_2CO_3) (mol cm^{-2}-sec^{-1})	-	Varied
Reaction rate constant (k_m) of metaschoepite ($UO_3.2H_2O$) (mol cm^{-2}-sec^{-1})	-	Varied
Porosity (φ)	0.25	Calculated, Fixed
Tortuosity (tau)	1	Assumed, Fixed
aqueous diffusion coefficient (m^2 s^{-1})	10^{-9}	From Literature, Fixed
Darcy's Flux, q (cm min^{-1})	1.496	Calculated, Fixed
Average U-V bearing mineral diameter (µm) Batch experiments (<63 µm)	32	Assumed based on size fractions to calculate average surface area, fixed
Average U-V bearing mineral diameter (µm) Column Experiments (120-355 µm)	240	Assumed based on size fractions to calculate average surface area, fixed

Table 7.3. Reaction rate constants of metaschoepite and rutherfordine estimated by modelling the reactive transport of U and V during mine waste reaction at circumneutral and acidic conditions.

Mineral phase	**Reaction rate constants (k_m) (mol cm^{-2}-sec^{-1})**
Rutherfordine (UO_2CO_3) (Circumneutral Batch)	$1x10^{-15}$
Metaschoepite ($UO_3.2H_2O$) (Circumneutral Batch)	$2x10^{-16}$

Table 7.4. Parameters used to consider the effect of grain size on the reactive transport of U and V during flow through column experiment with 10 mM $NaHCO_3$. The surface area of U-V bearing minerals was estimated using equation 13. The effective reaction rate constant ($k_{effective} = k*a_m^0$) accounts for the effect of grain surface area on the reactive transport of U and V, where k is the reaction rate constant and a_m^0 is the surface are of U-V bearing minerals.

U-V bearing minerals of different grain sizes	**Average U-V bearing mineral diameter (µm)**	**Estimated U-V bearing mineral surface area (a_m^0) (cm^2 cm^{-3})**	**Reaction rate constant (k_m) (mol cm^{-2}-sec^{-1})**	**Effective reaction rate constant ($k_{effective} = (k_m*a_m^0)$ (mol cm^{-3}-sec^{-1})**
U-V mineral	240	62.5	$4.8x10^{-13}$	$3.0x10^{-11}$
U-V mineral 1	200	75	$4.8x10^{-13}$	$3.6x10^{-11}$
U-V mineral 2	280	53.6	$4.8x10^{-13}$	$2.6x10^{-11}$
U-V mineral 3	120	125	$4.8x10^{-13}$	$6.0x10^{-11}$

Table 7.5. Elemental content of solid samples determined by acid extractions (measured using ICP-OES/MS) of unreacted mine waste and mine waste after sequential reaction with 10 mM $NaHCO_3$ and CH_3COOH solution during flow through column experiments.

Samples	U (mg Kg^{-1})	V (mg Kg^{-1})	As (mg Kg^{-1})	Fe (mg Kg^{-1})
Unreacted mine waste Acid extractable	1912.12	858.01	4.015	715.79
Reacted mine waste Acid extractable	17.79	62.01	1.17	456.89

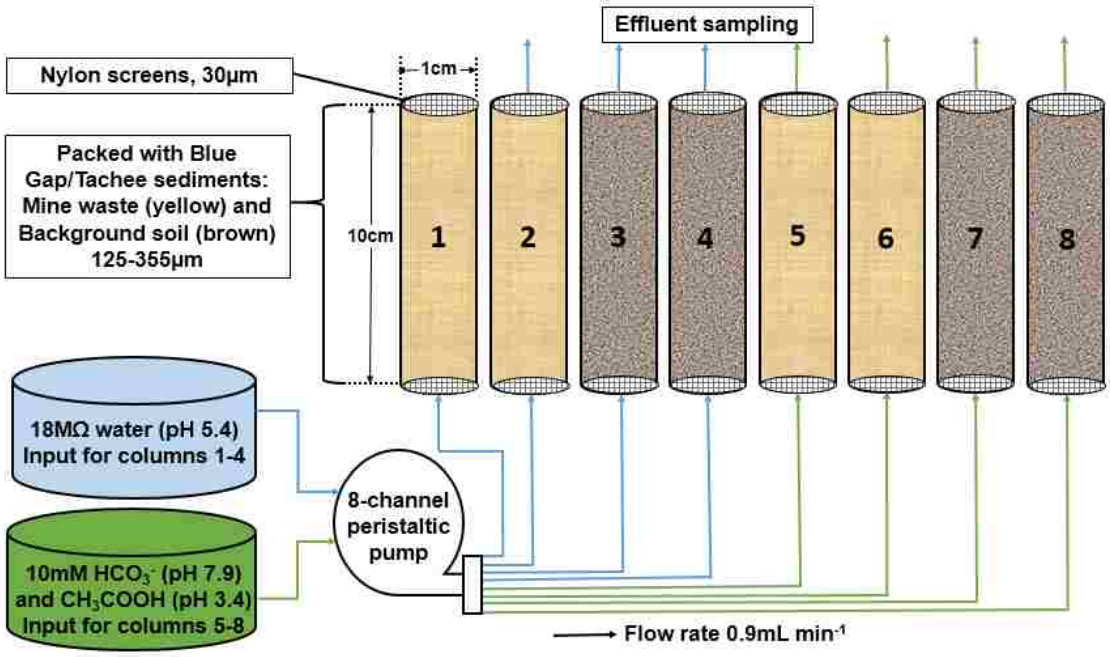

Figure 7.1. Experimental setup of sequential flow through column experiments

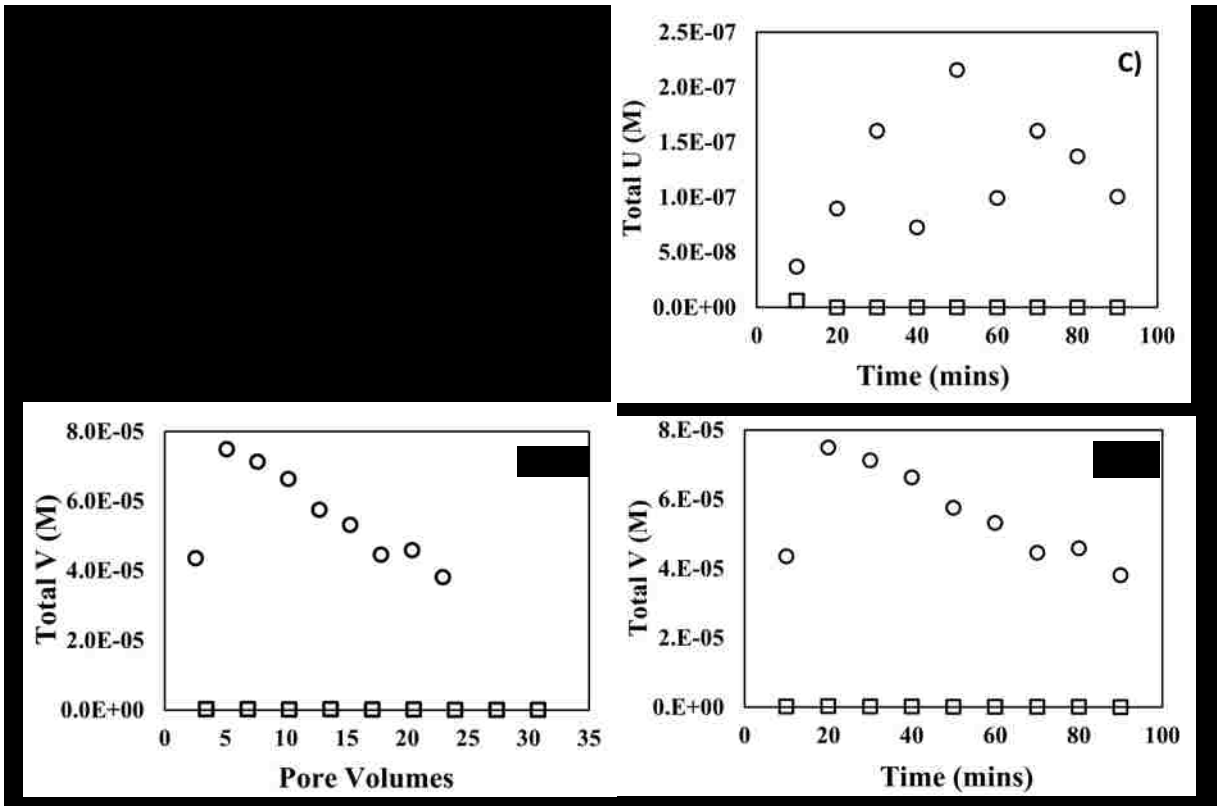

Figure 7.2. Effluent concentrations of U and V obtained after reaction of mine waste (circle) and background soil (squares) with 18MΩ water (pH 5.4), during continuous flow-through column experiments, as a function of pore volumes and time. **A)** U concentration versus pore volume; **B)** V concentration versus pore volume; **C)** U concentration versus time; **D)** V concentration versus time.

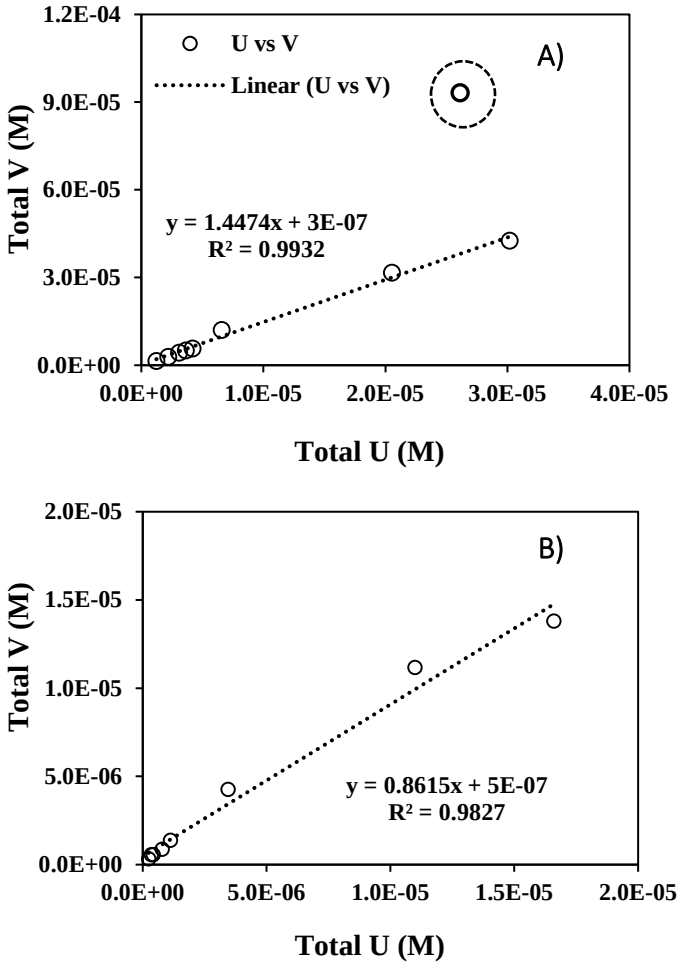

Figure 7.3. Molar correlation between U and V experimental release from mine waste (hollow circles) after reaction with **A)** 10 mM $NaHCO_3$.and **B)** 10 mM CH_3COOH during continuous flow through column experiments. The ideal slope should be 1:1 from the reaction $(K_2(UO_2)_2(VO_4)_2)^* = 2K^+ + 2UO2^{2+}\ VO4^{-3}$. The point in the dashed circle represents an outlier due to equilibration of the column with the influent solution on the early stages of the experiment (first 30 minutes).

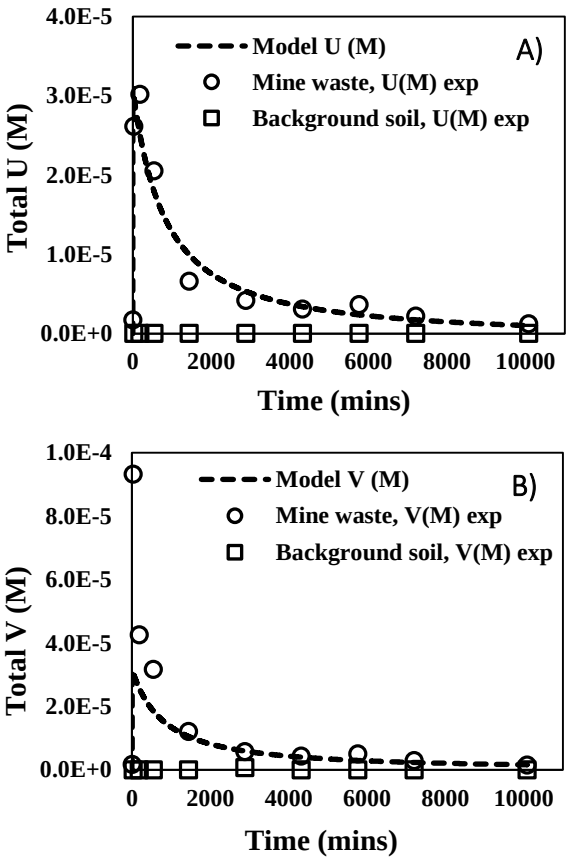

Figure 7.4. Measured effluent concentrations and reactive transport model (PFLOTRAN) of U and V, from mine waste (circle) and background soil (squares) during continuous flow-through column experiments at pH 7.9 (using 10 mM $NaHCO_3$), as a function of time. **A)** U concentration versus time; **B)** V concentration versus time. The curve fitting using PFLOTRAN are presented with dashed lines.

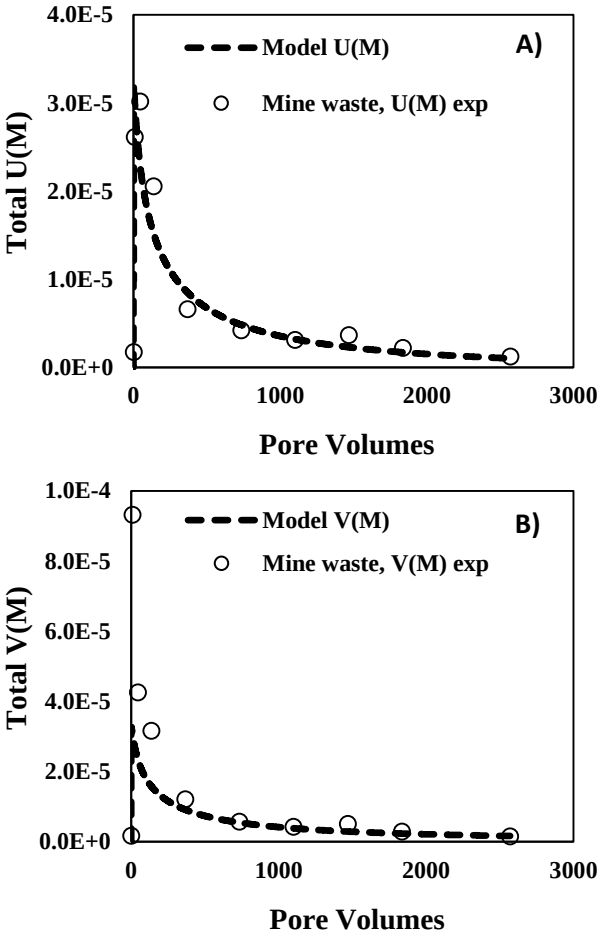

Figure 7.5. Measured effluent concentrations and reactive transport model (PFLOTRAN) of U and V from mine waste (circle) as a function of pore volumes after considering the effect of grain size during continuous flow-through column experiments at pH 7.9 (using 10 mM $NaHCO_3$). **A)** U concentrations versus pore volumes **B)** V concentrations versus pore volumes. The curve fitting using PFLOTRAN are presented with dashed lines.

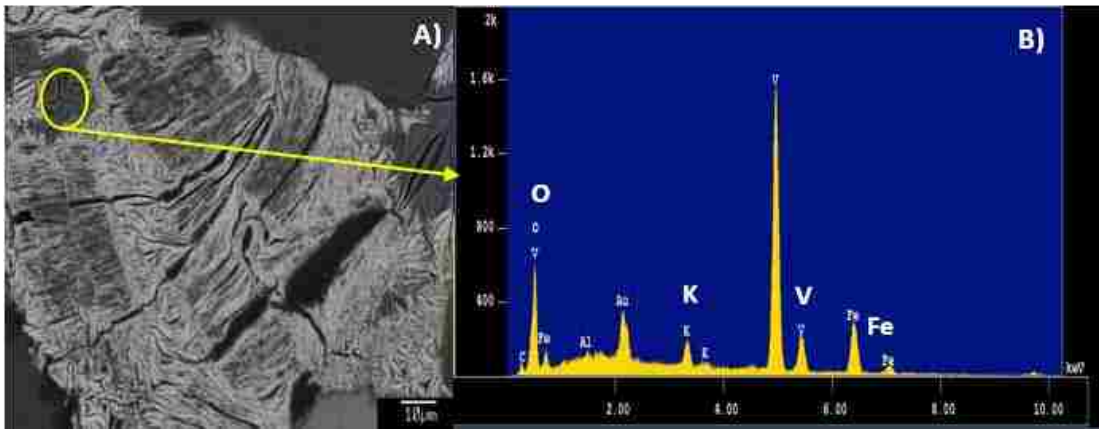

Figure 7.6. Microprobe identification of a V-Fe-K phase in the mine waste samples. **A)** Back Scatter Electron Imaging (BSE) of a V-Fe-K phase. **B)** EDS spectrum of the identified V-Fe-K phase.

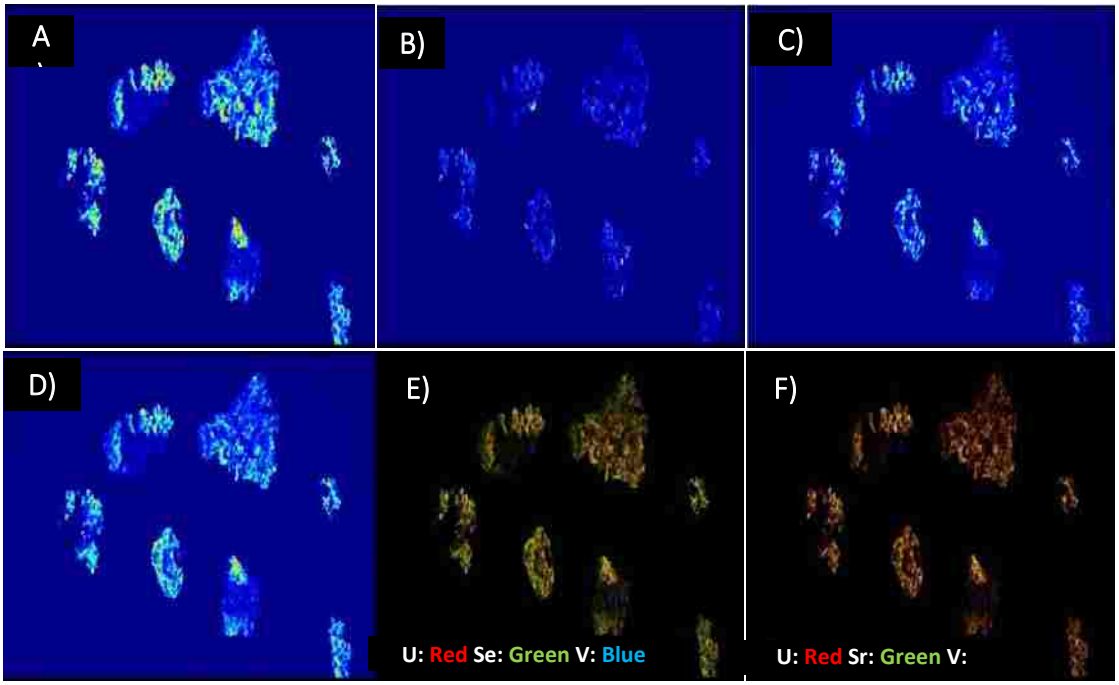

Figure 7.7. Synchrotron Micro- X-ray Fluorescence mapping for mine waste samples identifying the co-occurrence of U with other metals. **A)** Uranium map; **B)** Vanadium map; **C)** Selenium map ; **D)** Strontium map ; **E)** Overlay map of U- red, Se – green and V – blue; **F)** Overlay map of U- red, Sr – green and V – blue. Gradient yellow colors in E and F suggest potential co-occurrence of U and Se, and U and Sr respectively. Similarly cyan gradient colors in E and F suggest co-occurrence of U and V, possibly as a U-V mineral.

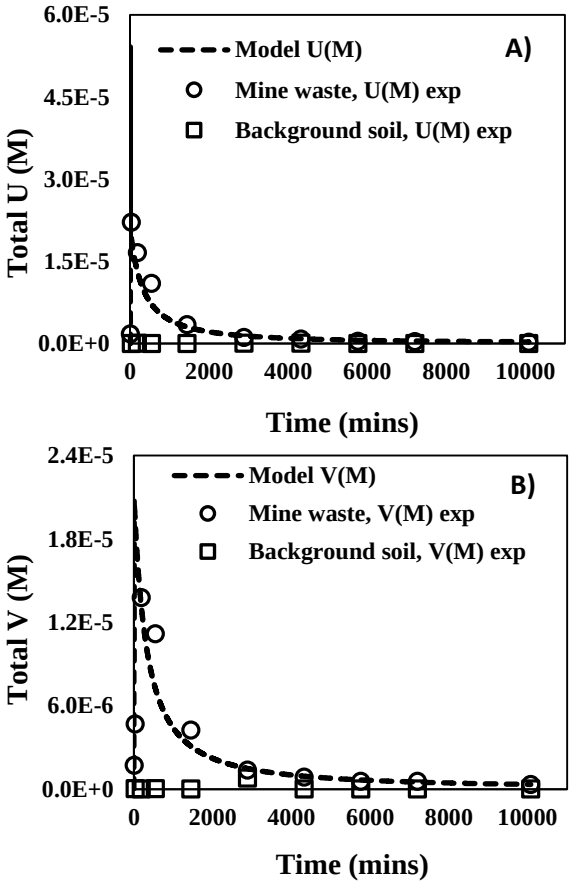

Figure 7.8. Measured effluent concentrations and reactive transport model (PFLOTRAN) of U and V, from mine waste (circle) and background soil (squares) during continuous flow-through column experiments at pH 3.4 (using 10 mM CH_3COOH) as a function of time. **A)** U concentration versus time; **B)** V concentration versus time. The curved fitting using PFLOTRAN are presented with solid lines.

[redacted]

[redacted] **Additional Materials and Methods.**

[redacted]

Acid digestions were conducted to assess and compare the total acid extractable trace metal concentrations between unreacted and reacted mine wastes. Acid digestions for unreacted sediments involved addition of 3ml of Hydrochloric acid (HCl), 3 ml of Nitric acid (HNO_3) and 3ml of Hydrofluoric acid (HF) into 50 ml Teflon digestion tubes to 2 ± 0.002g sediments. Similarly for reacted sediments 1 ml of HCl, HNO_3 and HF was added to 50 ml Teflon digestion tubes containing 0.5 ± 0.002g of sediments. All reagents are of high purity. The digestion tubes were then heated using a Digi prep MS SCP Science block digester at 95 °C for 2 h, followed by dilution of acid extracts from reacted and unreacted sediments to 50 and 25 ml. The diluted samples are then filtered using 0.45 μm filters to remove any suspended or undissolved solids before analysis.

[redacted]

Unreacted abandoned mine waste samples collected from the Jackpile-Paguate Mine, Laguna Pueblo were characterized for their bulk elemental and oxide composition using XRF with a detection limit around 0.1% of total elemental content. Sample preparation involved mixing about 9g of mine waste sample with 1g of binder “spectroblend” and homogenizing the mixture using a Spex mixer mill for 5 minutes in a plastic vial containing plastic balls for mixing. The homogenized sample was then transferred into a 40mm pressing container “9x38 mm Spec-Cap” that was placed inside a press pellet dye and pressed at 25 tons per square inch.

[redacted]

A Rigaku Smart Lab XRD was used to identify the U mineral phases that occur in the waste samples collected from the Jackpile-Paguate mine. The instrument uses Cu Ka radiation with a scintillation detector, a graphite monochromator and Jade® software to obtain this information. The samples are prepared by using a water separation technique with a settling time <30 s to concentrate the submicron U phases from the <63µm homogenized waste sample.

[redacted]

A STEM analysis was conducted on waste samples to identify the submicron-crystalline U phases and their composition which dominantly affect the reactivity and transport of U. A JEOL 2010F Field Emission Gun Scanning Transmission Electron Microscope (FEG/STEM) fitted with an Oxford ultrathin window Energy Dispersive Spectroscopy (EDS) detector, an Oxford ISIS/INCA X-ray analysis system and a GATAN multiscan CCD camera was used for the analysis. Apart from the traditional TEM techniques, this TEM is capable of conducting 1) energy filtered imaging (EFTEM), 2) electron energy loss spectroscopy (EELS), 3) X-ray microanalysis and X-ray mapping at the sub-nm level, and 4) bright- and dark-field STEM imaging. For this study, we used the TEM and STEM mode imaging, EDS analysis, high resolution selected area electron diffraction (HR-SAED) and STEM mapping capabilities of the instrument. Drops of unaltered waste sediment suspended in acetone were dropped onto standard holey carbon film-covered Cu TEM grids using a disposable pipette. The sample was then allowed to sit for a minute until all the acetone was vaporized. The dry samples were loaded onto the TEM holder for performing the analysis. The INCA EDS detector was used to determine the elemental composition of the specific targeted crystal. Later a HR-SAED analysis was

performed on the identified crystals to observe their crystallinity. A mapping analysis was then conducted on these samples to identify the composition of these U-phases that could be crucial to better understand their reactivity during waste reaction with various reagents.

[redacted]

The samples were analyzed using a JEOL JXA-8200 (JEOL Ltd., Tokyo, Japan) electron microprobe at the Department of Earth and Planetary Science/Institute of Meteoritics, University of New Mexico. The microprobe is equipped with 5 wavelength dispersive x-ray spectrometers (WDS) and an ultrathin-window energy dispersive spectrometer (EDS). A Sun Microsystems computer, running Solaris OS 10, hosts the JEOL operating software, which includes a qualitative X-ray mapping routine, the EDS analyzer, and image acquisition facilities. A Dell PC running Windows 7 handles the quantitative analysis and automation with third party software, Probe for EPMA (Probe Software, Inc., Eugene, Oregon).

X-ray maps were acquired at 20 kV and 30 nA beam current, mapping the following elements (see table below for analytical lines): Al, Si, P, S, K, Ca, V, Ti, Fe, and U (Appendix B: Table 8.1). All elements were mapped using WDS spectrometers except Al and Si which were mapped using the EDS spectrometer. The 10 elements measured by WDS required 2 complete passes to be made on each map since each WDS measures one element at a time. To accomplish this, the first 5 elemental lines on the WDS, a backscattered electron image, and the EDS lines were collected simultaneously, followed by a second pass on the map to acquire the remaining 5 lines measured by WDS. Maps were acquired over areas as large as 177 x 223 pixels down to 98 x 137

pixels where each pixel was 2 µm square, moving the stage from pixel to pixel. Stage movement is used over large areas to avoid defocusing the X-ray optics of the WDS spectrometer. Dwell time on all maps was 100 msec per pixel. Thus, the longest map stage map required 1 hour 17 minutes, including overhead for stage movement, while the smallest map (98 x 37 pixels) required 27 minutes acquisition time. One map of 100 x 200 pixels was acquired over a small area of 56 by 112 µm using the beam scan mode rather than stage movement since defocusing the WDS was not a problem. The acquisition time on this map was 2 hours using 3 accumulations or frames added together. The polished sections were analyzed at 20 kV and 30 nA beam current with a spot size less than 1 µm. Quantitative analyses were accomplished with WDS; the elements and their analytical lines with counting times and detection limits are provided in the SI table 1 below. Standard metals and minerals from C.M. Taylor Corp. (Sunnyvale, CA) and from the Smithsonian collection[176] were used for calibration, and Probe for EPMA software, utilizing a ZAF correction algorithm, was used to reduce the raw data. The elements analyzed using Electron Microprobe, their analytical line, peak counting time in seconds, counting time on each background (above and below peak, in seconds), and Minimum Detection Limit (in element wt%) are presented in a table below.

Element	**Al**	**Si**	**P**	**S**	**K**	**V**	**Fe**	**U**
Line	K_a	K_a	K_a	K_a	K_a	K_a	K_a	M_a
Peak counting Time (s)	20	20	40	60	20	20	20	60
Background Time (s)	10	10	10	20	10	10	10	20
Minimum Detection Limit (MDL) (wt%)	0.014	0.013	0.012	0.006	0.014	0.016	0.017	0.034

A XPS analysis was conducted on unreacted and reacted waste sediments surface oxidation states (top 5 nm) of the uranium (U). We used a Kratos AXIS-Ultra DLD XPS was used to acquire the near surface (5-10 nm) elemental composition and oxidation states. Monochromatic Al Kα source operating at 225W was used. Survey spectra were acquired at 80 eV and high resolution at 20 eV pass energy. The data obtained for every sample is an average of 3 different areas on the sample. Charge neutralization was accomplished using low energy electron that operate at a -3.1 V bias voltage, -1.0 V filament voltage and filament current of 2.1 A. Our spectra were calibrated using the 4f spectra acquired from gold powder that was deposited on each sample. All spectra of U were processed using CasaXPS software. Synthetic uraninite [UO_2] and becquerelite [$Ca(UO_2)_6O_4(OH)_6 \cdot 8(H_2O)$] procured from our collaborators in University of Notre Dame were used as reference standards for U(IV) and U(VI). Atomic percentage content for various elements was calculated using sensitivity factors provided by the manufacturer. A 70% Gaussian / 30% Lorentzian (GL (30)) line shape was used to fit our spectra. The full width at half maximum was kept between 1.6 and 1.9 eV for all peaks used in fitting. The position and area of peaks in U 4f 5/2 component was constrained to those in U4f 7/2 components by the values reported in database- 10.8 eV higher in position and 75% of the area. Several peaks from other elements contribute to the same binding energy range – K 2s at 378.9 eV, Mg auger peak at 385 eV and N 1s in the region above 399 eV.

We mapped a polished section of the waste sample at the advanced Stanford Synchrotron Radiation Light source (SSRL) beam line 10.3.2 using a µ-SXRF fitted with a Si (111) phi, 90 double crystal monochromator to observe the co-occurrence of U with P and Si. X-ray energies as high as 17.2 kev, just above the U LIII edge was used to acquire these maps. The acquired data was processed using the Microanalysis Toolkit software program.

[redacted]

The surface charge of the unreacted and reacted mine waste samples was obtained by using Malvern Zetasizer Nano-ZS which is equipped with a He−Ne laser (633 nm) and non-invasive backscatter optics (NIBS). All samples for zeta potential measurements were suspended in 10 mM NaCl solution at a 0.25 mg mL^{-1} concentration. Measurements were acquired at room temperature (22-25^{o}C) in triplicates. All reported values correspond to the average of at least three independent samples.

Table 8.1 Elemental percentage concentrations of metals at the surface of the unreacted and reacted Laguna mine wastes determined using X-ray Photoelectron Spectroscopy (XPS) survey scan.

Sample	O 1s %	C 1s %	Si 2p %	N 1s %	U 4f %
Unreacted Laguna Mine waste	37.5	47.8	9.0	0.2	0.1
Reacted - 10 mM $NaHCO_3$ pH 7.5	56.0	29.5	14.0	0.23	0.02
Reacted - 6% NaOCl @ pH 7.5	56.3	30.5	12.7	0.33	0.06
Reacted - 5.6-6% NaOCl + 10 mM $NaHCO_3$ pH 7.5	46.3	31.0	10.85	-	0.07

Table 8.2 Percentage distribution of U(IV) and U(VI) oxidation states at the surface (top 5 nm) of the unreacted and reacted Laguna mine wastes determined using XPS narrow scans (figure 8.8).

Sample	% U Content	
	U(VI)	U(IV)
Binding energy, eV	381.6	384.5
Unreacted mine waste	95	5
Reacted - 10 mM $NaHCO_3$ pH 7.5	100	0
Reacted - 6% NaOCl @ pH 7.5	100	0
Reacted - 5.6-6% NaOCl + 10 mM $NaHCO_3$ pH 7.5	100	0

Table 8.3 Chemical equilibrium simulations conducted using MINEQL 4.6 to observe the dominant aqueous complexes and mineral precipitates formed at a certain pH and reactivity conditions. The saturation indices (SI) for schoepite during reaction with 18MΩ water and 6% NaOCl are estimated to be, SI = 0.

Experiments	**Average pH**	**Aqueous complexes and mineral precipitates formed**	**Dominance of aqueous and solid phases in concentration%**
Reaction with 18MΩ water	6.5 (when concentrations start dropping)	UO_2OH^+	13.8
		$(UO_2)_3(OH)_5^+$	8.7
		$UO_2(OH)_2$ (aq)	5.5
		Schoepite	71.7
Reaction with 10 mM $NaHCO_3$	8	$UO_2(CO_3)_3^{4-}$	4.6
		$Ca_2UO_2(CO_3)_3^0$	18.9
		$Ca_2UO_2(CO_3)_3^{2-}$	75.8
Reaction with 6% NaOCl	6.5 (when concentrations start dropping)	UO_2OH^+	1.1
		Schoepite	97.9
6% NaOCl + 10 mM $NaHCO_3$	5.9 (when concentrations start dropping)	UO_2CO_3 (aq)	5.4
		$UO_2(CO_3)_2^{-2}$	2.4
		$Ca_2UO_2(CO_3)_3^0$	77.8
		$Ca_2UO_2(CO_3)_3^{2-}$	14.1

Table 8.4 Dissolved Organic Carbon (DOC) content dissolved from Laguna mine wastes after reaction with 1) 18MΩ water pH 5.4 2) 10 mM $NaHCO_3$ pH 7.5 3) 6% NaOCl pH 7.5 and 4) 6% NaOCl + 10mM $NaHCO_3$ pH 7.5.

Reagents	**Dissolved Organic Carbon (DOC) (mg/L)**
Reaction with 18MΩ water	1.6
Reaction with 10 mM $NaHCO_3$	2.6
Reaction with 6% NaOCl	5.5
6% NaOCl + 10 mM $NaHCO_3$	3.3

Table 8.5 Atomic content of elements in acid extracts obtained through acid digestion of unreacted and reacted Laguna mine wastes used during batch experiments.

Jackpile-Paguate mine waste Samples	**U (mg Kg^{-1})**	**V (mg Kg^{-1})**	**Fe (mg Kg^{-1})**	**P (mg Kg^{-1})**
Unreacted XRF	7345	919	77006	2675
Acid extractable from Unreacted sample	5876	271	64880	1381
Reacted - 18MΩ water pH 5.4	5654	357	58020	2341
Reacted - 10 mM $NaHCO_3$ pH 7.5	4882	369	57915	2155
Reacted - 6% NaOCl pH 7.5	5188	343	52580	2415
Reacted - 6% NaOCl + 10 mM $NaHCO_3$ pH 7.5	4526	359	55483	1099

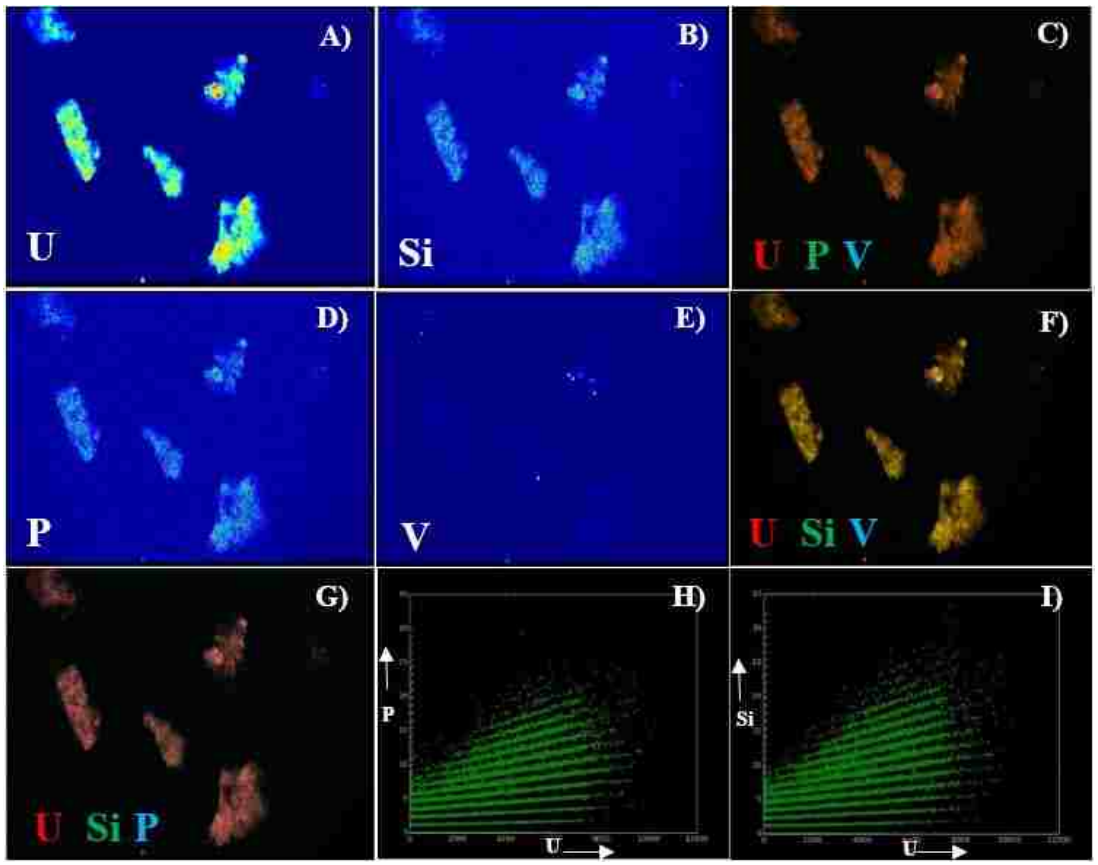

Figure 8.1 Micro X-Ray Fluorescence (µXRF) mapping on unreacted Laguna mine waste showing co-occurrence of U, Si and P. **A**, **B**, **D** and **E**) Mapping images showing distribution of U, Si, P and V in the elemental grains of the mine waste. **C)** Overlaid image of U (red), P (green) and V (blue), showing correlation between U and P in orange which is due to dominance of U over P. **F)** Overlaid image of U (red), Si (green) and V (blue), showing correlation between U and Si in yellow. **G)** Overlaid image of U (red), Si (green) and P (blue), showing correlation between U and Si in yellow and correlation between U and P in magenta. **H and I**) Correlations plots between U-P and U-Si maps, where the mapping intensities of U are plotted against those of Si and P, clearly indicating correlation between U, P and Si.

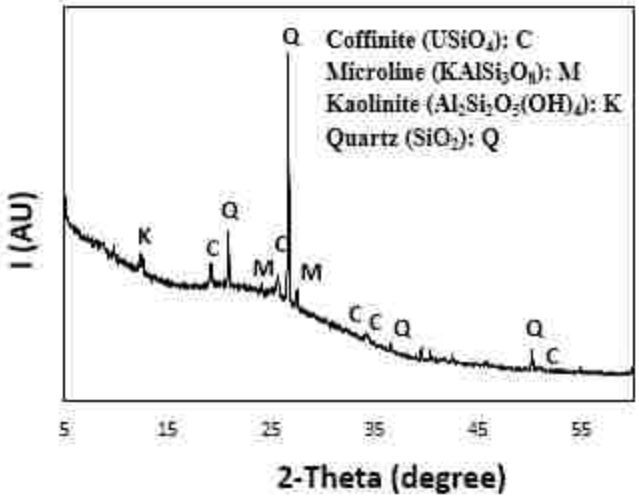

Phase ID	Weight %
Coffinite	1.4
Kaolinite	0.4
Microcline	2.6
Quartz	49
Amorphous and others	47

Figure 8.2 X-Ray Diffraction patterns of unreacted Laguna mine waste indicating presence of Kaolinite (K), Quartz (Q), Coffinite (C, U(IV) phase) and Microcline (M). Normalized weight percentages of each of these identified phases were indicated in the table on the right

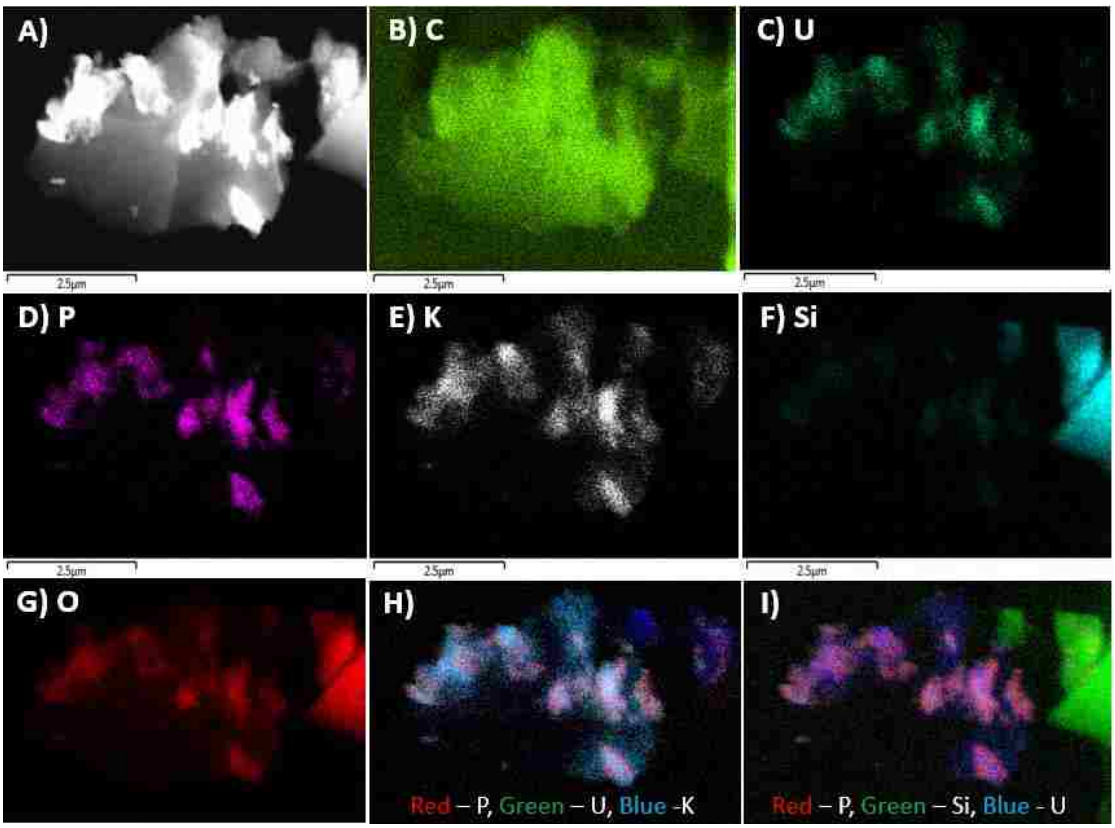

Figure 8.3 Scanning Transmission Electron Microscopy (STEM) mapping of the U-K-P phase in the unreacted mine waste sample. **A)** STEM image of the waste sample **B)** C (carbon) map **C)** U map **D)** P map **E)** K map and **F)** Si map **G)** O map **H)** Overlay map of P in red, U in green and K in Blue suggests co-occurrence of U, K and P, cyan shows co-occurrence of U and K. **I)** Overlay map of P in red, Si in green and U in Blue. Magenta areas show co-occurrence of U and P, cyan shows co-occurrence of U and Si.

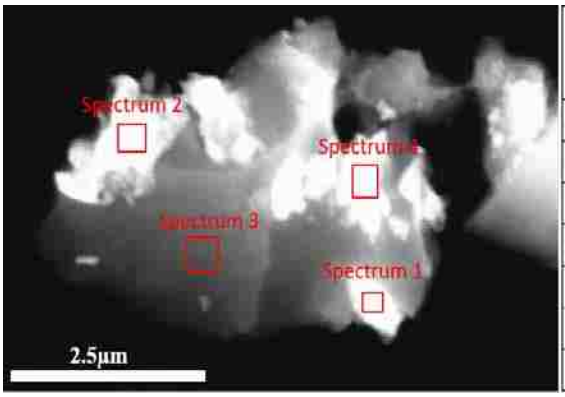

Elements	Atomic weight %			
	Spectrum 1	Spectrum 2	Spectrum 3	Spectrum 4
O	69.86	69.94	66.55	70.3
Si	6.49	11.84		10.78
P	9.15	6.7		7.02
K	3.79	2.01		1.81
U	10.7	9.5		10.09
C	-	-	33.28	-
Cl	-	-	0.17	-

Figure 8.4 Scanning Transmission Electron Microscopy (STEM) image of an area in the waste sample where the predominance of carbon encapsulated U-P-K phases are observed **(Table)** Shows atomic composition of the U-K-P phase in spectrums 1, 2 and 4 highlighted in red boxes in the figure. Spectrum 3 shows the composition of the carbon that encapsulates the micro crystalline U-P-K phase in the waste sample.

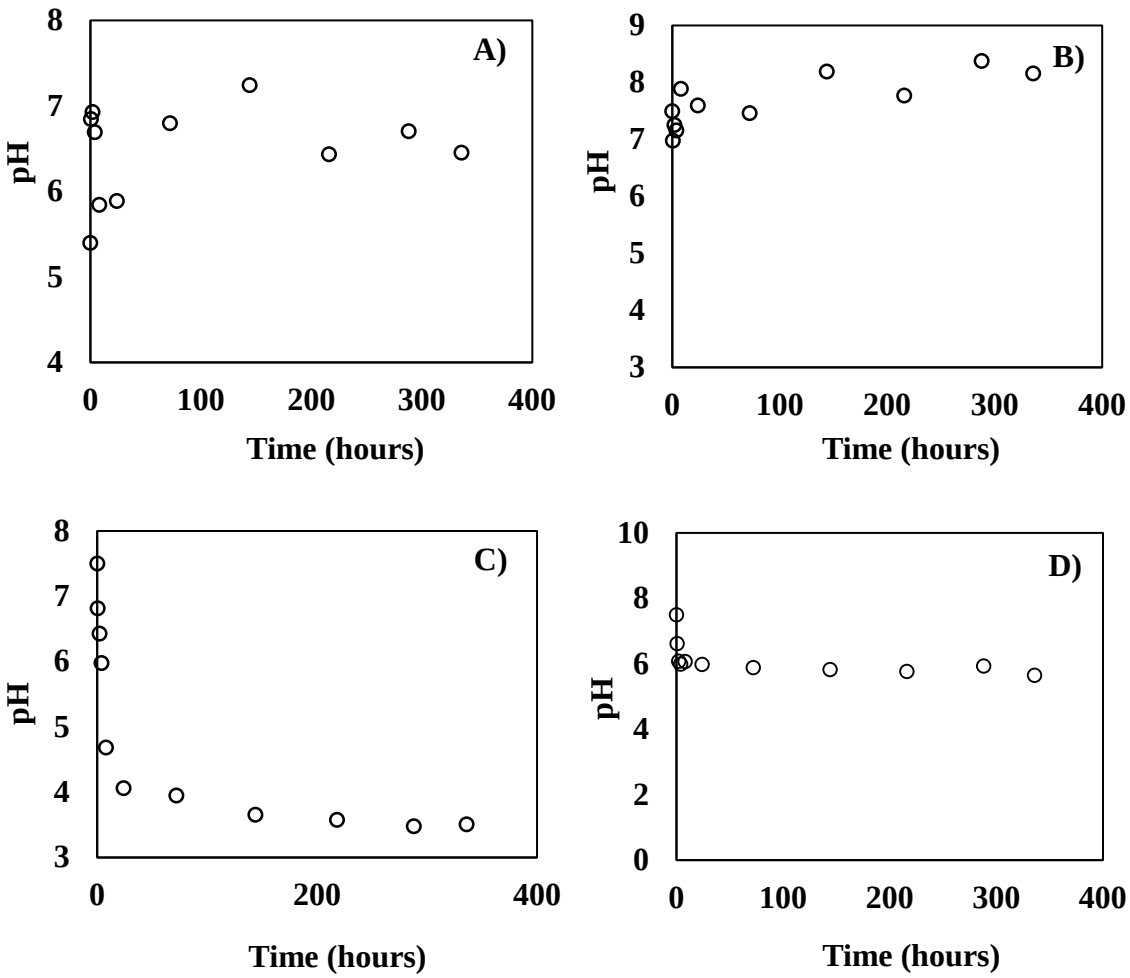

Figure 8.5 The average pH change during batch reactions of Laguna mine wastes with **A)** 18MΩ water pH 5.4 **B)** 10 mM $NaHCO_3$ pH 7.5 **C)** 6% NaOCl pH 7.5 **D)** 6% NaOCl + 10 mM $NaHCO_3$ pH 7.5, conducted in triplicates.

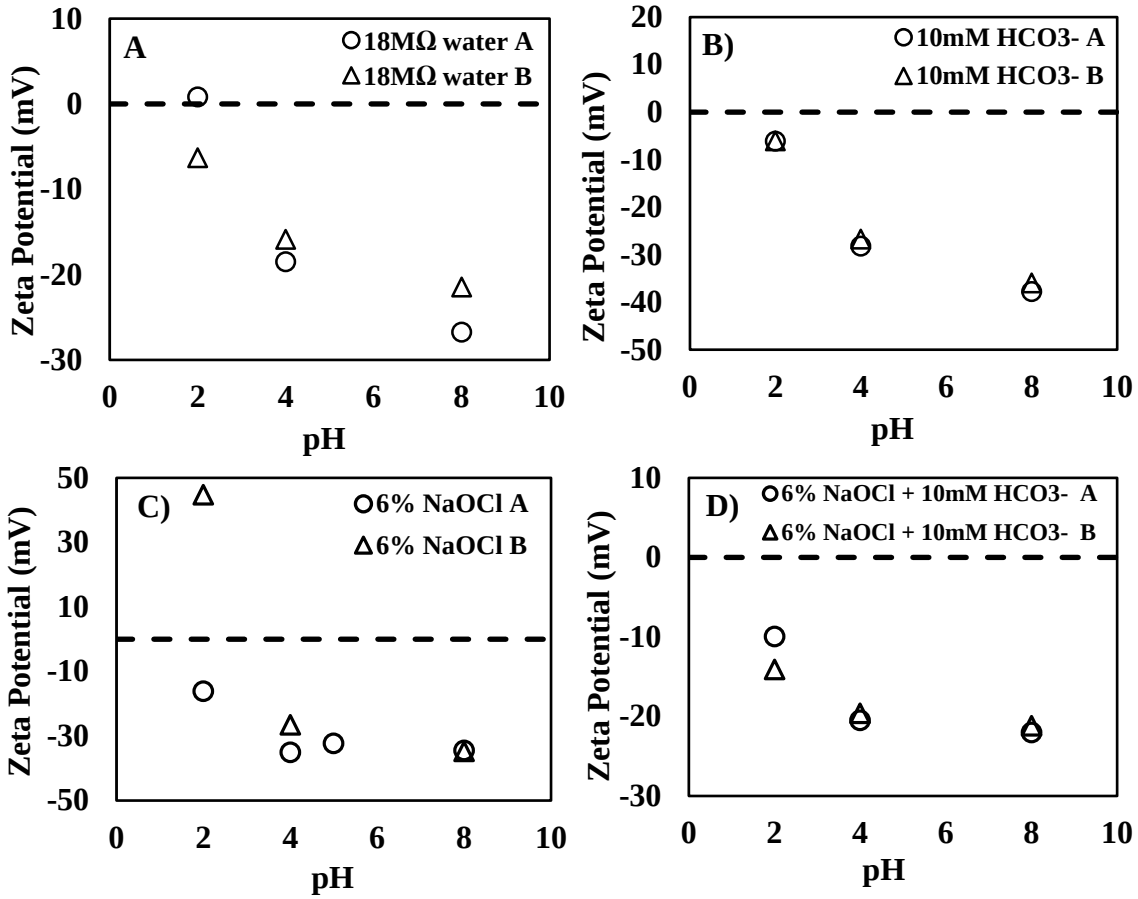

Figure 8.6 Zeta Potential of unreacted and reacted Laguna mine waste. **A)** unreacted mine wastes **B)** mine wastes reacted with 18MΩ water pH 5.4 **C)** mine wastes reacted with 10 mM $NaHCO_3$ pH 7.5 **D)** mine wastes reacted with 6% NaOCl pH 7.5 **E)** mine wastes reacted with 6% NaOCl + 10 mM $NaHCO_3$ pH 7.5.

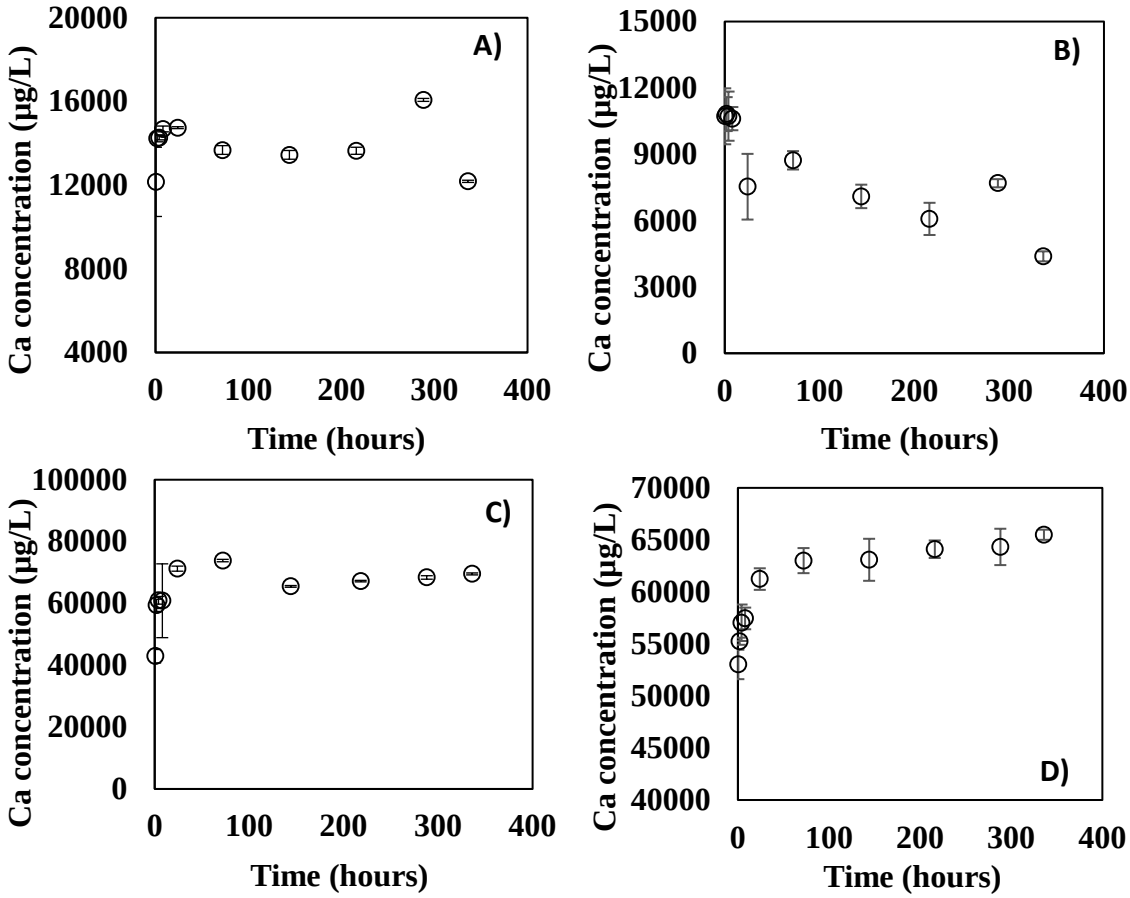

Figure 8.7 Calcium trends for batch experiments on Laguna mine waste reacted with **A)** 18MΩ water pH 5.4 **B)** 10 mM sodium bicarbonate ($NaHCO_3$) solution pH 7.5 **C)** 6% NaOCl solution, pH 7.5 **D)** 10 mM $NaHCO_3$ + 6% NaOCl solution, pH 7.5. The pH of the reagents used in B-D were adjusted using 0.5N NaOH, 0.1N HCl and 35.6N HNO_3.

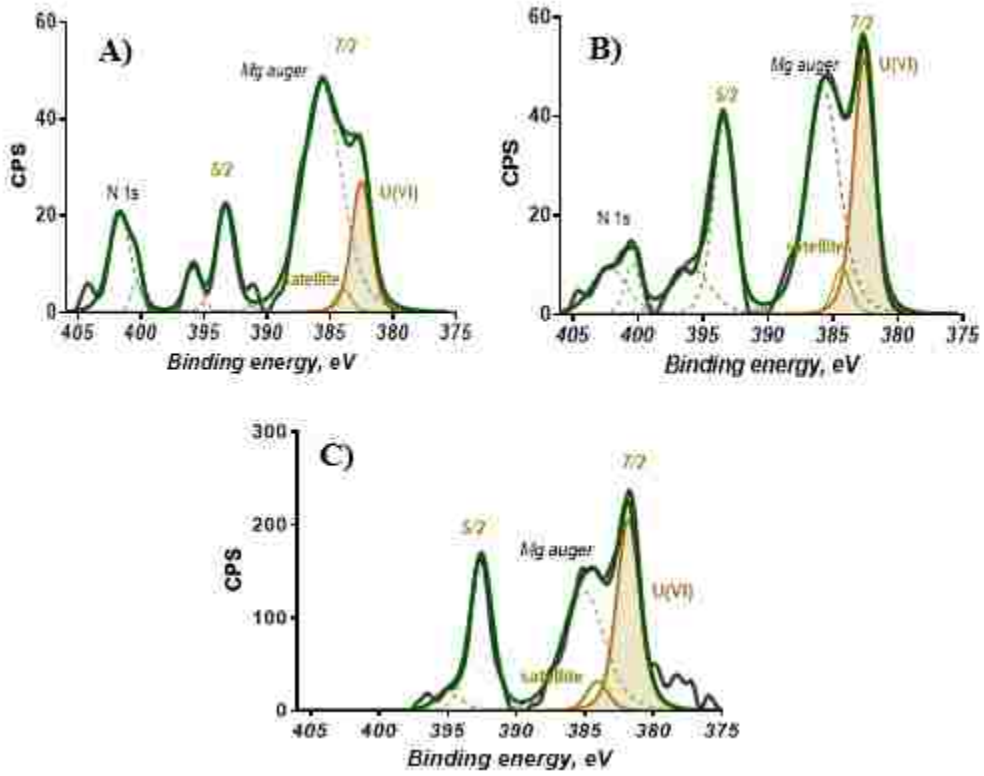

Figure 8.8 High resolution X-ray Photoelectron Spectroscopy (XPS) spectra of reacted mine wastes to identify the surface oxidation states of U. **A)** Mine waste reacted with 10 mM $NaHCO_3$. **B)** Mine waste reacted with 6% NaOCl. **C)** Mine waste reacted with 6% NaOCl +10 mM $NaHCO_3$. Black line represents the experimental spectra obtained while the green line represents the curve fitting by cumulating the individual peaks under the curve. Percentage of different U oxidation states observed in the top 5nm of the mine waste surface through these high resolution spectra are reported in table 8.2.

1. Blake, J. M.; Avasarala, S.; Artyushkova, K.; Ali, A.-M. S.; Brearley, A. J.; Shuey, C.; Robinson, W. P.; Nez, C.; Bill, S.; Lewis, J., Elevated concentrations of U and co-occurring metals in abandoned mine wastes in a northeastern Arizona Native American community. *Environmental science & technology* **2015,** *49* (14), 8506-8514.
2. Riley, R. G.; Zachara, J. Chemical contaminants on DOE lands and selection of contaminant mixtures for subsurface science research; Pacific Northwest Lab., Richland, WA (United States): 1992.
3. Archer, V. E., Hazards to health in uranium mining and milling. *Journal of Occupational and Environmental Medicine* **1962,** *4* (2), 55-60.
4. Byrne, J.; Hoffman, S. M., Governing the Atom: The Politics of Risk. North Atlantic Books: 1996; Vol. 7.
5. Sovacool, B. K., The costs of failure: a preliminary assessment of major energy accidents, 1907–2007. *Energy Policy* **2008,** *36* (5), 1802-1820.
6. Moore-Nall, A., The legacy of uranium development on or near Indian reservations and health implications rekindling public awareness. *Geosciences* **2015,** *5* (1), 15-29.
7. United States government, abandoned mines portal **2016**.
8. USEPA, Addressing uranium contamination on the Navajo Nation. U.S. Environmental Protection Agency, Pacific Southwest, Region 9: San Francisco, CA. **2015**.
9. USEPA, Technical Report on Technologically Enhanced Naturally Occurring Radioactive Materials from Uranium Mining Vol. 1: Mining and Reclamation Background. U.S. Environmental Protection Agency, Office of Radiation and Indoor Air **April, 2008a,** *EPA 402-R-08-005* (Washington, D.C.).
10. Congress, U. S., Uranium Mill Tailings Radiation Control Act of 1978. *Public Law* **1978**, 95−604.
11. USEPA, Technical Report on Technologically Enhanced Naturally Occurring Radioactive Materials from Uranium Mining Vol. 1: Mining and Reclamation Background; U.S. Environmental Protection Agency, Office of Radiation and Indoor Air, EPA 402-R-08-005:. Washington,*D.C.* **2008a**.
12. USEPA, Addressing uranium contamination on the Navajo Nation. U.S. Environmental Protection Agency, Pacific Southwest, Region 9. San Francisco, CA **2015**.
13. USEPA, Federal actions to address impacts of uranium contamination in the Navajo Nation: Five-year plan summary report. U.S. Environmental Protection Agency, Pacific Southwest, Region 9. San Francisco, CA **2013**.
14. Dawson, S., Navajo uranium workers and the effects of occupational illnesses: A case study. *Human Organization* **1992,** *51* (4), 389-397.
15. Hopenhayn, C., Arsenic in drinking water: Impact on human health. *Elements* **2006,** *2*, 103-107.
16. D'amore, J.; Al-Abed, S.; Scheckel, K.; Ryan, J., Methods for speciation of metals in soils. *Journal of environmental quality* **2005,** *34* (5), 1707-1745.

17. Menzel, D. C., Implementation of the federal surface mining control and reclamation act of 1977. *Public Administration Review* **1981**, 212-219.
18. Cothern, C. R.; Lappenbusch, W. L.; Cotruvo, J. A., Health effects guidance for uranium in drinking water. *Health physics* **1983,** *44*, 377-384.
19. Agency, U. S. E. P., Jackpile-Paguate Uranium Mine NPL Listing Support Document, U.S. Government Publishing Office. *Washington, D.C.* **2013**.
20. Blake, J. M.; De Vore, C. L.; Avasarala, S.; Ali, A.-M.; Roldan, C.; Bowers, F.; Spilde, M. N.; Artyushkova, K.; Kirk, M. F.; Peterson, E., Uranium mobility and accumulation along the Rio Paguate, Jackpile Mine in Laguna Pueblo, NM. *Environmental Science: Processes & Impacts* **2017,** *19* (4), 605-621.
21. Santos, E. n. A.; Ladeira, A. C., Recovery of uranium from mine waste by leaching with carbonate-based reagents. *Environmental science & technology* **2011,** *45* (8), 3591-3597.
22. Benjamin, M. M., Water chemistry. Waveland Press: 2014.
23. Ledin, M.; Pedersen, K., The environmental impact of mine wastes—roles of microorganisms and their significance in treatment of mine wastes. *Earth-Science Reviews* **1996,** *41* (1), 67-108.
24. Byczkowski, J. Z.; Kulkarni, A. P., Oxidative stress and pro-oxidant biological effects of vanadium. *Advances in Environmental Science and Technology -New York-* **1998,** *31*, 235-264.
25. Stohs, S.; Bagchi, D., Oxidative mechanisms in the toxicity of metal ions. *Free radical biology and medicine* **1995,** *18* (2), 321-336.
26. Panichev, N.; Mandiwana, K.; Moema, D.; Molatlhegi, R.; Ngobeni, P., Distribution of vanadium (V) species between soil and plants in the vicinity of vanadium mine. *Journal of hazardous materials* **2006,** *137* (2), 649-653.
27. Keith, S.; Faroon, O.; Roney, N.; Scinicariello, F.; Wilbur, S.; Ingerman, L.; Llados, F.; Plewak, D.; Wohlers, D.; Diamond, G., Toxicological profile for uranium. **2013**.
28. Zota, A. R.; Willis, R.; Jim, R.; Norris, G. A.; Shine, J. P.; Duvall, R. M.; Schaider, L. A.; Spengler, J. D., Impact of mine waste on airborne respirable particulates in northeastern Oklahoma, United States. *Journal of the Air & Waste Management Association* **2009,** *59* (11), 1347-1357.
29. Health, U. D. o.; Services, H., Toxicological profile for arsenic. 2000.
30. Extraction of values from ores. Google Patents: 1935.
31. McLeod, C., Uranium Mines and Mills May Have Caused Birth Defects among Navajo Indians. *Energy Resources* **1985,** (12:49), 196-204.
32. Churchill, W., American Indian lands: The Native ethic amid resource development. *Environment: Science and Policy for Sustainable Development* **1986,** *28* (6), 13-34.
33. Gofman, J. W., Radiation and human health. **1981**.
34. Organization, W. H., Uranium in drinking-water. Background document for preparation of WHO Guidelines for drinking-water quality. Geneva. *World Health Organization (WHO/SDE/WSH/03.04/118)* **2003**.
35. Domingo, J. L., Reproductive and developmental toxicity of natural and depleted uranium: a review. *Reproductive Toxicology* **2001,** *15* (6), 603-609.

36. Hund, L.; Bedrick, E. J.; Miller, C.; Huerta, G.; Nez, T.; Ramone, S.; Shuey, C.; Cajero, M.; Lewis, J., A Bayesian framework for estimating disease risk due to exposure to uranium mine and mill waste on the Navajo Nation. *Journal of the Royal Statistical Society: Series A (Statistics in Society)* **2015,** *178* (4), 1069-1091.
37. EPA, Navajo Nation: Cleaning Up Abandoned Uranium Mines. **2016**.
38. Wuana, R.; Okieimen, F.; Imborvungu, J., Removal of heavy metals from a contaminated soil using organic chelating acids. *International Journal of Environmental Science & Technology* **2010,** *7* (3), 485-496.
39. Chenoweth, W. L., The Geology and Production Histroy of the Uranium Deposits in the Toreve A formation, Black Mesa, Apache county, Arizona. **1990**.
40. Franczyk, K. J., Stratigraphic revision and depositional environments of the Upper Cretaceous Toreva Formation in the northern Black Mesa area, Navajo and Apache Counties, Arizona. *U.S. Geological Survey: Reston,* VA **1988**.
41. Hostetler, P.; Garrels, R., Transportation and precipitation of uranium and vanadium at low temperatures, with special reference to sandstone-type uranium deposits. *Economic Geology* **1962,** *57* (2), 137-167.
42. Mann, A. Chemical ore genesis models for the precipitation of carnotite in calcrete; Commonwealth Scientific and Industrial Research Organisation: **1974**.
43. Hillebrand, W., Carnotite and tyuyamunite and their ores in Colorado and Utah. *American Journal of Science* **1924,** (45), 201-216.
44. Crook, T.; Blake, G., On Carnotite and an associated mineral complex from South Australia. *Mineralogical Magazine* **1910,** *15* (71), 271-284.
45. Sharma, R. K.; Putirka, K. D.; Stone, J. J., Stream sediment geochemistry of the upper Cheyenne River watershed within the abandoned uranium mining region of the southern Black Hills, South Dakota, USA. *Environmental Earth Sciences* **2016,** *75* (9), 1-12.
46. Xu, J.; Zhu, S.-Y.; Luo, T.-Y.; Zhou, W.; Li, Y.-L., Uranium mineralization and its radioactive decay-induced carbonization in a black shale-hosted polymetallic sulfide ore layer, southwest China. *Economic Geology* **2015,** *110* (6), 1643-1652.
47. Abed, A. M.; Saffarini, G. A.; Sadaqah, R. M., Spatial distribution of uranium and vanadium in the upper phosphorite member in Eshidiyya basin, southern Jordan. *Arabian Journal of Geosciences* **2014,** *7* (1), 253-271.
48. Kim, C.; Chi, C.; Miller, S.; Rosales, R.; Sugihara, E.; Akau, J.; Rytuba, J.; Webb, S., (Micro) spectroscopic analyses of particle size dependence on arsenic distribution and speciation in mine wastes. *Environmental science & technology* **2013,** *47* (15), 8164-8171.
49. Nelkin, D., Native Americans and nuclear power. *Science, Technology & Human Values* **1981,** *6* (2), 2-13.
50. Moench, R. H.; Schlee, J. S., Geology and uranium deposits of the Laguna district, New Mexico. US Government Printing Office: 1967.
51. Risser, D. W.; Davis, P. A.; Baldwin, J. A.; McAda, D. P., Aquifer tests at the Jackpile-Paguate uranium mine, Pueblo of Laguna, west-central New Mexico. *US Geol. Surv. Water Resour. Invest. Rep* **1984,** *84* (4255), 26.
52. Maxwell, C. H. In Mesozoic stratigraphy of the Laguna-Grants region, Albuquerque Country II. NM Geol. Soc., 33rd Annual Field Conf, 1982; pp 261-266.

53. Nash, J. T., Uranium deposits in the Jackpile Sandstone, New Mexico. *Economic Geology* **1968,** *63* (7), 737-750.
54. Blake, J.; DeVore, C.; Avasarala, S.; Ali, A.-M.; Roldan, C.; Bowers, F.; Spilde, M.; Artyushkova, K.; Kirk, M. F.; Peterson, E., Uranium Mobility and Accumulation along the Rio Paguate, Jackpile Mine in Laguna Pueblo, New Mexico. *Environmental Science: Processes & Impacts* **2017**.
55. Alessi, D. S.; Uster, B.; Veeramani, H.; Suvorova, E. I.; Lezama-Pacheco, J. S.; Stubbs, J. E.; Bargar, J. R.; Bernier-Latmani, R., Quantitative separation of monomeric U (IV) from UO_2 in products of U (VI) reduction. *Environmental science & technology* **2012,** *46* (11), 6150-6157.
56. Ilton, E. S.; Boily, J.-F.; Buck, E. C.; Skomurski, F. N.; Rosso, K. M.; Cahill, C. L.; Bargar, J. R.; Felmy, A. R., Influence of dynamical conditions on the reduction of UVI at the magnetite− solution interface. *Environmental science & technology* **2009,** *44* (1), 170-176.
57. Kohler, M.; Curtis, G.; Kent, D.; Davis, J., Experimental investigation and modeling of uranium (VI) transport under variable chemical conditions. *Water Resources Research* **1996,** *32* (12), 3539-3551.
58. Morss, L. R.; Edelstein, N. M.; Fuger, J., The Chemistry of the Actinide and Transactinide Elements (Set Vol. 1-6): Volumes 1-6. *Springer Science & Business Media*: 2010; Vol. 1.
59. Stumm, W.; Morgan, J. J., Aquatic chemistry: chemical equilibria and rates in natural waters. John Wiley & Sons: 2012; Vol. 126.
60. Langmuir, D., Aqueous Environmental Geochemistry, Prentice Hall, Upper Saddle River, NJ,. **1997**, 600.
61. Maurice, P. A., Environmental surfaces and interfaces from the nanoscale to the global scale. Wiley: 2009.
62. Naeem, A.; Westerhoff, P.; Mustafa, S., Vanadium removal by metal (hydr) oxide adsorbents. *Water research* **2007,** *41* (7), 1596-1602.
63. Gerke, T. L.; Scheckel, K. G.; Schock, M. R., Identification and distribution of vanadinite (Pb5 (V^{5+} O_4) 3Cl) in lead pipe corrosion by-products. *Environmental science & technology* **2009,** *43* (12), 4412-4418.
64. Dong, W.; Ball, W. P.; Liu, C.; Wang, Z.; Stone, A. T.; Bai, J.; Zachara, J. M., Influence of calcite and dissolved calcium on uranium (VI) sorption to a Hanford subsurface sediment. *Environmental science & technology* **2005,** *39* (20), 7949-7955.
65. Merritt, R. In The Extractive Metallurgy of Uranium, Colorado School of Mines Research Institute, Library of Congress Catalog Card, 1971.
66. Stewart, B. D.; Nico, P. S.; Fendorf, S., Stability of uranium incorporated into Fe (hydr) oxides under fluctuating redox conditions. *Environmental Science & Technology* **2009,** *43* (13), 4922-4927.
67. Stewart, B. D.; Cismasu, A. C.; Williams, K. H.; Peyton, B. M.; Nico, P. S., Reactivity of uranium and ferrous iron with natural iron oxyhydroxides. *Environmental science & technology* **2015,** *49* (17), 10357-10365.
68. Hsi, C.-k. D.; Langmuir, D., Adsorption of uranyl onto ferric oxyhydroxides: application of the surface complexation site-binding model. *Geochimica et Cosmochimica Acta* **1985,** *49* (9), 1931-1941.

69. Hattori, T.; Saito, T.; Ishida, K.; Scheinost, A. C.; Tsuneda, T.; Nagasaki, S.; Tanaka, S., The structure of monomeric and dimeric uranyl adsorption complexes on gibbsite: A combined DFT and EXAFS study. *Geochimica et Cosmochimica Acta* **2009,** *73* (20), 5975-5988.
70. Sachs, S.; Bernhard, G., Sorption of U (VI) onto an artificial humic substance-kaolinite-associate. *Chemosphere* **2008,** *72* (10), 1441-1447.
71. Yang, Y.; Saiers, J. E.; Barnett, M. O., Impact of interactions between natural organic matter and metal oxides on the desorption kinetics of uranium from heterogeneous colloidal suspensions. *Environmental science & technology* **2013,** *47* (6), 2661-2669.
72. Wang, Y.; Frutschi, M.; Suvorova, E.; Phrommavanh, V.; Descostes, M.; Osman, A. A.; Geipel, G.; Bernier-Latmani, R., Mobile uranium (IV)-bearing colloids in a mining-impacted wetland. *Nature communications* **2013,** *4*, 2942.
73. Yang, Y.; Saiers, J. E.; Xu, N.; Minasian, S. G.; Tyliszczak, T.; Kozimor, S. A.; Shuh, D. K.; Barnett, M. O., Impact of natural organic matter on uranium transport through saturated geologic materials: from molecular to column scale. *Environmental science & technology* **2012,** *46* (11), 5931-5938.
74. Luo, W.; Gu, B., Dissolution and mobilization of uranium in a reduced sediment by natural humic substances under anaerobic conditions. *Environmental science & technology* **2008,** *43* (1), 152-156.
75. Mibus, J.; Sachs, S.; Pfingsten, W.; Nebelung, C.; Bernhard, G., Migration of uranium (IV)/(VI) in the presence of humic acids in quartz sand: A laboratory column study. *Journal of contaminant hydrology* **2007,** *89* (3), 199-217.
76. Steelink, C., Peer reviewed: investigating humic acids in soils. ACS Publications: 2002.
77. Keiluweit, M.; Kleber, M., Molecular-level interactions in soils and sediments: the role of aromatic π-systems. *Environmental science & technology* **2009,** *43* (10), 3421-3429.
78. McCarthy, J. F.; Zachara, J. M., Subsurface transport of contaminants. *Environmental science & technology* **1989,** *23* (5), 496-502.
79. Kretzschmar, R.; Borkovec, M.; Grolimund, D.; Elimelech, M., Mobile subsurface colloids and their role in contaminant transport. *Advances in agronomy* **1999,** *66*, 121-193.
80. Bone, S. E.; Dynes, J. J.; Cliff, J.; Bargar, J. R., Uranium (IV) adsorption by natural organic matter in anoxic sediments. *Proceedings of the National Academy of Sciences* **2017**, 201611918.
81. Bhattacharyya, A.; Campbell, K. M.; Kelly, S. D.; Roebbert, Y.; Weyer, S.; Bernier-Latmani, R.; Borch, T., Biogenic non-crystalline U (IV) revealed as major component in uranium ore deposits. *Nature Communications* **2017,** *8*.
82. Mikutta, C.; Langner, P.; Bargar, J. R.; Kretzschmar, R., Tetra-and hexavalent uranium forms bidentate-mononuclear complexes with particulate organic matter in a naturally uranium-enriched peatland. *Environmental science & technology* **2016,** *50* (19), 10465-10475.
83. Bargar, J. R.; Williams, K. H.; Campbell, K. M.; Long, P. E.; Stubbs, J. E.; Suvorova, E. I.; Lezama-Pacheco, J. S.; Alessi, D. S.; Stylo, M.; Webb, S. M., Uranium

redox transition pathways in acetate-amended sediments. *Proceedings of the National Academy of Sciences* **2013,** *110* (12), 4506-4511.
84. Veeramani, H.; Alessi, D. S.; Suvorova, E. I.; Lezama-Pacheco, J. S.; Stubbs, J. E.; Sharp, J. O.; Dippon, U.; Kappler, A.; Bargar, J. R.; Bernier-Latmani, R., Products of abiotic U (VI) reduction by biogenic magnetite and vivianite. *Geochimica et Cosmochimica Acta* **2011,** *75* (9), 2512-2528.
85. Lovley, D. R.; Phillips, E. J., Microbial reduction of uranium. *Nature* **1991,** *350* (6317), 413.
86. Bargar, J. R.; Bernier-Latmani, R.; Giammar, D. E.; Tebo, B. M., Biogenic uraninite nanoparticles and their importance for uranium remediation. *Elements* **2008,** *4* (6), 407-412.
87. O'Loughlin, E. J.; Kelly, S. D.; Cook, R. E.; Csencsits, R.; Kemner, K. M., Reduction of uranium (VI) by mixed iron (II)/iron (III) hydroxide (green rust): formation of UO2 nanoparticles. *Environmental science & technology* **2003,** *37* (4), 721-727.
88. Nenoff, T. M.; Jacobs, B. W.; Robinson, D. B.; Provencio, P. P.; Huang, J.; Ferreira, S.; Hanson, D. J., Synthesis and low temperature in situ sintering of uranium oxide nanoparticles. *Chemistry of Materials* **2011,** *23* (23), 5185-5190.
89. Mkandawire, M.; Dudel, E. G., Natural occurring uranium nanoparticles and the implication in bioremediation of surface mine waters. *Uranium, Mining and Hydrogeology* **2008**, 487-496.
90. Schindler, M.; Lussier, A. J.; Bellrose, J.; Rouvimov, S.; Burns, P. C.; Kyser, T. K., Mobilization and agglomeration of uraninite nanoparticles: A nano-mineralogical study of samples from the Matoush Uranium ore deposit. *American Mineralogist* **2017,** *102* (9), 1776-1787.
91. Singh, A.; Catalano, J. G.; Ulrich, K.-U.; Giammar, D. E., Molecular-scale structure of uranium (VI) immobilized with goethite and phosphate. *Environmental science & technology* **2012,** *46* (12), 6594-6603.
92. Troyer, L. D.; Maillot, F.; Wang, Z.; Wang, Z.; Mehta, V. S.; Giammar, D. E.; Catalano, J. G., Effect of phosphate on U (VI) sorption to montmorillonite: Ternary complexation and precipitation barriers. *Geochimica et Cosmochimica Acta* **2016,** *175*, 86-99.
93. Tokunaga, T. K.; Kim, Y.; Wan, J., Potential remediation approach for uranium-contaminated groundwaters through potassium uranyl vanadate precipitation. *Environmental science & technology* **2009,** *43* (14), 5467-5471.
94. Giammar, D. E.; Hering, J. G., Time scales for sorption− desorption and surface precipitation of uranyl on goethite. *Environmental science & technology* **2001,** *35* (16), 3332-3337.
95. Singer, D. M.; Zachara, J. M.; Brown Jr, G. E., Uranium speciation as a function of depth in contaminated Hanford sediments-A micro-XRF, micro-XRD, and micro-and bulk-XAFS study. *Environmental science & technology* **2009,** *43* (3), 630-636.
96. Buck, E. C.; Brown, N. R.; Dietz, N. L., Contaminant uranium phases and leaching at the Fernald site in Ohio. *Environmental science & technology* **1995,** *30* (1), 81-88.
97. Kanematsu, M.; Perdrial, N.; Um, W.; Chorover, J.; O'Day, P. A., Influence of phosphate and silica on U (VI) precipitation from acidic and neutralized wastewaters. *Environmental science & technology* **2014,** *48* (11), 6097-6106.

98. Avasarala, S.; Lichtner, P. C.; Ali, A.-M. S.; González-Pinzón, R.; Blake, J. M.; Cerrato, J. M., Reactive Transport of U and V from Abandoned Uranium Mine Wastes. *Environmental Science & Technology* **2017**.
99. Minelli, L.; Veschetti, E.; Giammanco, S.; Mancini, G.; Ottaviani, M., Vanadium in Italian waters: monitoring and speciation of V (IV) and V (V). *Microchemical journal* **2000,** *67* (1), 83-90.
100. Schock, M.; Kelly, K. In *Vanadium chemistry essentials for treatment studies*, USEPA Inorganics Workshop, 2002.
101. Veschetti, E.; Maresca, D.; Lucentini, L.; Ferretti, E.; Citti, G.; Ottaviani, M., Monitoring of V (IV) and V (V) in Etnean drinking-water distribution systems by solid phase extraction and electrothermal atomic absorption spectrometry. *Microchemical journal* **2007,** *85* (1), 80-87.
102. Wehrli, B.; Stumm, W., Vanadyl in natural waters: adsorption and hydrolysis promote oxygenation. *Geochimica et Cosmochimica Acta* **1989,** *53* (1), 69-77.
103. Baes Jr, C.; Mesmer, R., T he Hydrolysis of Cations. Wiley, New York: 1976.
104. Burke, I. T.; Mayes, W. M.; Peacock, C. L.; Brown, A. P.; Jarvis, A. P.; Gruiz, K., Speciation of arsenic, chromium, and vanadium in red mud samples from the Ajka spill site, Hungary. *Environmental science & technology* **2012,** *46* (6), 3085-3092.
105. Catana, G.; Rao, R. R.; Weckhuysen, B. M.; Van Der Voort, P.; Vansant, E.; Schoonheydt, R. A., Supported vanadium oxide catalysts: Quantitative spectroscopy, preferential adsorption of $V^{4+/5+}$, and Al_2O_3 coating of zeolite Y. *The Journal of Physical Chemistry B* **1998,** *102* (41), 8005-8012.
106. Manohar, D.; Noeline, B.; Anirudhan, T., Removal of vanadium (IV) from aqueous solutions by adsorption process with aluminum-pillared bentonite. *Industrial & engineering chemistry research* **2005,** *44* (17), 6676-6684.
107. Davis, J. A.; Meece, D. E.; Kohler, M.; Curtis, G. P., Approaches to surface complexation modeling of uranium (VI) adsorption on aquifer sediments. *Geochim Cosmochim Ac* **2004,** *68* (18), 3621-3641.
108. Curtis, G. P.; Davis, J. A.; Naftz, D. L., Simulation of reactive transport of uranium (VI) in groundwater with variable chemical conditions. *Water Resources Research* **2006,** *42* (4).
109. Qafoku, N. P.; Zachara, J. M.; Liu, C.; Gassman, P. L.; Qafoku, O. S.; Smith, S. C., Kinetic desorption and sorption of U (VI) during reactive transport in a contaminated Hanford sediment. *Environmental science & technology* **2005,** *39* (9), 3157-3165.
110. Hammond, G. E.; Lichtner, P. C., Field-scale model for the natural attenuation of uranium at the Hanford 300 Area using high-performance computing. *Water Resources Research* **2010,** *46* (9).
111. Zachara, J. M.; Chen, X.; Murray, C.; Hammond, G., River stage influences on uranium transport in a hydrologically dynamic groundwater-surface water transition zone. *Water Resources Research* **2016**.
112. Stubbs, J. E.; Veblen, L. A.; Elbert, D. C.; Zachara, J. M.; Davis, J. A.; Veblen, D. R., Newly recognized hosts for uranium in the Hanford Site vadose zone. *Geochim Cosmochim Ac* **2009,** *73* (6), 1563-1576.
113. Wolff-Boenisch, D.; Gislason, S. R.; Oelkers, E. H., The effect of crystallinity on dissolution rates and CO2 consumption capacity of silicates. *Geochimica et Cosmochimica Acta* **2006,** *70* (4), 858-870.

114. Stefánsson, A.; Gíslason, S. R., Chemical weathering of basalts, Southwest Iceland: effect of rock crystallinity and secondary minerals on chemical fluxes to the ocean. *American Journal of Science* **2001,** *301* (6), 513-556.
115. Gorman-Lewis, D.; Burns, P. C.; Fein, J. B., Review of uranyl mineral solubility measurements. *The Journal of Chemical Thermodynamics* **2008,** *40* (3), 335-352.
116. Abraham, F.; Dion, C.; Saadi, M., Carnotite analogues: synthesis, structure and properties of the $Na_{1-x}K_xUO_2VO_4$ solid solution ($0 \leqslant x \leqslant 1$). *Journal of Materials Chemistry* **1993,** *3* (5), 459-463.
117. Weigel, F.; Hoffmann, G., The phosphates and arsenates of hexavalent actinides. Part I. Uranium. *Journal of the Less Common Metals* **1976,** *44*, 99-123.
118. Plášil, J.; Veselovský, F.; Hloušek, J.; Škoda, R.; Novák, M.; Sejkora, J.; Čejka, J.; Škácha, P.; Kasatkin, A. V., Mathesiusite, $K_5(UO_2)_4(SO_4)_4(VO_5)(H_2O)_4$, a new uranyl vanadate-sulfate from Jachymov, Czech Republic. *American Mineralogist* **2014,** *99* (4), 625-632.
119. Karyakin, N.; Chernorukov, N.; Suleimanov, E.; Alimzhanov, M., Chemical thermodynamics of alkaline-earth metal uranovanadates. *Radiochemistry* **2003,** *45* (5), 457-468.
120. Burns, P. C., U^{6+} minerals and inorganic compounds: insights into an expanded structural hierarchy of crystal structures. *The Canadian Mineralogist* **2005,** *43* (6), 1839-1894.
121. Krivovichev, S. V.; Plášil, J., Mineralogy and crystallography of uranium. *Uranium: From Cradle to Grave. Mineralogical Association of Canada Short Courses* **2013,** *43*, 15-119.
122. Troyer, L. D.; Stone, J. J.; Borch, T., Effect of biogeochemical redox processes on the fate and transport of As and U at an abandoned uranium mine site: an X-ray absorption spectroscopy study. *Environmental Chemistry* **2014,** *11* (1), 18-27.
123. Stokes, W. L., Carnotite Deposits in the Carrizo Mountains Area, Navajo Indian Reservation, Apache County, Arizona and San Juan County, New Mexico. *USGS Circular* **1951,** *111*.
124. Dixon, E. The Legacy Uranium Mining and Milling Cleanup Plan: Evaluation of the EPA Five-Year Plan, Grants Mining District, New Mexico. 2015
125. Dawson, S. E., Navajo Uranium Workers and the Effects of Occupational Illnesses - a Case-Study. *Hum Organ* **1992,** *51* (4), 389-397.
126. Hopenhayn, C., Arsenic in drinking water: Impact on human health. *Elements* **2006,** *2* (2), 103-107.
127. Chenoweth, W., Vanadium mining in the Carrizo Mountains, 1942-1947. San Juan County, New Mexico and Apache County Arizona: New Mexico Bureau of Mines and Mineral Resources, Open-file Report **1991,** *378*, 33.
128. Dong, W.; Brooks, S. C., Determination of the Formation Constants of Ternary Complexes of Uranyl and Carbonate with Alkaline Earth Metals (Mg^{2+}, Ca^{2+}, Sr^{2+}, and Ba^{2+}) Using Anion Exchange Method. *Environmental Science & Technology* **2006,** *40* (15), 4689-4695.
129. Bargar, J. R.; Reitmeyer, R.; Davis, J. A., Spectroscopic confirmation of uranium (VI)-carbonato adsorption complexes on hematite. *Environmental Science & Technology* **1999,** *33* (14), 2481-2484.

130. Peacock, C. L.; Sherman, D. M., Vanadium (V) adsorption onto goethite (α-FeOOH) at pH 1.5 to 12: a surface complexation model based on ab initio molecular geometries and EXAFS spectroscopy. *Geochim Cosmochim Ac* **2004,** *68* (8), 1723-1733.
131. Sylwester, E.; Hudson, E.; Allen, P., The structure of uranium (VI) sorption complexes on silica, alumina, and montmorillonite. *Geochimica et Cosmochimica Acta* **2000,** *64* (14), 2431-2438.
132. Liu, C.; Shang, J.; Shan, H.; Zachara, J. M., Effect of subgrid heterogeneity on scaling geochemical and biogeochemical reactions: A case of U (VI) desorption. *Environmental science & technology* **2014,** *48* (3), 1745-1752.
133. Kosmulski, M., pH-dependent surface charging and points of zero charge: III. Update. *Journal of Colloid and Interface Science* **2006,** *298* (2), 730-741.
134. Schroth, B. K.; Sposito, G. In *Surface charge properties of kaolinite*, MRS Proceedings, Cambridge Univ Press: 1996; p 87.
135. Bernier-Latmani, R.; Veeramani, H.; Vecchia, E. D.; Junier, P.; Lezama-Pacheco, J. S.; Suvorova, E. I.; Sharp, J. O.; Wigginton, N. S.; Bargar, J. R., Non-uraninite products of microbial U (VI) reduction. *Environmental science & technology* **2010,** *44* (24), 9456-9462.
136. Hansley, P. L.; Spirakis, C. S., Organic matter diagenesis as the key to a unifying theory for the genesis of tabular uranium-vanadium deposits in the Morrison Formation, Colorado Plateau. *Economic Geology* **1992,** *87* (2), 352-365.
137. Franczyk, K. J., Stratigraphic revision and depositional environments of the Upper Cretaceous Toreva Formation in the northern Black Mesa area, Navajo and Apache Counties, Arizona. **1988**.
138. Giammar, D. E.; Hering, J. G., Time scales for sorption-desorption and surface precipitation of uranyl on goethite. *Environmental science & technology* **2001,** *35* (16), 3332-3337.
139. Tokunaga, T. K.; Kim, Y.; Wan, J.; Yang, L., Aqueous uranium (VI) concentrations controlled by calcium uranyl vanadate precipitates. *Environmental science & technology* **2012,** *46* (14), 7471-7477.
140. Langmuir, D., Aqueous environmental geochemistry. 1997.
141. Liu, C.; Zachara, J. M.; Qafoku, N. P.; Wang, Z., Scale-dependent desorption of uranium from contaminated subsurface sediments. *Water Resources Research* **2008,** *44* (8).
142. Steefel, C. I.; DePaolo, D. J.; Lichtner, P. C., Reactive transport modeling: An essential tool and a new research approach for the Earth sciences. *Earth and Planetary Science Letters* **2005,** *240* (3), 539-558.
143. Shabansefidan, F.; Reddy, M. A., Investigation of Uranium Solubility and its Transport Path in the Razgah Basin's Groundwater in the Northwest of Iran, Using Saturation Indexes.
144. Puigdomenech, I.; Bruno, J., Modelling uranium solubilities in aqueous solutions: Validation of a thermodynamic data base for the EQ3/6 geochemical codes. Swedish Nuclear Fuel and Waste Management Company: 1988.
145. Kubatko, K.-A.; Helean, K. B.; Navrotsky, A.; Burns, P. C., Thermodynamics of uranyl minerals: Enthalpies of formation of rutherfordine, UO_2CO_3, andersonite, $Na_2CaUO_2(CO_3)_3(H_2O)_5$, and grimselite, K_3NaUO_2 (CO_3) $3H_2O$. *American Mineralogist* **2005,** *90* (8-9), 1284-1290.

146. Bond, D. L.; Davis, J. A.; Zachara, J. M., Uranium (VI) release from contaminated vadose zone sediments: Estimation of potential contributions from dissolution and desorption. *Developments in Earth and Environmental Sciences* **2007,** *7*, 375-416.
147. Lollar, B. S., Environmental geochemistry. *Elsevier*: 2005; Vol. 9.
148. Riba, O.; Walker, C.; Ragnarsdottir, K. V., Kinetic studies of synthetic metaschoepite under acidic conditions in batch and flow experiments. *Environmental science & technology* **2005,** *39* (20), 7915-7920.
149. Yoshida, S.; Iguchi, T.; Ishida, S.; Tarama, K., Some physico-chemical properties of vanadium oxide supported on silica or γ-alumina. *Bulletin of the Chemical Society of Japan* **1972,** *45* (2), 376-380.
150. Langmuir, D., Uranium solution-mineral equilibria at low temperatures with applications to sedimentary ore deposits. *Geochim Cosmochim Ac* **1978,** *42* (6), 547-569.
151. Hochella, M. F.; Lower, S. K.; Maurice, P. A.; Penn, R. L.; Sahai, N.; Sparks, D. L.; Twining, B. S., Nanominerals, mineral nanoparticles, and earth systems. *science* **2008,** *319* (5870), 1631-1635.
152. Um, W.; Wang, Z.; Serne, R. J.; Williams, B. D.; Brown, C. F.; Dodge, C. J.; Francis, A. J., Uranium phases in contaminated sediments below Hanford's U tank farm. *Environmental science & technology* **2009,** *43* (12), 4280-4286.
153. Delemos, J. L.; Bostick, B. C.; Quicksall, A. N.; Landis, J. D.; George, C. C.; Slagowski, N. L.; Rock, T.; Brugge, D.; Lewis, J.; Durant, J. L., Rapid dissolution of soluble uranyl phases in arid, mine-impacted catchments near Church Rock, NM. *Environmental science & technology* **2008,** *42* (11), 3951-3957.
154. Goss, K.-U., The p K a values of PFOA and other highly fluorinated carboxylic acids. *Environmental science & technology* **2007,** *42* (2), 456-458.
155. Kim, K.-W.; Hyun, J.-T.; Lee, K.-Y.; Lee, E.-H.; Lee, K.-W.; Song, K.-C.; Moon, J.-K., Effects of the different conditions of uranyl and hydrogen peroxide solutions on the behavior of the uranium peroxide precipitation. *Journal of hazardous materials* **2011,** *193*, 52-58.
156. Schoonen, M.; Barnes, H., Reactions forming pyrite and marcasite from solution: I. Nucleation of FeS 2 below 100 C. *Geochim Cosmochim Ac* **1991,** *55* (6), 1495-1504.
157. Lippmann, F., Sedimentary carbonate minerals. *Springer Science & Business Media*: 2012; Vol. 6.
158. Smith, S. C.; Douglas, M.; Moore, D. A.; Kukkadapu, R. K.; Arey, B. W., Uranium extraction from laboratory-synthesized, uranium-doped hydrous ferric oxides. *Environmental science & technology* **2009,** *43* (7), 2341-2347.
159. Ilton, E. S.; Zachara, J. M.; Moore, D. A.; Mckinley, J. P.; Eckberg, A. D.; Cahill, C. L.; Felmy, A. R., Dissolution study of metatorbernite: Thermodynamic properties and the effect of pH and phosphate. *Environmental science & technology* **2010,** *44* (19), 7521-7526.
160. Graham, J.; Butt, C.; Vigers, R., Sub-surface charging, a source of error in microprobe analysis. *X-Ray Spectrometry* **1984,** *13* (3), 126-133.
161. Stubbs, J. E.; Post, J. E.; Elbert, D. C.; Heaney, P. J.; Veblen, D. R., Uranyl phosphate sheet reconstruction during dehydration of metatorbernite [$Cu(UO_2)_2(PO_4)_2 \cdot 8H_2O$]. *American Mineralogist* **2010,** *95* (8-9), 1132-1140.

162. Barton Jr, P. B. Synthesis and properties of carnotite and its alkali analogues; 1957.
163. Abraham, F.; Dion, C.; Tancret, N.; Saadi, M. In $Ag_2(UO_2)_2V_2O_8$: a new compound with the carnotite structure. Synthesis, structure and properties, *Advanced Materials Research, Trans Tech Publ*: 1994; pp 511-520.
164. Obbade, S.; Dion, C.; Duvieubourg, L.; Saadi, M.; Abraham, F., Synthesis and crystal structure of α and β-Rb 6 U 5 V 2 O 23, a new layered compound. *Journal of Solid State Chemistry* **2003,** *173* (1), 1-12.
165. Murata, K.; CISNEY, E.; Stieff, L.; Zworykin, E. In Hydration and Base-Exchange Properties of Carnotite, Tyuyamunite and Related Compounds, *Geologican Society of America Bulltetin, Assoc Engineering Geologists Geological society Amer Texas A & M Univ*, Dept Geology $ Geophysics, College Stn, *TX*77843-3115: 1950; pp 1489-1490.
166. Piret, P.; Declerq, J.; Wautersstoop, D., Crystal Structure of Sengierite, *Bulletin De Mineralogie* **1980,** *103* (2), 176-178.
167. Ginderow, D.; Cesbron, F., Structure de la demesmaekerite, $Pb_2Cu_5(SeO_3)6(UO_2)_2(OH)_6.2H_2O$. *Acta Crystallographica Section C: Crystal Structure Communications* **1983,** *39* (7), 824-827.
168. Borene, J., Crystal Structure Of Nickel Uranyl Vanadate Tetrahydrate $Ni(UO_2)_2(VO_4)$ $2.4H_2O$. *Bulletin De La Societe Franciase Mineralogie Et Dt Cristallographie* **1970,** *93* (4), 426.
169. Dickens, P. G.; Stuttard, G. P.; Ball, R. G.; Powell, A. V.; Hull, S.; Patat, S., Powder neutron diffraction study of the mixed uranium–vanadium oxides $Cs_2(UO_2)_2(V_2O_8)$ and UVO_5. *Journal of Materials Chemistry* **1992,** *2* (2), 161-166.
170. Spano, T. L.; Dzik, E. A.; Sharifironizi, M.; Dustin, M. K.; Turner, M.; Burns, P. C., Thermodynamic investigation of uranyl vanadate minerals: Implications for structural stability. *American Mineralogist* **2017,** *102* (6), 1149-1153.
171. Frost, R. L.; Čejka, J.; Weier, M. L.; Martens, W.; Henry, D. A., Vibrational spectroscopy of selected natural uranyl vanadates. *Vibrational spectroscopy* **2005,** *39* (2), 131-138.
172. Senchyk, G.; Wylie, E.; Prizio, S.; Szymanowski, J.; Sigmon, G.; Burns, P., Hybrid uranyl–vanadium nano-wheels. *Chemical Communications* **2015,** *51* (50), 10134-10137.
173. Catalano, J. G.; Brown, G. E., Analysis of uranyl-bearing phases by EXAFS spectroscopy: Interferences, multiple scattering, accuracy of structural parameters, and spectral differences. *American Mineralogist* **2004,** *89* (7), 1004-1021.
174. Burns, P. C.; Ewing, R. C.; Miller, M. L., Incorporation mechanisms of actinide elements into the structures of U6+ phases formed during the oxidation of spent nuclear fuel. *Journal of Nuclear materials* **1997,** *245* (1), 1-9.
175. McGuire, A. V.; Francis, C. A.; Dyar, M. D., Mineral standards for electron microprobe analysis of oxygen. *American Mineralogist* **1992,** *77*, 1087-1087.
176. Jarosewich, E., Smithsonian microbeam standards. *Journal of Research of the National Institute of Standards and Technology* **2002,** *107* (6), 681.
177. Donovan, J. J.; Snyder, D. A.; Rivers, M. L. In An improved interference correction for trace element analysis, Proceedings of the Annual Meeting-Electron Microscopy Society of America, San Francisco Press: 1992; pp 1646-1646.

178. Donovan, J. J.; Lowers, H. A.; Rusk, B. G., Improved electron probe microanalysis of trace elements in quartz. *American Mineralogist* **2011,** *96* (2-3), 274-282.
179. Bastin, G.; Heijligers, H., Quantitative electron probe microanalysis of carbon in binary carbides. I—principles and procedures. *X-Ray Spectrometry* **1986,** *15* (2), 135-141.
180. Poppe, L.; Paskevich, V.; Hathaway, J.; Blackwood, D., A laboratory manual for X-ray powder diffraction. *US Geological Survey Open-File Report* **2001,** *1* (041), 1-88.
181. Abreu, N. M.; Brearley, A. J., Early solar system processes recorded in the matrices of two highly pristine CR3 carbonaceous chondrites, MET 00426 and QUE 99177. *Geochim. Cosmochim. Acta* **2010,** *74* (3), 1146-1171.
182. Anthony, J. W., Handbook of mineralogy: Arsenates, phosphates, vanadates. arsenates, phosphates, vanadates. Mineral Data Pub.: 2000; Vol. 4.
183. Nasdala, L.; Kronz, A.; Wirth, R.; Váczi, T.; Pérez-Soba, C.; Willner, A.; Kennedy, A. K., The phenomenon of deficient electron microprobe totals in radiation-damaged and altered zircon. *Geochim Cosmochim Ac* **2009,** *73* (6), 1637-1650.
184. Jones, A.; Palmer, D.; Islam, M.; Mortimer, M., Alkali ion migration in albite and K-feldspar. *Physics and Chemistry of Minerals* **2004,** *31* (5), 313-320.
185. Craw, D., Oxidation and microprobe-induced potassium mobility in iron-bearing phyllosilicates from the Otago schists, New Zealand. *Lithos* **1981,** *14* (1), 49-57.
186. Katrinak, K.; Rez, P.; Buseck, P., Structural variations in individual carbonaceous particles from an urban aerosol. *Environmental science & technology* **1992,** *26* (10), 1967-1976.
187. Comelli, G.; Stöhr, J.; Robinson, C.; Jark, W., Structural studies of argon-sputtered amorphous carbon films by means of extended x-ray-absorption fine structure. *Physical Review B* **1988,** *38* (11), 7511.
188. Sundberg, I.; Sillén, L., On the Crystal Structure of KUO_2VO_4 (Synthetic Anhydrous Carnotite). *Arkiv Kemi* **1950,** *1*.
189. Stern, T.; Stieff, L.; Girhard, M.; Meyrowitz, R., The Occurrence And Properties of Metatyuyamunite, $Ca(UO_2)_2(VO_4)_2$.3-5H2O. *Am. Mineralogist* **1956,** *41*.
190. Donnay, G.; Donnay, J. In Tyuyamunite, Carnotite, And Sengierite, American Mineralogist, *Mineralogical Soc Amer* 1015 Eighteenth ST, NW suite 601, Washington, DC 20036: 1954; pp 323-324.
191. Hilpert, L. S.; Moench, R. H., Uranium deposits of the southern part of the San Juan Basin, New Mexico. *Economic Geology* **1960,** *55* (3), 429-464.
192. Laverty, R.; Ashwill, W.; Chenoweth, W.; Norton, D., Ore processes. *Geology and technology of the Grants uranium region: New Mexico Bureau of Mines and Mineral Resources Memoir* **1963,** *15*, 191-204.
193. Kittel, D. F., Geology of the Jackpile mine area. *Geology and Technology of the Grants Uranium Region, Memoir* **1963,** *15*.
194. Zehner, H. H., Hydrology and water-quality monitoring considerations, Jackpile uranium mine, northwestern New Mexico. **1985**.
195. Adams, S.; Curtis, H.; Hafen, P.; Salek-Nejad, H., Interpretation of postdepositional processes related to the formation and destruction of the Jackpile-Paguate uranium deposit, northwest New Mexico. *Economic Geology* **1978,** *73* (8), 1635-1654.

196. Kelley, V. C., *Geology and technology of the Grants uranium region*. State Bureau of Mines and Mineral Resources: Society of Economic Geologists, 1963.
197. Ginder-Vogel, M.; Criddle, C. S.; Fendorf, S., Thermodynamic constraints on the oxidation of biogenic UO2 by Fe (III)(hydr) oxides. *Environmental science & technology* **2006,** *40* (11), 3544-3550.
198. Deditius, A. P.; Utsunomiya, S.; Ewing, R. C., The chemical stability of coffinite, $USiO_4 \cdot nH_2O$; 0<n<2, associated with organic matter: A case study from Grants uranium region, New Mexico, USA. *Chemical Geology* **2008,** *251* (1), 33-49.
199. Ruiz, O.; Thomson, B. M.; Cerrato, J. M., Investigation of in situ leach (ISL) mining of uranium in New Mexico and post-mining reclamation. *New Mexico Geology* **2016,** *38* (4).
200. Learn, D.; Brestel, E.; Seetharama, S., Hypochlorite scavenging by Pseudomonas aeruginosa alginate. *Infection and immunity* **1987,** *55* (8), 1813-1818.
201. Schultz, M. K.; Burnett, W. C.; Inn, K. G., Evaluation of a sequential extraction method for determining actinide fractionation in soils and sediments. *Journal of Environmental Radioactivity* **1998,** *40* (2), 155-174.
202. Blanco, P.; Tome, F. V.; Lozano, J., Fractionation of natural radionuclides in soils from a uranium mineralized area in the south-west of Spain. *Journal of environmental radioactivity* **2005,** *79* (3), 315-330.
203. Schecher, W.; MINEQL, D. M., A Chemical Equilibrium Modeling System, Version 4.6, 4.5. *Environmental Research Software: Hallowell, ME* **2007**.
204. Grenthe, I.; Fuger, J.; Konings, R.; Lemire, R.; Muller, A.; Nguyen-Trung, C., Chemical Thermodynamics of Uranium, edited by H. Wanner and I. *Forest (North Holland, Amsterdam, 1992)* **1992**.
205. Guillaumont, R.; Mompean, F. J., Update on the chemical thermodynamics of uranium, neptunium, plutonium, americium and technetium. **2003**.
206. Dong, W.; Brooks, S. C., Formation of aqueous $MgUO_2(CO_3)_3^{2-}$ complex and uranium anion exchange mechanism onto an exchange resin. *Environmental science & technology* **2008,** *42* (6), 1979-1983.
207. Ilton, E. S.; Bagus, P. S., XPS determination of uranium oxidation states. *Surface and Interface Analysis* **2011,** *43* (13), 1549-1560.
208. Uyuşur, B.; Li, C.; Baveye, P. C.; Darnault, C. J., pH-dependent reactive transport of uranium (VI) in unsaturated sand. *Journal of soils and sediments* **2015,** *15* (3), 634-647.
209. Bi, Y.; Hayes, K. F., Surface passivation limited UO2 oxidative dissolution in the presence of FeS. *Environmental science & technology* **2014,** *48* (22), 13402-13411.
210. Wang, G.; Um, W.; Wang, Z.; Reinoso-Maset, E.; Washton, N. M.; Mueller, K. T.; Perdrial, N.; O'Day, P. A.; Chorover, J., Uranium Release from Acidic Weathered Hanford Sediments: Single-Pass Flow-Through and Column Experiments. *Environmental Science & Technology* **2017**.
211. Gorman-Lewis, D.; Shvareva, T.; Kubatko, K.-A.; Burns, P. C.; Wellman, D. M.; McNamara, B.; Szymanowski, J. E.; Navrotsky, A.; Fein, J. B., Thermodynamic properties of autunite, uranyl hydrogen phosphate, and uranyl orthophosphate from solubility and calorimetric measurements. *Environmental science & technology* **2009,** *43* (19), 7416-7422.

212. Liu, C.; Zachara, J. M.; Qafoku, O.; McKinley, J. P.; Heald, S. M.; Wang, Z., Dissolution of uranyl microprecipitates in subsurface sediments at Hanford Site, USA. *Geochimica et Cosmochimica Acta* **2004,** *68* (22), 4519-4537.
213. Lichtner, P. C., Continuum model for simultaneous chemical reactions and mass transport in hydrothermal systems. *Geochim Cosmochim Ac* **1985,** *49* (3), 779-800.
214. Lichtner, P. C., Kinetic rate laws invariant to scaling the mineral formula unit. *American Journal of Science* **2016,** *316* (5), 437-469.
215. Lasaga, A. C., Chemical kinetics of water-rock interactions. *Journal of geophysical research: solid earth* **1984,** *89* (B6), 4009-4025.
216. Brantley, S. L., Kinetics of mineral dissolution. In *Kinetics of water-rock interaction*, Springer: 2008; pp 151-210.
217. Bai, J.; Liu, C.; Ball, W. P., Study of sorption-retarded U (VI) diffusion in Hanford silt/clay material. *Environmental science & technology* **2009,** *43* (20), 7706-7711.
218. Appelo, C. A. J.; Postma, D., Geochemistry, groundwater and pollution. CRC press: 2004.
219. Shock, E. L.; Helgeson, H. C., Calculation of the thermodynamic and transport properties of aqueous species at high pressures and temperatures: Correlation algorithms for ionic species and equation of state predictions to 5 kb and 1000 C. *Geochim Cosmochim Ac* **1988,** *52* (8), 2009-2036.
220. Ulrich, K.-U.; Singh, A.; Schofield, E. J.; Bargar, J. R.; Veeramani, H.; Sharp, J. O.; Bernier-Latmani, R.; Giammar, D. E., Dissolution of biogenic and synthetic UO_2 under varied reducing conditions. *Environmental science & technology* **2008,** *42* (15), 5600-5606.
221. Cox, J.; Wagman, D. D.; Medvedev, V. A., Codata key values for thermodynamics. Chem/Mats-Sci/E: 1989.
222. Pokrovskii, V. A.; Helgeson, H. C., Thermodynamic properties of aqueous species and the solubilities of minerals at high pressures and temperatures; the system Al_2O_3-H_2O-NaCl. *American Journal of Science* **1995,** *295* (10), 1255-1342.
223. Baes, C. F.; Mesmer, R. E., Hydrolysis of cations. Wiley: 1976.
224. Johnson, J. W.; Oelkers, E. H.; Helgeson, H. C., SUPCRT92: A software package for calculating the standard molal thermodynamic properties of minerals, gases, aqueous species, and reactions from 1 to 5000 bar and 0 to 1000 C. *Computers & Geosciences* **1992,** *18* (7), 899-947.
225. Wagman, D. D.; Evans, W. H.; Parker, V. B.; Schumm, R. H.; Halow, I. The NBS tables of chemical thermodynamic properties. Selected values for inorganic and C1 and C2 organic substances in SI units; DTIC Document: 1982.
226. Turner, D.; Whitfield, M.; Dickson, A., The equilibrium speciation of dissolved components in freshwater and sea water at 25 C and 1 atm pressure. *Geochim Cosmochim Ac* **1981,** *45* (6), 855-881.
227. Mattigod, S. V.; Sposito, G., Chemical modeling of trace metal equilibria in contaminated soil solutions using the computer program Geochem. ACS Publications: 1979.
228. Grenthe, I.; Fuger, J.; Konings, R. J.; Lemire, R. J.; Muller, A. B.; Nguyen-Trung, C.; Wanner, H., *Chemical thermodynamics of uranium*. North-Holland Amsterdam: 1992; Vol. 1.

229. Bernhard, G.; Geipel, G.; Reich, T.; Brendler, V.; Amayri, S.; Nitsche, H., Uranyl (VI) carbonate complex formation: Validation of the Ca2UO2 (CO3) 3 (aq.) species. *Radiochimica Acta* **2001,** *89* (8), 511-518.
230. Israel, Y.; Meites, L.; Bard, A., Encyclopedia of Electrochemistry of the Elements. *Vol. 7Dekker, New York* **1976**, 293.
231. Sergeyeva, E.; Khodakovskiy, I., Physicochemical conditions of formation of native arsenic in hydrothermal deposits. **1969**.
232. Helgeson, H. C., Summary and critique of the thermodynamic properties of rock-forming minerals. *American Journal of Science* **1978,** *278*, 1-229.
233. Casas, I.; Bruno, J.; Cera, E.; Finch, R. J.; Ewing, R. C., Characterization and dissolution behavior of a becquerelite from Shinkolobwe, Zaire. *Geochim Cosmochim Ac* **1997,** *61* (18), 3879-3884.
234. Robie, R. A.; Hemingway, B. S. Thermodynamic properties of minerals and related substances at 298.15 K and 1 bar (10^ 5 Pascals) pressure and at higher temperatures; USGPO; For sale by US Geological Survey, Information Services: 1995.
235. Stumm, W.; Morgan, J., Aquatic Chemistry. Interscience, New York: 1970.
236. Meinrath, G.; Kimura, T., Behaviour of U (VI) solids under conditions of natural aquatic systems. *Inorganica chimica acta* **1993,** *204* (1), 79-85.